VOL. 107 NO. WW2. MAY 1981

JOURNAL OF THE WATERWAY PORT COASTAL AND OCEAN DIVISION

PROCEEDINGS OF
THE AMERICAN SOCIETY
OF CIVIL ENGINEERS

VOL.107 NO.WW2. MAY 1981

JOURNAL OF THE WATERWAY PORT COASTAL AND OCEAN DIVISION

PROCEEDINGS OF
THE AMERICAN SOCIETY
OF CIVIL ENGINEERS

ISSN 0148-9895

AMERICAN SOCIETY OF CIVIL ENGINEERS

CONTENTS

This Journal is published quarterly by the American Society of Civil Engineers. Publications office is at 345 East 47th Street, New York, N.Y. 10017. Address all ASCE correspondence to the Editorial and General Offices at 345 East 47th Street, New York, N.Y. 10017. Allow six weeks for change of address to become effective. Subscription price to members is $8.00. Nonmember subscriptions available; prices obtainable on request. Second-class postage paid at New York, N.Y. and at additional mailing offices. WW.

DISCUSSION

Proc. Paper 16220

INFORMATION RETRIEVAL

The key words, abstract, and reference "cards" for each article in this Journal represent part of the ASCE participation in the EJC information retrieval plan. The retrieval data are placed herein so that each can be cut out, placed on a 3 × 5 card and given an accession number for the user's file. The accession number is then entered on key word cards so that the user can subsequently match key words to choose the articles he wishes. Details of this program were given in an August, 1962 article in CIVIL ENGINEERING, reprints of which are available on request to ASCE headquarters.

*Discussion period closed for this paper. Any other discussion received during this discussion period will be published in subsequent Journals.

16265 FLUSHING STUDY OF OREGON MARINA

KEY WORDS: Comparative studies; Dye releases; Dyes; **Flushing; Hydraulic models; Marinas; Mathematical models;** Oregon; Tidal effects; Time factors

ABSTRACT: A newly constructed single-opening marina was evaluated to determine flushing characteristics by comparison of a hydraulic model and a mathematical model with field studies of dye releases. Both models simulated well-mixed conditions and agreed well with each other. The dye study was conducted by mixing rhodamine-wt throughout the marina on a flood tide and monitoring dye concentration versus time over several tidal cycles following release. Over the initial 7-10 hours of the field studies, all three methods agreed well; field results thereafter showed three to six times less dye than model predictions. For marinas of simple geometry with single openings and width-to-length ratios similar to the marina studied here, flushing estimates may be conservatively approximated by elementary mathematical methods.

REFERENCE: Callaway, Richard J., "Flushing Study of South Beach Marina, Oregon," *Journal of the Waterway, Port, Coastal and Ocean Division,* ASCE, Vol. 107, No. WW2, **Proc. Paper 16265**, May, 1981, pp. 47-58

16255 BREAKING-LIMITED WAVE HEIGHTS

KEY WORDS: Narrowband; **Probability; Probability distribution functions;** Rayleigh waves; **Stokes law;** Stokes law (fluid mechanics); **Wave action; Wave height;** Wave measurement; **Wave spectrum**

ABSTRACT: Empirical distributions of wave heights derived from field data differ from the theoretical distribution of wave heights as given by the Rayleigh law. A principal cause of this discrepancy is suggested to be that the conventional theory does not in any way account for wave breaking. Based on the assumption that the sea surface is characterized with a narrow-band spectrum, the probability distribution of wave heights limited by breaking, due to a Stokes-type limiting steepness in deep or finite water depths, is derived. The breaking-limited distribution provides a probability discription which compares with two well documented field observations more favorably than the Rayleigh law.

REFERENCE: Tayfun, M. Aziz, "Breaking-Limited Wave Heights," *Journal of the Waterway, Port, Coastal and Ocean Division,* ASCE, Vol. 107, No. WW2, **Proc. Paper 16255**, May, 1981, pp. 59-69

16272 WAVE FORCES ON RIGID PIPES

KEY WORDS: Hawaii; Kinematics; **Ocean engineering; Offshore structures;** Pipe design; **Pipelines; Pipe tests; Rigid pipes;** Time factors; **Wave pressure; Waves**

ABSTRACT: A test pipe rig was designed, fabricated, and then placed in the ocean, offshore from Honolulu. The pipe diameter was 16 inches, its length 17.5 feet, and the water depth was 37 feet. During four seasons of swell from Southern Hemisphere winter storms, data were obtained for the forces exerted on a 40-inch-long portion of the test pipe. Four separate angles between the swell fronts and the test pipe were involved: 0^{o}, 15^{o}, 35^{o}, and 52^{o}. the measured forces were combined with concurrently measured wave-induced kinematic values to derive horizontal and vertical pipe force coefficients of use to offshore pipeline designers.

REFERENCE: Grace, Robert A., and Zee, Gabriel T.Y., "Wave Forces on Rigid Pipes Using Ocean Test Data," *Journal of the Waterway, Port, Coastal and Ocean Division,* ASCE, Vol. 107, No. WW2, **Proc. Paper 16272**, May, 1981, pp. 71-92

16277 LONG-TERM DISTRIBUTIONS OF OCEAN WAVES

KEY WORDS: **Coastal engineering; Ocean engineering;** Ocean waves; Offshore structures; Probability distribution functions; Statistical analysis; Wave equations; Wave forecasting; **Wave height;** Wave measurement

ABSTRACT: The various steps involved in the estimation of an extreme design wave are reviewed. These include the following: methods of data collection, the use of a plotting formula, the selection of a suitable distribution and its parameters, the plotting of confidence bands about the best-fit line, and the selection of a design wave corresponding to a prescribed return period or encounter probability. The probability distributions commonly used, including the log-normal and Extremal Types I, II, and III distributions (Gumbel, Fretchet, and Weibull respectively), are described, and their properties are summarized in tabular form for ready reference.

REFERENCE: Isaacson, Michael de St. Q., and MacKenzie, Neil G., "Long-Term Distributions of Ocean Waves: A Review," *Journal of the Waterway, Port, Coastal and Ocean Division,* ASCE, Vol. 107, No. WW2, **Proc. Paper 16277,** May, 1981, pp. 93-109

Flushing Study of South Beach Marina, Oregon

By Richard J. Callaway[1]

Introduction

Recent increases in recreational and small commercial craft activities have resulted in the construction of many new marinas. Local, state, and Federal governments must evaluate applications for marina construction permits. Little information exists on ecological impacts of marinas or of construction events such as dredging and spoil disposal.

This report concerns one aspect of the marina permit evaluation process: water quality impacts related to marina circulation and flushing efficiency. These physical properties vary with the wind, tide range, water density, and physical dimensions of a marina. Water quality is affected by the degree of flushing, and sediment redistribution by currents. Detrimental water quality can determine, e.g., the fate of migrating juvenile fish and benthic organisms (5,7).

Ecological studies of marinas are few. The most comprehensive have been performed on Marina del Rey, Calif. (3,15,16,17,22). Slotta and Noble (21) analyzed the use of benthic sediments as indicators of marina flushing in several Pacific Northwest marinas. Puget Sound marina water quality studies have also been conducted (10, 11, and an unpublished work by Yearsley).

Marina Model Studies

Most mathematical studies of marina circulation and flushing have been concerned with vertically well-mixed waters in one and two dimensions (1,2,4,6, 18,20).

Hydraulic model studies of small harbors provide an alternative method of assessing flushing ability, although not without deficiencies related to scale distortion. Several hydraulic model studies of Pacific Northwest marinas have been conducted by Nece and Richey and their associates at the University of Washington (9,12,13), and by Slotta and others at Oregon State University (1,20,21).

[1]Oceanographer, Environmental Protection Agency, Marine Div., Environmental Research Lab., 200 S.W. 35 St., Corvallis, Oreg. 97330.

Note.—Discussion open until October 1, 1981. To extend the closing date one month, a written request must be filed with the Manager of Technical and Professional Publications, ASCE. Manuscript was submitted for review for possible publication on July 16, 1980. This paper is part of the Journal of the Waterway, Port, Coastal and Ocean Division, Proceedings of the American Society of Civil Engineers, ©ASCE, Vol. 107, No. WW2, May, 1981.

Because of the small size of most Pacific Northwest marinas, use of numerical models employing finite difference grids or finite elements is not always practical. In order to utilize the numerical method to its best advantage, very small grids would need to be used; for finite difference analogs employing explicit solutions, this would in turn require small time steps less than the grid size, Δx, divided by the speed of a shallow water wave, $\sqrt{gh}$, for a one-dimensional simulation. For a 328-ft (100-m) grid size in, e.g., a 20-ft (6-m) deep marina [depth + 3.3-ft (1-m) tide amplitude], the time step would need to be less than 13 sec. Smaller grid sizes or greater depth, h, require proportionately smaller time steps and increased computer time.

The Oregon marinas examined at Oregon State University used Froude scale models, as did those constructed at the University of Washington. All of the model studies (except that reported in Ref. 13) were site-specific.

One advantage of an hydraulic model over a numerical one is that small-scale operations relating to mixing can be readily observed and photographically recorded. These phenomena approximate mixing processes which take place in the prototype. No attempt has been made to study vertical exchange processes in either the numerical or hydraulic models. Rather, time and space averages were taken; the water column is assumed to be well-mixed in the vertical. This assumption prevents the reproduction of vertical or horizontal convection currents.

Field Surveys

Dye releases have been used to determine flushing rates in Florida finger canals (2,8,23). Slotta and Tang (20) released dye in Oregon's Chetco estuary boat basin, and compared results with an hydraulic and a finite element model. Discrepancies between field and hydraulic model results were due to the difficulty of obtaining the proper density differences between dye and the receiving water in the hydraulic model. However, depth-averaged concentration versus time curves were similar.

In the field experiments to be described, dye as a tracer was distributed throughout the marina during the middle stage of a flood tide. The last two hours of the flood tide were used to permit the dye to continue mixing. An initial average dye concentration, C_o, was achieved at maximum high tide; ideally this concentration remains constant on the following ebb tide, while dye mass decreases. Assuming no return of dye on the next flood tide, the mass of dye in the marina remains constant while the concentration decreases with an increase of volume during the flood.

These assumptions can be expressed as follows, for dye mass, M, at concentration, C, with increasing volumes represented as +, decreasing volumes as −, constant volumes as o, for flow, Q, and volume, V:

$$Q^+, V^+ \overset{\text{Flood}}{\rightarrow} M^o, C^-; \quad Q^-, V^- \overset{\text{Ebb}}{\rightarrow} M^-, C^o \quad \ldots\ldots\ldots\ldots\ldots\ldots (1)$$

Then, on a flood tide, mass is constant, but $C^- \rightarrow M^o/V^+$; on an ebb, $M^- \rightarrow M^o - C^o V^-$ in which M^o = the mass at the end of a flood tide. Note that it is assumed that the dye is uniformly mixed throughout the basin at the time of initial high tide.

For the case of no direct fresh-water inflow, the volume of water present in a marina can be evaluated in terms of a mean tide level volume, V_o, and variations about the mean. For a mean low tide volume $V_l = V_o - A_oR/2$, in which A_o = mean marina surface area; and R = the tidal range from mean low to mean high water.

The tidal prism volume is $V_p = V_h - V_l = A_oR$. This is the amount of water on an ebb tide carrying with it a mass, M (for the first ebb), at concentration, C_o. At the end of the ebb the mass is, as in the preceding

$$M_1 = M_o - C_o(A_oR) \quad (2)$$

On the following flood tide, the concentration decreases; at the end of the flood

$$C_1 = \frac{M_1}{A_o(R+d)} \quad (3)$$

in which d = depth to mean low water level, while the mass is unchanged. There is a stepwise decrease in both M and C; however the time change between

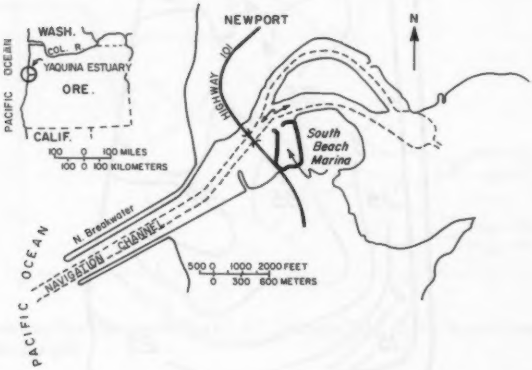

FIG. 1.—Yaquina Estuary Entrance and South Beach Marina (Inset: Place Map)

constant values is gradual rather than abrupt, and C and M are out of phase by 90°. It follows that the concentration after the ith flood cycle is $C_i = C_o(V_1/V_h)^i$. This relationship can be explored through analysis of a first-order differential equation. The rate of change of concentration is assumed proportional to the concentration present:

$$\frac{dC}{dt} = -\left(\frac{Q}{V}\right)C \quad (4)$$

in which $Q = 1/2A_oR\omega \sin(\omega t)$; $V = V_o + 1/2A_oR \sin(\omega t + \alpha)$; $\omega = 2\pi/T$ = the frequency at tidal period, T; and α = a phase angle.

Solving by numerical differentiation

$$C_{t+1} = C_t - \frac{QC}{V'} \Delta t \quad \text{. . . . . (5)}$$

where the subscripts = time; and Δt = the time step. The t_i are in any given time units, not necessarily tidal cycles, with the restriction that on an ebb cycle, $C_{t+1} = C_t$. The equation can also be solved by direct integration.

South Beach Marina Characteristics.—The entrance to South Beach marina is 1.5 nautical miles (2.8 km) upstream of the end of the north jetty at Newport,

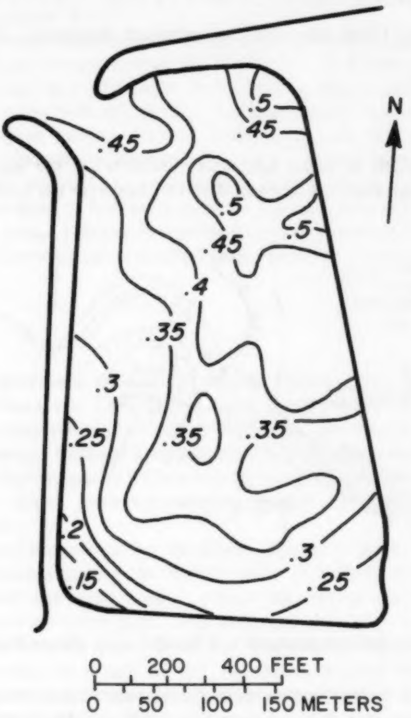

FIG. 2.—Exchange Coefficient Isopleths, South Beach Marina Hydraulic Model (19); Tide Range = 6 ft (1.83 m)

Oreg. (see Fig. 1). Approximate marina dimensions are: length, L = 1,574 ft (480 m); width, W = 623 ft (190 m); depth, *d*, at mean tide level = 13.4 ft (4.1 m), resulting in a mean tide level (MTL) volume, $V_o = 1.34 \times 10^{-7}$ cu ft (3.74×10^5 m^3); and a mean low tide volume, $V_1 = 1.04 \times 10^7$ cu ft (2.90 $\times$ 10^5 m^3). The mean tide range, R = 6.0 ft (1.83 m), resulting in a mean tidal prism volume, $V_p = R \times L \times W$ of 6.07×10^6 cu ft (1.7×10^5 m^3).

The entrance width is 157 ft (48 m), resulting in a mean cross-sectional entrance area, A, of 2,118 sq ft (197 m^2).

The marina is designed to hold 600 boats. At the time of the field work, no boat slips or piles were in place. Dredge spoil was disposed of on the east bank of the marina. The marina breakwater jetty restricts rapid flowthrough.

South Beach Marina Hydraulic Model Studies.—An hydraulic model study of South Beach marina was made by Richey and Skjelbreia (19). The model used a 1:10 horizontal/vertical distortion ratio; Froude scaling was employed with the following scale ratios: horizontal length = 1:480; vertical length = 1:48; velocity = 1:6.93; time = 1:69.3. The prototype tidal cycle was taken as 12.4 h, which required 10.74 min to reproduce in the model. Sinusoidal tides were used for 0.9-m, 1.8-m, and 2.7-m ranges. Model water density was uniform; boat slips and pilings and wind stress were not modeled.

A 20% solution of rhodamine-WT diluted 1:100 was used as a tracer. Thirty milliliters of dye were completely mixed in the model at high water location.

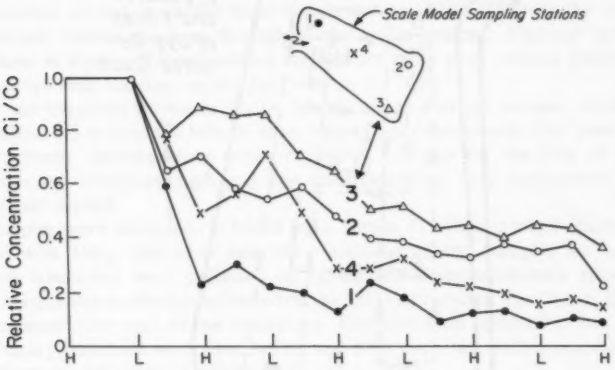

FIG. 3.—Relative Dye Concentration (C_i/C_o) Versus Tidal Cycle, South Beach Marina Hydraulic Model (19)

A Turner Model 110 fluorometer was used to determine relative concentration at the end of four tide cycles.

This procedure was augmented by time-lapse photography of the loss of water-soluble dye with time. The photos were analyzed by a densitometer to obtain relative concentration versus time. Exchange coefficients, defined as $E = 1 - (C_i/C_o)^{1/i}$, were determined from both the dye and densitometer data. Here, C_i = concentration at the ith tidal cycle; and C_o = initial concentration. Exchange coefficients thus calculated are shown for the 5.9-ft (1.8-m) tide in Figs. 2 and 3. Fig. 2 shows E values at the end of four cycles. These are averaged values and range from about 0.15 in the southwest corner to 0.5 in the northeast corner. Low values correspond to relatively low flushing, while higher values indicate greater flushing. This is shown in Fig. 3, where individual C_i/C_o values are 0.35 for station 3, and 0.1 for station 4. This corresponds to $E = 0.23$ and $E = 0.44$ for stations 3 and 1, respectively, which is in the

range of the values given in the previous figure.

The main conclusions of the hydraulic model study were as follows: (1) The basin had good hydraulic characteristics except for poor exchange in the south corners; (2) good exchange is due to strong currents in the main channel passing the marina entrances, which can introduce turbulent eddies on flood tide and prevent recirculation on the ebb; and (3) the currents past the entrance improve the exchange coefficient by about 25% over that where the entrance is situated on a quiet bay.

Field Float Studies.—Weighted poles of 6-ft, 8-ft, 10-ft, and 12-ft (1.83-m, 2.44-m, 3.05-m, and 3.66-m) submerged length were released and followed on

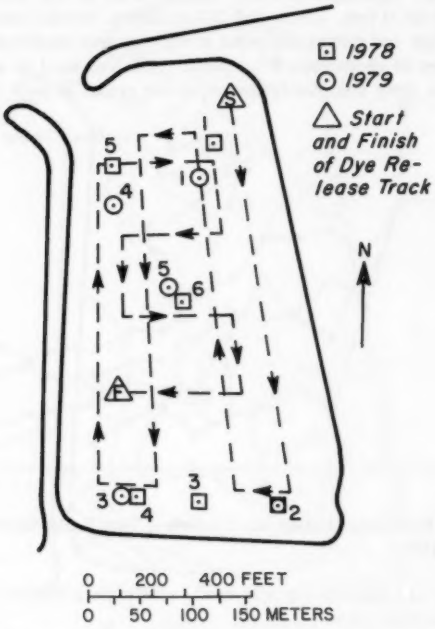

FIG. 4.—South Beach Marina Field Sampling Stations, 1978–1979; Dashed Line Is Approximate Dye Release Track

January 17–18, 1979, in conjunction with a dye release; pole positions were fixed by sextant. Easterly winds ranged from 3 knots–10 knots (1.5 m/s–5 m/s) on the first survey day which was conducted on an ebb tide; 10-knot winds determined the main direction of all pole trajectories during this ebb cycle although a northwest water current component toward the entrance was present. Tide decreased from a maximum [lower high water (LHW)] height of 6.9 ft–3.9 ft (2.1 m–1.2 m), about midtide. Maximum pole velocities observed for the 6-ft and 8-ft poles were 0.8 fps and 0.9 fps (26 cm/s and 27 cm/s), respectively.

Winds were less than 3 knots from the west on the January 18 survey. Tides increased from 6.2 ft–7.5 ft (1.9 m–2.3 m) [higher high water (HHW)]. Although this study was only conducted for a short time, pole trajectories show that surface water near the entrance had a net outward direction, while the deeper layer showed inward motion. Thus, there was some flushing on the incoming tide in the upper layers.

Field Dye Studies.—Rhodamine-WT was released for about 1 h over the entire marina (see Fig. 4) starting about 4 h before slack water on flood tide. Visual observations from the United States Highway 101 bridge at Newport and a light plane did not reveal any obvious high or low surface dye patch concentrations.

Fifty-one lb (23 kg) of 20% dye was diluted with 50 gal (190 L) of seawater to approximate receiving water density from a 55-gal (210-L) drum; it was discharged at about 0.8 gal/min (3 L/min). Two methods of release were used. On the first survey, a 15-ft (4.6-m) hollow aluminum pole with a horizontal discharge tube at the bottom was raised and lowered as the dye was released. The outboard motor vessel made right angle paths throughout the marina. On the second survey, a garden hose was towed at about 45° from the surface to bottom behind the boat throughout the water column; discharge ports in the hose at about 1.5-ft increments allowed for more even vertical distribution of the dye than occurred on the first survey.

At the locations shown in Fig. 4, hourly samples at the surface, middepth, and about 1.5 m from the bottom were drawn from a continuous flow hose-pump arrangement. Samples were taken at hourly intervals for the first 14 h and at mid- and maximum high and low tides thereafter until background levels were approached.

Samples were analyzed on board by a Turner 111 flow-through fluorometer fitted with 546-μ excitation and 590-μ emission filters. Samples for analysis in the laboratory were collected in 125-ml screw-cap containers after local equilibrium was reached as indicated on the field fluorometer. The Turner Designs fluorometer was used in the laboratory. Frequent field calibration was made; laboratory standards were used before and after each run, values reported here are from the laboratory analyses.

Field Study Results

The 1978 study was similar to that of 1979 except for the following differences: (1) Average tide ranges were 7.9 ft and 4.9 ft (2.4 m and 1.5 m), respectively; (2) water column density was different, with a greater rate of change of density with depth for the 1978 study; and (3) the method of introducing the dye was different.

Stratification was slight on each study, the main differences being due to temperature. Salinity and temperature-depth profiles showed a gradual decrease in temperature from 15.6° C to 14.6° C and increase in salinity from 31.6 ‰ to 32.1 ‰ from surface to bottom for 1978.

1978 Survey.—Attempts to distribute dye evenly throughout the water column were not completely satisfactory. Fig. 5 shows surface, mid, and bottom dye concentrations at station 6 (refer to Fig. 4). The surface and middle concentrations were nearly equal to about 1400 on September 15, 1978, but the bottom sample was initially quite low; all samples approached equality after about 0600 on

September 16, 1978. Surface concentrations for all six stations over the duration of the experiment showed similar concentrations except for station 1, which decreased rapidly to about 1800 on the first day. Bottom concentration with time showed station 1 having lower concentrations than all the others until 2200 (September 15) when, again, the concentration lines merged. Stations 2 and 3 showed several spikes which were not apparent in the other values.

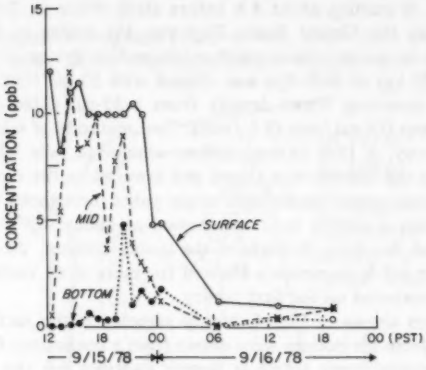

FIG. 5.—Surface, Middle, and Bottom Rhodamine-wt Concentration, in parts per billion, South Beach Marina, September 15–16, 1978

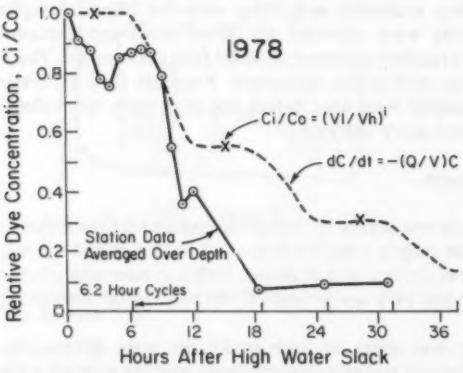

FIG. 6.—Relative Dye Concentration (C_i/C_o) Averaged Over Depth and Model Computations Versus Time, South Beach Marina, September 15–16, 1978

Fig. 6 shows values of C_i/C_o averaged for all stations. The modified tidal prism and numerical model results are also shown. Considering the variability of the dye patches, the first 7 h are in reasonable agreement. A rapid decrease in concentration is shown from hours 7–12 in the models and in the field data.

The latter, however, continue to show decreases to about hour 18.

The 1978 field data can also be compared with the hydraulic model results for the 8.8-ft (2.7-m) range tests. Exchange coefficients in the hydraulic model ranged from 0.44–0.52. Interpolation between the 6-ft (1.83-m) and 9-ft (2.74-m) ranges give $E = 0.44$ for the 8-ft (2.4-m) range found in the field. The exchange coefficient based on the prism method is 0.5 for the 8-ft range. This gives C_i values of 1, 0.55, 0.30, ... on alternate high tides starting with $C_i/C_o = 1$. Field, hydraulic, and mathematical model results all clearly show rapid flushing for this tide range. The hydraulic and mathematical model results are essentially equivalent, but underestimate the dye removed when compared with the field study.

1979 Survey.—For the 1979 survey, the sampling station location was essentially the same as before except that station 3 of the 1978 survey was eliminated (Fig. 4).

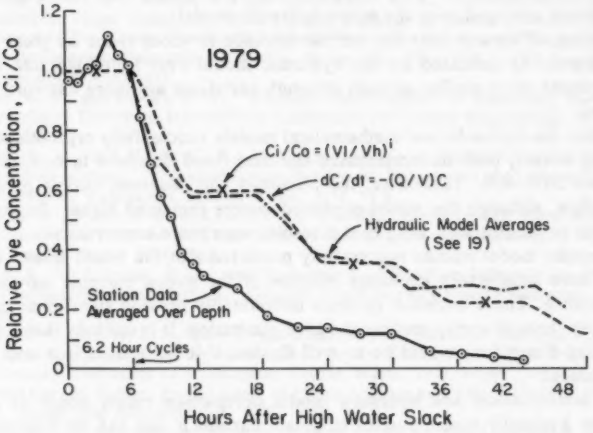

FIG. 7.—Relative Dye Concentration (C_i/C_o) Averaged Over Depth and Model Computations Versus Time, South Beach Marina, January 17–18, 1979

Plots (not shown) of all stations at the surface, middle, and bottom show better initial mixing than in 1978. Station 1, in the northeast corner, initially showed higher concentrations than the other stations but quickly merged with the rest. All data showed an increase in C_i/C_o ratios from about hour 3–7 (ebb cycle), while values at station 4 indicated recirculation south along the west side of the marina.

The hydraulic model results (19) show an average interpolated exchange coefficient of 0.3 for the 6-ft range. The high tide C_i/C_o values at station 1 in the model and field are close; there is an initial rapid decrease in concentration to about $C_i/C_o = 0.2$, followed by a gradual decrease to 0.1 at the fourth tide cycle. Fig. 7 shows the average C_i/C_o results for the hydraulic model as taken from Fig. 3, and the mathematical model values.

For the average results, the discrepancy is rather large giving $V_t/V_h = 0.64$ which results in alternate high tide C_t/C_o values of 1, 0.64, 0.41 .... After hour 12, on the second ebb tide, when the concentration should remain constant, there was only a slight straightening out of the curve; the predicted and observed curves merged after the second flood tide.

Comparisons of Figs. 6 and 7 show that normalized concentration-time curves were quite similar with respect to the sharp decline during the first flood cycle. The 1979 curve shows a steeper exponential decrease toward background concentration.

Summary and Conclusions

South Beach marina has a single entrance and is uncomplicated geometrically; it has free exchange with the main navigation channel where rather large currents develop during ebb and flood tides.

Mathematical and hydraulic models results agreed well when exchange coefficients were averaged over the entire hydraulic model.

Flushing efficiency near the marina entrance is about twice as great as the inner harbor as indicated by the hydraulic model over four high tide cycles. Field results show similar spreads although variations are more extreme among stations.

Neither the hydraulic nor mathematical models successfully reproduced early flushing events; both underestimated the first flood decrease in concentration by about 30%–40%. Thereafter, the predicted and observed curves parallelled each other, although the model-predicted curves remained higher. In terms of pollutant concentrations, both model results were more conservative.

Hydraulic model studies successfully predicted that the South Beach marina would have satisfactory exchange because of the strong currents moving past the entrance. These entrance currents undoubtedly provide significant transfer processes through vortex motion and gyre generation. It is unlikely that a marina of similar dimensions would be as well flushed if it were sited in a less active environment.

The mathematical and hydraulic model comparison raises doubt as to the need for hydraulic model studies of small marinas *if* one can be content with conservative predictions. For marinas of similar dimensions in similar locations, good approximations of flushing efficiency can be made in a matter of minutes using simple box-model assumptions. However, these results cannot be extrapolated to other marinas with multiple entrances, significantly different width-to-length ratios, or environmental settings.

Acknowledgments

I thank Bill McDougal for field assistance; he was primarily responsible for the success of the 1979 dye release. Mike Gates assisted in data reduction; George Ditsworth, Allen Teeter, Lon Bentsen, and Karl Rukavina assisted in the field and laboratory. R. E. Nece, L. S. Slotta, and R. C. Swartz made many helpful comments on the manuscript.

Appendix I.—References

1. Askren, D. R., "Numerical Simulation of Sedimentation and Circulation in Rectangular Marine Basins," thesis presented to Oregon State University, at Corvallis, Oreg.,

in 1977, in partial fulfillment of the requirements for the degree of Master of Science.
2. Barnwell, T., Jr., and Cavinder, T. R., "Application of Water Quality Models to Finger Fill Canals," *Symposium on Modeling Techniques*, ASCE, 1975, pp. 709–728.
3. Bowerman, F. R., and Chen, K. Y., "Marina del Rey: A Study of Environmental Variables in a Semi-Enclosed Coastal Water," *USC-SG-4-71*, University of Southern California, Los Angeles, Calif., 1971, p. 59.
4. Brandsma, M. G., Lee, J. J., and Bowerman, F. R., "Marina del Rey: Computer Simulation of Pollutant Transport in Semi-Enclosed Water Body," *Sea Grant Pub. USC-SG-1-73*, University of Southern California, Los Angeles, Calif., 1973, 113 p.
5. Chmura, G. L., and Ross, N. W., "The Environmental Impacts of Marinas and Their Boats: A Literature Review With Management Considerations," Marine Advisory Service, University of Rhode Island, Kingston, R.I., 1978, 32 p.
6. Fischer, H. B., "Some Remarks on Computer Modeling of Coastal Flows," *Journal of the Waterways Harbors and Coastal Engineering Division*,CU, Vol. 102, No. WW4, Proc. Paper 12520, Nov., 1976, pp. 395–406.
7. Heiser, D. W., and Finn, E. L., Jr., "Observations of Juvenile Chum and Pink Salmon in Marine and Bulkheaded Areas," Supplementary Progress Report, Puget Sound Stream Studies, Washington State Department of Fisheries, 1970.
8. Morris, F. W., IV, Walton, R., and Christensen, B. A., "Hydrodynamic Factors Involved in Finger Canal and Borrow Lake Flushing in Florida's Coastal Zone," *Project R/OE-4, Grant Number 04-6-158-44*, Hydraulics Laboratory, Department of Civil Engineering, University of Florida, Gainesville, Fla., Vol. 1, 704 p., and Vol. 2, Appendices A–K, 1978.
9. Nece, R. E., and Richey, P. R., "Flushing Characteristics of Small-Boat Marinas," *Proceedings*, Thirteenth International Conference on Coastal Engineering, 1972, pp. 2499–2512.
10. Nece, R. E., and Knoll, C. R., "Flushing and Water Quality Characteristics of Small-Boat Marinas," *Technical Report Number 40*, Department of Civil Engineering, University of Washington, Seattle, Wash., 1974, 58 p.
11. Nece, R. E., Welch, E. B., and Reed, J. R., "Flushing Criteria for Salt Water Marinas," *Technical Report Number 72*, Department of Civil Engineering, University of Washington, Seattle, Wash., 1975, 50 p.
12. Nece, R. E., Falconer, R. A., and Tsutsumi, T., "Planform Influence on Flushing and Circulation in Small Harbors," *Fifteenth Conference on Coastal Engineering*, ASCE, 1976.
13. Nece, R. E., Richey, E. P., Rhee, J., and Smith, H. N., "Effects of Planform Geometry on Tidal Flushing and Mixing in Marinas," *Report No. 62*, C. W. Harris Hydraulics Laboratory, University of Washington, Seattle, Wash., 1979, 74 pp.
14. "Tidal Current Tables: Pacific Coast of North America and Asia," National Oceanic and Atmospheric Administration, 1978, 1979.
15. Reish, D. J., "An Ecological Study of Pollution in Los Angeles–Long Beach Harbors, California," *Occasional Paper No. 22*, Allen Hancock Foundation, 1959, 119 p.
16. Reish, D. J., "A Study of Benthic Fauna in a Recently Constructed Boat Harbor in Southern California," *Ecology*, Vol. 42, 1961, pp. 84–91.
17. Reish, D. J., "Further Studies on the Benthic Fauna in a Recently Constructed Boat Harbor in Southern California," Southern California Academy of Science, Vol. 62, 1963, pp. 23–32.
18. Richey, E. P., "Hydro-Ecological Problems of Marinas in Puget Sound," *Proceedings*, 1971 Technical Conference on Estuaries in the Pacific Northwest, *Circular 42*, Engineering Experiment Station, Oregon State University, Corvallis, Oreg., 1971, pp. 249–271.
19. Richey, E. P., and Skjelbreia, N. K., "Yaquina Bay Marina: Circulation and Exchange Characteristics," *Technical Report 56*, C. W. Harris Hydraulic Laboratory, University of Washington, Seattle, Wash., 1978, 25 p.
20. Slotta, L., and Tang, S. S., "Chetco River Tidal Hydrodynamics and Associated Marina Flushing," final report, Ocean Engineering Program, School of Engineering, Oregon State University, Corvallis, Oreg., 1976, 55 p.
21. Slotta, L. S., and Noble, S. M., "Use of Benthic Sediments as Indicators of Marina Flushing," *Publication ORESO-T-77-007*, Ocean Engineering, Oregon State University, Corvallis, Oreg., 1977, 56 p.

22. Soule, D. F., and Oguri, M., "The Marine Ecology of Marina del Rey Harbor, California," *USC-SG-2-77*, Allen Hancock Foundation, University of Southern California, Los Angeles, Calif., 1977, 424 p.
23. van de Kreeke, J., Carpenter, J. H., and McKeehan, D. S., "Water Motions in Closed-End Residential Canal," *Journal of the Waterways Harbors and Coastal Engineering Division*, ASCE, Vol. 103, No. WW1, Proc. Paper 12710, Feb., 1977, pp. 161–166.

Appendix II.—Notation

The following symbols were used in this paper:

A = cross-sectional or planform area;
C = concentration;
d = mean tidal depth;
E = exchange coefficient;
g = gravity;
h = maximum depth, shallow water wave;
i = tide cycle;
L = marina length;
M = dye mass;
R = tide range;
T = tidal period;
V = volume;
W = marina width;
α = phase angle;
Δx = grid length; and
ω = frequency ($= 2\pi/T$).

Subscripts

h = high water;
l = low water;
o = mean tide;
p = tidal prism; and
t = time step.

Superscripts

$-$ = denotes decreasing values;
$+$ = denotes increasing values; and
0 = denotes constant values.

BREAKING-LIMITED WAVE HEIGHTS

By M. Aziz Tayfun,[1] A. M. ASCE

INTRODUCTION

Distribution of wave heights in a wave field is of particular relevance to ocean engineers. For sea states in which the free surface is approximately linear Gaussian with a narrow-band spectrum, this distribution is given theoretically by the Rayleigh law. Numerous field data confirm the validity of the Rayleigh theory, particularly for low and medium wave heights. However, a systematic discrepancy between empirical data and the theory is often noted towards the high wave tail, the theory overpredicting the observations. Likely causes of this discrepancy include the nonlinear non-Gaussian nature of sea waves, bandwidth effects, wave breaking, and possibly others. Some studies (3,10) demonstrate various compensating procedures for the discrepancy, but fail to explain why the conventional Rayleigh theory overpredicts field observations. Others (6,12,13) examine some effects of nonlinearity, finite bandwidth, and differences in the definitions employed in data analysis versus theory. In particular, Longuet-Higgins (6) and Tayfun (12,13) suggest that the observed discrepancy cannot be attributed to a finite-amplitude effect but to effects associated with finite bandwidth, and to differences in certain basic definitions employed in data analysis versus theory.

It appears likely that the skew non-Gaussian nature of the sea surface due to finite-amplitude effects would not directly result in reducing theoretical wave heights in a manner consistent with field observations (6,7,12). A more plausible mechanism is wave breaking, which is a finite-amplitude effect unaccounted for in the analytical wave models and in the development of the Rayleigh law. A previous study by the writer (14) qualitatively demonstrated that wave breaking will introduce a deficiency in wave heights towards the high wave extreme. This result followed an indirect approach in which Longuet-Higgins' (5) approximate solution for the joint distribution of wave heights and periods was constrained to satisfy the Stokes limiting steepness in deep water. It is aimed herein to derive a distribution for breaking-limited wave heights by following a direct approach in which the statistical description of the free surface is modified

[1]Assoc. Prof., Civ. Engrg. Dept., Coll. of Engrg. and Petroleum, Kuwait Univ., P.O. Box 5969, Kuwait.

Note.—Discussion open until October 1, 1981. To extend the closing date one month, a written request must be filed with the Manager of Technical and Professional Publications, ASCE. Manuscript was submitted for review for possible publication on May 13, 1980. This paper is part of the Journal of the Waterway, Port, Coastal and Ocean Division, Proceedings of the American Society of Civil Engineers, ©ASCE, Vol. 107, No. WW2, May, 1981. ISSN 0148-9895/81/0002-0059/$01.00.

to satisfy a Stokes-type limiting steepness in deep or finite water depths. On the basis of this distribution, it is seen that wave breaking contributes to the deficiency in wave heights towards the high wave tail in a manner dependent on various moments of the surface spectrum and the still water depth. Comparisons with two well-documented field observations are given to demonstrate that the distribution of wave heights limited by breaking compares more favorably with reality than the conventional Rayleigh law.

Definitions and Conventional Results

The oscillations of the sea surface at a given point as a function of time is represented by

$$X(t) = \int_0^\infty [2S(\omega)d\omega]^{1/2} \cos(\omega t + \epsilon) \quad \ldots\ldots\ldots\ldots\ldots\ldots\ldots\ldots (1)$$

in which $S(\omega)$ = spectral density of the surface; $\epsilon(\omega)$ = independent and identically distributed random phase angles with a uniform density function $1/2\pi$ in $[0, 2\pi]$; and ω = radian frequency which is related to the wave number, k, at a uniform water depth, D, through the dispersion relation

$$\omega^2 = gk \tanh kD \quad \ldots\ldots\ldots\ldots\ldots\ldots\ldots\ldots\ldots\ldots\ldots\ldots (2)$$

The jth moment of the spectrum is defined by

$$\mu_j = \int_0^\infty \omega^j S(\omega)\, d\omega \quad \ldots\ldots\ldots\ldots\ldots\ldots\ldots\ldots\ldots\ldots\ldots\ldots (3)$$

In particular, μ_0 = variance of X; and $\omega_0 = \mu_1/\mu_0$ = mean frequency. The spectrum is narrow band if

$$\nu^2 = \left(\frac{\mu_2}{\mu_0 \omega_0^2}\right) - 1 << 1 \quad \ldots\ldots\ldots\ldots\ldots\ldots\ldots\ldots\ldots\ldots (4)$$

Under this condition, the wave envelope or amplitude of $X(t)$ is defined as (see, e.g., Refs. 9, 12, and 16)

$$A(t) = (X^2 + \hat{X}^2)^{1/2} \quad \ldots\ldots\ldots\ldots\ldots\ldots\ldots\ldots\ldots\ldots\ldots\ldots (5)$$

in which $$\hat{X}(t) = \int_0^\infty [2S(\omega)\, d\omega]^{1/2} \sin(\omega t + \epsilon) \quad \ldots\ldots\ldots\ldots\ldots (6)$$

These definitions suggest that each realization of X can be viewed as an amplitude-modulated wave form with an apparent mean frequency ω_0, i.e.:

$$X(t) = A(t) \cos(\omega_0 t + \phi) \quad \ldots\ldots\ldots\ldots\ldots\ldots\ldots\ldots\ldots\ldots\ldots (7)$$

in which ϕ = a random phase with the uniform density $1/2\pi$ in $[0, 2\pi]$ (9). Therefore, $A(t)$ and $-A(t)$ represent two symmetrical curves passing through wave crests and troughs, respectively; and

$$H = 2A(t) \quad \ldots\ldots\ldots\ldots\ldots\ldots\ldots\ldots\ldots\ldots\ldots\ldots\ldots\ldots (8)$$

is defined as the wave height with

$$H_{rms} = 2(2\mu_0)^{1/2} \quad \ldots\ldots (9)$$

Finally, the probability density of the scaled heights

$$\xi = \frac{H}{H_{rms}} = \frac{A}{A_{rms}} \quad \ldots\ldots (10)$$

is recognized as the Rayleigh density (5,9,11) with the invariant form

$$f_\xi(x) = 2x \exp(-x^2); \quad (x \geq 0) \quad \ldots\ldots (11)$$

The preceding formalism is underlined with the assumption that the sea surface is linear and can be represented as the sum of many constituent wavelets with different amplitudes, frequencies, and random phases, i.e.:

$$X(t) = \sum_{n=1}^{N} c_n \cos(\omega_n t + \epsilon_n) \quad \ldots\ldots (12)$$

$$\text{Similarly} \quad \hat{X}(t) = \sum_{n=1}^{N} c_n \sin(\omega_n t + \epsilon_n) \quad \ldots\ldots (13)$$

The amplitudes c_n are chosen so that

$$c_n = [2S(\omega_n)\Delta\omega_n]^{1/2} \quad \ldots\ldots (14)$$

$$\mu_0 = \sum_{n=1}^{N} \left(\frac{1}{2}\right) c_n^2 \quad \ldots\ldots (15)$$

If the conditions necessary for the central limit theorem are satisfied, i.e., as $N \to \infty$, $\max \Delta\omega_n \to 0$, with μ_0 being fixed, X and $\hat{X}$ asymptotically approach two independent Gaussian variates with zero means and variance, μ_0. Consequently, the density of both A and H becomes the Rayleigh law (9,11). Strictly speaking, this limiting operation requires that the spectral representation of X and $\hat{X}$ as stationary random functions be expressed by Fourier-Stieltjes integrals as in Eqs. 1 and 6, respectively. As shown by Yang (17), the convergence of X and $\hat{X}$ to Gaussian variates is fairly rapid for small and midrange values of these variables, but considerably slow towards the extremes. In general, then, X and $\hat{X}$ are not exactly Gaussian unless $N \to \infty$, and the distribution of wave heights for a fixed N must deviate from the Rayleigh law particularly towards the extreme tail.

The question which arises now is whether there is any need at all to consider Eqs. 12 and 13 as opposed to their respective theoretical limits, i.e., Eqs. 1 and 6, which imply $N \to \infty$. This is answered readily by noting that Eqs. 1 and 6 require that the range of X and $\hat{X}$ be unrestricted, which is not physically acceptable. In reality, extremes of both X and $\hat{X}$ are limited by whitecapping or breaking. Therefore, Eqs. 12 and 13 with a bounded range should offer a more realistic stochastic representation for the sea surface when N is constrained properly on physical grounds.

Breaking Criterion

In a deep-water progressive wave, whose limiting form at the crest is the Stokes 120° angle, the acceleration is equal to $(1/2)\,g$. Thus, in a typical sea

state whitecaps appear whenever the vertical acceleration at the crest approaches $-(1/2)\,g$. The limiting form in finite water depth is given by Miche's (8) approximate analysis as

$$(kH)_{max} = \frac{2\pi}{7} \tanh kD \quad \ldots\ldots\ldots\ldots\ldots\ldots\ldots\ldots\ldots\ldots \quad (16)$$

Evidently, Eq. 16 provides a semitheoretical transition from the Stokes limiting steepness in deep water, i.e., $(kH)_{max} \simeq 2\pi/7$, to transitional water depths where its validity has been established reasonably well-based on field and laboratory data (see, e.g., Ref. 15).

Assume for the moment that the wave is described by the linear theory. On this basis, the limiting steepness in deep water corresponding to a downward acceleration of $(1/2)\,g$ is

$$(kH)_{max} = 1 \quad \ldots\ldots\ldots\ldots\ldots\ldots\ldots\ldots\ldots\ldots\ldots\ldots\ldots\ldots \quad (17)$$

as compared to the theoretical value $2\pi/7$. Therefore although it might be thought unacceptable to use the linear theory for an obviously nonlinear effect, doing so involves an error of only 11% as an overestimate.

The extension of these arguments to an irregular sea state is not immediate in general. However, for a sea state characterized with a narrow-band spectrum such that $\nu^2 << 1$ strictly, each realization of the surface has the form of a progressive wave train with a slowly varying amplitude, $A(t)$, and an apparent mean frequency, ω_0. Under these conditions, Eq. 16 should do reasonably well to describe the limiting form of an irregular wave packet locally. Therefore, with $H = 2A$ being correct to second order (12), Eq. 6 becomes

$$(kA)_{max} \simeq k_0 A_{max} \simeq \frac{\pi}{7} \tanh k_0 D \quad \ldots\ldots\ldots\ldots\ldots\ldots\ldots\ldots \quad (18)$$

in which k_0 represents the mean apparent wave number, which is related to ω_0 through Eq. 2.

Nonlinear corrections to μ_0 are of $O(g^{-2})$ and, therefore, can be neglected (12). Now, without any loss of generality, let

$$c_n = [2S(\omega_n)\,\Delta\omega_n]^{1/2} = C \quad \ldots\ldots\ldots\ldots\ldots\ldots\ldots\ldots\ldots \quad (19)$$

be a constant so that

$$\mu_0 = \frac{1}{2} NC^2 \quad \ldots\ldots\ldots\ldots\ldots\ldots\ldots\ldots\ldots\ldots\ldots\ldots \quad (20)$$

It is implied that the more peaked the spectrum $S(\omega)$, at $\omega = \omega_n$, the smaller $\Delta\omega_n$ should be used and vice versa. On this basis, Eqs. 5, 12, and 13 can be rewritten as

$$\eta = \frac{X}{(2\mu_0)^{1/2}} = N^{-1/2} \sum_{n=1}^{N} \cos \chi_n \quad \ldots\ldots\ldots\ldots\ldots\ldots\ldots \quad (21)$$

$$\hat{\eta} = \frac{\hat{X}}{(2\mu_0)^{1/2}} = N^{-1/2} \sum_{n=1}^{N} \sin \chi_n \quad \ldots\ldots\ldots\ldots\ldots\ldots\ldots \quad (22)$$

$$\bar{\xi} = \frac{A}{(2\mu_o)^{1/2}} = (\eta^2 + \hat{\eta}^2)^{1/2} \quad \ldots\ldots\ldots\ldots\ldots\ldots\ldots\ldots\ldots\ldots \quad (23)$$

in which $\chi_n = \omega_n t + \epsilon_n$; and $\bar{\xi}$ = the scaled wave height when N is fixed. Therefore, $\bar{\xi} \to \xi$ as $N \to \infty$. Now, noting that $\bar{\xi}_{max} = \sqrt{2N}$, Eqs. 18 and 23 can be combined to show that

$$N^{1/2} \simeq \frac{\pi}{7\sqrt{2}} \frac{\tanh k_o D}{k_o(2\mu_o)^{1/2}} \quad \ldots\ldots\ldots\ldots\ldots\ldots\ldots\ldots\ldots\ldots \quad (24)$$

Thus, N is inversely related to $k_o(2\mu_o)^{1/2}$ and also depends on the relative depth $k_o D$ in a manner which requires no elaboration. The parameter $k_o(2\mu_o)^{1/2}$ can be regarded as a measure of sea state with a typical range varying from 0.1–0.2 for larger waves in a hurricane to much smaller values representative of gentle seas with no apparent whitecaps or breakers. Since N is a function of both $k_o(2\mu_o)^{1/2}$ and $k_o D$, the distribution of $\bar{\xi}$ in a narrow-band wave field is, in essence, dependent on the first two spectral moments and the local water depth.

Distribution of Heights Limited by Breaking

Consider now the probability structure of $\bar{\xi}$. It can be shown (see, e.g., Ref. 17) that the characteristic function of η and $\hat{\eta}$ is given by

$$M_{\eta\hat{\eta}}(u, \hat{u}) = E\left[e^{i(u\eta + \hat{u}\hat{\eta})}\right] = J_0^N\left(\frac{q}{\sqrt{N}}\right) \quad \ldots\ldots\ldots\ldots\ldots\ldots \quad (25)$$

in which $q = (u^2 + \hat{u}^2)^{1/2}$; and $J_o(\cdot)$ = the zero-order Bessel function. The joint density of η and $\hat{\eta}$ is the inverse Fourier transform of Eq. 25, i.e.:

$$f_{\eta\hat{\eta}}(x, \hat{x}) = (2\pi)^{-2} \int_{-\infty}^{\infty}\int J_0^N\left(\frac{q}{\sqrt{N}}\right) e^{-i(ux + \hat{u}\hat{x})}\, du\, d\hat{u}$$

$$= (2\pi)^{-1} \int_0^{\infty} u\, J_0^N\left(\frac{u}{\sqrt{N}}\right) J_0\left[u(x^2 + \hat{x}^2)^{1/2}\right] du \quad \ldots\ldots\ldots\ldots\ldots \quad (26)$$

in which $|x|$ and $|\hat{x}| \leq \sqrt{N}$, and the simplification leading to the last step follows from a change of variables from $(u, \hat{u})$ to polar coordinates. The cumulative distribution of $\bar{\xi}$ is defined by

$$F_{\bar{\xi}}(x; N) = \text{Prob}\left[(\eta^2 + \hat{\eta}^2)^{1/2} \leq x\right] \quad \ldots\ldots\ldots\ldots\ldots\ldots \quad (27)$$

Using Eq. 26 and paying careful attention to the region of integration implied in Eq. 27, it can be verified that

$$F_{\bar{\xi}}(x; N) = \int_0^{\infty} u\, J_0^N\left(\frac{u}{\sqrt{N}}\right) \int_0^x r\, J_0(ur)\, dr\, du, \quad (0 \leq x \leq \sqrt{N});$$

$$F_{\bar{\xi}}(x; N) = \frac{2}{\pi} \int_0^{\infty} (G_1 + G_{12} + G_2)\, u\, J_0^N\left(\frac{u}{\sqrt{N}}\right) du,$$

$$(\sqrt{N} \leq x \leq \sqrt{2N}) \quad \ldots\ldots\ldots\ldots\ldots\ldots\ldots\ldots\ldots\ldots \quad (28)$$

in which $G_1 = \int_0^{\tau_1} \int_0^{r_1} r J_0(ur)\, dr\, d\tau$ . . . . . (29)

$G_{12} = (\tau_2 - \tau_1) \int_0^{x} r J_0(ur)\, dr$ . . . . . (30)

$G_2 = \int_{\tau_2}^{\pi/2} \int_0^{r_2} r J_0(ur)\, dr\, d\tau$ . . . . . (31)

with $\tau_1 = \cos^{-1}\left(\frac{\sqrt{N}}{x}\right)$ . . . . . (32)

$\tau_2 = \sin^{-1}\left(\frac{\sqrt{N}}{x}\right)$ . . . . . (33)

$r_1 = \frac{\sqrt{N}}{\cos(\tau)}$ . . . . . (34)

$r_2 = \frac{\sqrt{N}}{\sin(\tau)}$ . . . . . (35)

The probability density of $\bar{\xi}$ follows from Eq. 28 by differentiation with respect to x as

$$f_{\bar{\xi}}(x; N) = x \int_0^{\infty} u J_0^N\left(\frac{u}{\sqrt{N}}\right) J_0(xu)\, du, \quad (0 \le x \le \sqrt{N});$$

$$f_{\bar{\xi}}(x; N) = x\left[1 - \frac{4}{\pi}\cos^{-1}\left(\frac{\sqrt{N}}{x}\right)\right] \int_0^{\infty} u J_0^N\left(\frac{u}{\sqrt{N}}\right) J_0(xu)\, du,$$

$(\sqrt{N} \le x \le \sqrt{2N})$ . . . . . (36)

This can be simplified further, by using $\mathcal{U}(\cdot)$ = Heaviside unit step function and a change of variables in the integrals, as

$$f_{\bar{\xi}}(x; N) = xN\left[1 - \frac{4}{\pi}\cos^{-1}\left(\frac{\sqrt{N}}{x}\right)\mathcal{U}\left(1 - \frac{\sqrt{N}}{x}\right)\right] \int_0^{\infty} u J_0^N(u)\, J_0(xu\sqrt{N})\, du, \quad (0 \le x \le \sqrt{2N})$$ . . . . . (37)

Note that $J_0^N\left(\frac{u}{\sqrt{N}}\right) = e^{N \ln J_0(u/\sqrt{N})} = e^{N[-(u^2/4N) + O(u^4/N^2)]}$ . . . . . (38)

which can be substituted in Eq. 36 to show that

$\lim_{N\to\infty} f_{\bar{\xi}}(x; N) = f_{\xi}(x) = 2x\, e^{-x^2}; \quad (x \ge 0)$ . . . . . (39)

The exceedance probability distribution of $\bar{\xi}$ is

$$\text{Prob}\,(\bar{\xi} > x) = 1 - F_{\bar{\xi}}(x; N) = 1 - \int_0^x f_{\bar{\xi}}(v; N)\, dv \quad \ldots\ldots\ldots\ldots\ldots \quad (40)$$

The numerical integration of Eq. 40 is straight forward by using Simpson's rule. Fig. 1 shows some typical results constructed in this manner for N = 5, 10, 15, 30, and 60. The Rayleigh law is also included in the same figure for comparison. It is observed that the Rayleigh law overpredicts waves with heights towards the extreme tail in a manner increasing with smaller N values.

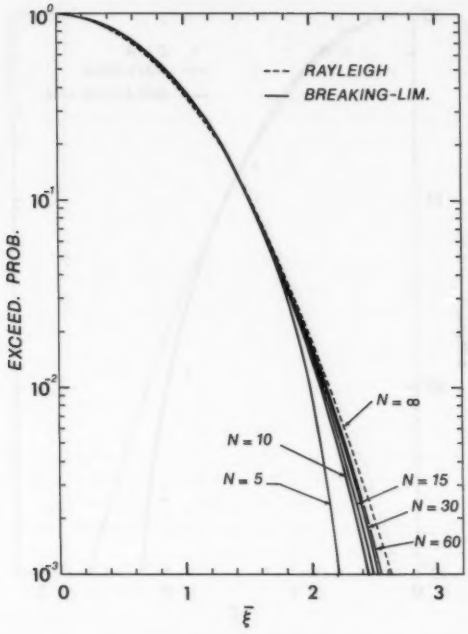

FIG. 1.—Theoretical Exceedance Distribution of Breaking-Limited Wave Heights under Narrow-Band Conditions and for Different Sea States as Implied by N

The convergence to the Rayleigh limit becomes increasingly slow for larger N values.

Comparison with Field Data

Deep Water Case.—The data examined for this case consist of approx 400 waves collected in the Gulf of Mexico under reasonably homogeneous conditions. It is contained in records e-11–e-15 of Ref. 1, with all pertinent information listed in Tables 4.1-2, and Fig. 5.1 of the same reference. These data are considered

also by Longuet-Higgins (5). The empirical exceedance distribution shown in Fig. 2 was constructed on the basis of the scatter diagram given in Fig. 5.1 of Ref. 1 in a manner consistent with the notation here. Statistics listed in Tables 4.1-2 of Ref. 1 suggest that $\bar{H} = 1.487$ m, $H_{rms} = 1.636$ m, $k_0 = 0.174$ m^{-1}, and $\mu_0 = 0.334$ m^2. The parameter ν as estimated by Longuet-Higgins (5) is 0.234. Therefore, $k_0(2\mu_0)^{1/2} = 0.142$, and Eq. 24 with $k_0 D = \infty$ requires that $N \simeq 5$. The corresponding theoretical exceedance distribution is given in Fig. 2 together with the Rayleigh counterpart. It is evident that the empirical

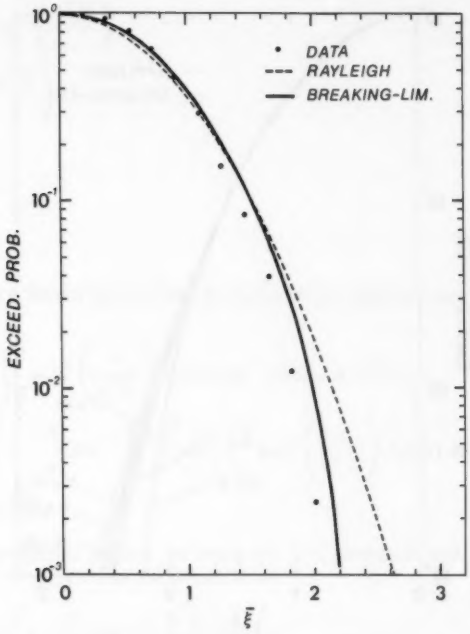

FIG. 2.—Empirical Exceedance Distribution Based on Bretschneider Data (1) in Comparison with Present Theory ($N = 5$) and Rayleigh Distribution

points are approximated by the $N = 5$ distribution more favorably than the conventional Rayleigh law. Furthermore, note that $\bar{\xi}_{max} \leq \sqrt{2N} = 3.162$ theoretically, in comparison with the observed $\bar{\xi}_{max} = 2.198$.

Finite Water Depth Case.—The data for this case are from Dattari, et. al (2), consisting of 1,509 waves collected in a water depth of $D = 13$ m. Unfortunately, the data represent a collective summary of 15 different records, each containing approx 100 waves. Statistics pertinent to each individual record are summarized in Table 2 of Ref. 2, which indicates a variability between these records. On the average, $k_0 = 0.056$ m^{-1}; $\mu_0 = 0.208$ m^2; and $\nu \simeq 0.350$

for the majority of the records. Therefore, $k_0(2\mu_0)^{1/2} \simeq 0.036$, and Eq. 24 requires that $N \simeq 30$. The empirical exceedance distribution constructed on the basis of Fig. 5 of Ref. 2 is shown in Fig. 3 here together with the distributions corresponding to $N = 30$ and the Rayleigh law. The comparison indicates again that the distribution with $N = 30$ is more favorable than the conventional Rayleigh theory. In this case, $\bar{\xi}_{max} = \sqrt{2N} = 7.746$ in contrast with $\bar{\xi}_{max} \simeq 2.903$ observed. This cannot be considered too contradictory considering that the actual sample size is approx 100 waves for each constituent record. It may be of interest

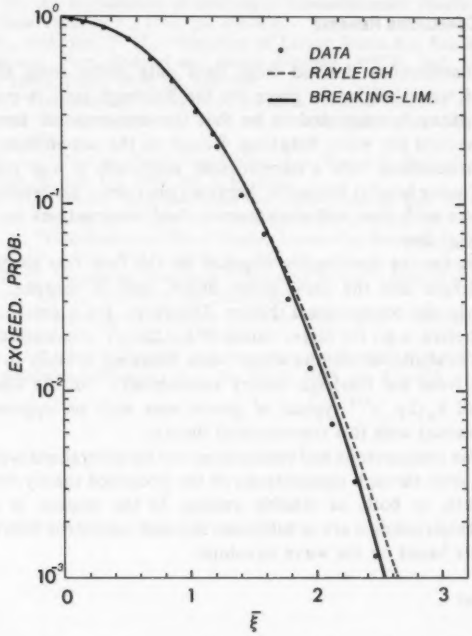

FIG. 3.—Empirical Exceedance Distribution Based on Data of Dattari et. al (2) in Comparison with Present Theory ($N = 30$) and Rayleigh Distribution

also to indicate that if these waves were in deep water Eq. 6 would require $N = 78$, and the corresponding distribution would be shifted slightly towards the Rayleigh limit.

The wave heights in these two cases and in almost all other field observations are based conventionally on a zero-crossing definition. The Rayleigh law and the distribution derived herein are relevant to an envelope or amplitude definition. The two have a fundamental difference. Specifically, a zero-crossing wave height in a scaled form is roughly equivalent to $(\xi_1 + \xi_2)/2$, in which ξ_1 and ξ_2 represent two points on $\xi(t)$ separated by half the mean period, π/ω_0. As

such this definition represents an averaging operation on ξ, damping variations of ξ about its mean. As demonstrated by the writer (13), the resulting sample space must have the same mean, show an excess of waves with heights about the mean, and a deficiency towards both extremes away from it. Therefore, histograms and empirical exceedance distributions constructed from zero-crossing wave heights could display the discrepancy in question in a manner further enhanced by this difference in definitions. In fact, this appears to be quite likely so for the aforementioned deep water case because the corresponding wave height histogram given in Fig. 4 of Ref. 5 displays these characteristics.

Summary and Concluding Remarks

Empirical distributions derived from field data differ from the theoretical distribution of wave heights as given by the Rayleigh law. A principal cause of this discrepancy is suggested to be that the conventional theory does not in any way account for wave breaking. Based on the assumption that the sea surface is characterized with a narrow-band spectrum, it was shown that the distribution of wave heights limited by breaking provides a probability description which compares with two well-documented field observations more favorably than the Rayleigh law.

The breaking-limited distribution depends on the first two spectral moments of the sea surface and the local water depth, and in essence, represents a generalization to the conventional theory. Therefore, for a certain combination of these parameters, e.g., for larger values of $k_0(2\mu_0)^{1/2}$ representative of rough sea states and in shallower depths where wave breaking is likely to be observed, it can deviate from the Rayleigh theory substantially. On the other hand, for small values of $k_0(2\mu_0)^{1/2}$ typical of gentle seas with no apparent breakers, it becomes identical with this conventional theory.

Whether these comparisons and conclusions can be generalized with confidence remains to be seen through comparisons of the proposed theory with additional field or lab data, or both, of reliable quality. In ths respect, it is imperative to ensure that empirical data are of sufficient size and consistent with the definition of wave heights based on the wave envelope.

Acknowledgment

Thanks are due to Daisy Mathew for the preparation of this manuscript. The writer is also grateful to the reviewers for their valuable comments.

Appendix.—References

1. Bretschneider, C. L., "Wave Variability and Wave Spectra for Wind-Generated Gravity Waves," *Technical Memorandum 118*, U.S. Beach Erosion Board, Washington, D.C., 1959.
2. Dattari, J., Raman, H., and Shankar, N. J., "Height and Period Distributions for Waves off Mangalore Barbour-West Coast," *Journal of Geophysical Research*, Vol. 84, No. C7, 1979, pp. 3767–3772.
3. Forristall, G., "On the Statistical Distribution of Wave Heights in a Storm," *Journal of Geophysical Research*, Vol. 83, No. C5, May, 1978, pp. 2353–2358.
4. Longuet-Higgins, M. S., "On the Statistical Distribution of the Heights of Sea Waves," *Journal of Marine Research*, Vol. XI, No. 3, 1952, p. 245.

5. Longuet-Higgins, M. S., "On the Joint Distribution of the Periods and Amplitudes of Sea Waves," *Journal of Geophysical Research*, Vol. 80, No. 18, p. 975, p. 2688.
6. Longuet-Higgins, M. S., "On the Distribution of Sea Waves: Some effects of Nonlinearity and Finite Band Width, *Journal of Geophysical Research*, Vol. 85, No. C3, 1980, pp. 1519–1523.
7. Longuet-Higgins, M. S., "The Effect of Non-Linearities on Statistical Distributions in the Theory of Sea Waves," *Journal of Fluid Mechanics*, Vol. 17, No. 3, 1963, pp. 450–480.
8. Miche, R., "Mouvements Ondulatoires de la Mer en Profondeur Constante ou Decroissante," *Annales des Ponts Chaussees*, Chap. 114, 1944, pp. 25–78, 131–164, 270–292, 369–406.
9. Middleton, D., *An Introduction to Statistical Communication Theory*, McGraw-Hill Book Co., New York, N.Y., 1960, pp. 396–436.
10. Nolte, K. G., and Hsu, F. H., "Statistics of Larger Wave in a Sea State," *Journal of the Waterway, Port, Coastal and Ocean Division*, ASCE, Vol. 105, No. WW4, Proc. Paper 14963, Nov., 1979, pp. 389–404.
11. Rice, S. O., "Mathematical Analysis of Random Noise," *Selected Papers on Noise and Stochastic Processes*, Nelson Wax, ed., Dover Publications, Inc., New York, N.Y., 1954, p. 836.
12. Tayfun, M. A., "Narrow-Band Non-Linear Sea Waves," *Journal of Geophysical Research*, Vol. 85, No. C3, 1980, pp. 1548–1552.
13. Tayfun, M. A., "Wave Heights Based on Zero-Crossing and Wave Envelope," submitted to *Journal of the Waterway, Port, Coastal and Ocean* Division, ASCE.
14. Tayfun, M. A., "Distribution of Wave Heights Limited by Breaking," *Civil Engineering in the Oceans IV*, ASCE, Vol. I, 1979, pp. 336–343.
15. Van Dorn, W. G., "Breaking-Invariants in Shoaling Waves," *Journal of the Geophysical Research*, Vol. 83, No. C6, 1978, pp. 2981–2988.
16. Yang, J.-N., "Simulation of Random Envelope Processes," *Journal of Sound and Vibration*, Vol. 21, No. 1, 1972, pp. 73–85.
17. Yang, J.-N., "On the Normality and Accuracy of Simulated Random Processes," *Journal of Sound and Vibration*, Vol. 26, No. 3, 1973, pp. 417–428.

WAVE FORCES ON RIGID PIPES USING OCEAN TEST DATA

By Robert A. Grace[1] and Gabriel T. Y. Zee[2]

INTRODUCTION

This paper concerns a 4-year experiment in Hawaiian waters dealing with the forces exerted by long-period swell on a test pipe mounted on the sea floor in 37 ft (11.3 m) of water. Four separate angles were involved between the wave fronts and the pipe: 0°, 15°, 35°, and 52°. The wave-induced water motion near the test structure was measured as were the horizontal and vertical forces on an instrumented portion of the test pipe. Although two earlier presentations (7,8) have dealt with data obtained in this investigation, it has not been possible to consider the complete set of data until this point. Instantaneous force values at times of zero velocity have been used with concurrent accelerations to derive information on (horizontal) inertia coefficients. These correspond closely to ideal flow predictions. The focus of this paper is on peak forces, however, and maximum force coefficients have been obtained by normalizing peak forces as for drag coefficients. The trends of these horizontal and vertical maximum force coefficients with changes in wave-pipe angle and (adapted) period parameter are examined for the data in both mean-value and extreme-value forms. Results from the experiment are used in a simulated submarine pipeline design problem.

EQUATIONS, PARAMETERS, AND COEFFICIENTS

Introduction.—Consider a rigid pipe of outside diameter D set parallel to and a distance Δ above a level sea floor. In the context of this paper, the intent is to determine the peak horizontal and vertical forces on a short length l of this pipe during the passage of a certain surface wave defined by its height H, its period T, the water depth at the location of the pipe, d, and the angle of the wave front with the pipe, α. The maximum horizontal force, perpendicular

[1]Visiting Prof., Oregon State Univ., Dept. of Civ. Engrg., Corvallis, Oreg. 97331; on leave from Dept. of Civ. Engrg., Univ. of Hawaii at Manoa, Honolulu, Hawaii.

[2]Engr., United States Navy Shipyard, Pearl Harbor, Hawaii; formerly Grad. Student, Univ. of Hawaii at Manoa, Dept. of Ocean Engrg., Honolulu, Hawaii.

Note.—Discussion open until October 1, 1981. To extend the closing date one month, a written request must be filed with the Manager of Technical and Professional Publications, ASCE. Manuscript was submitted for review for possible publication on July 1, 1980. This paper is part of the Journal of the Waterway, Port, Coastal, and Ocean Division, Proceedings of the Amercan Society of Civil Engineers, ©ASCE, Vol. 107, No. WW2, May, 1981. ISSN 0148-9895/81/0002-0071/$01.00.

to the pipe, that occurs during the passage of this wave will be represented by F'_{max}; the peak vertical force will be written P'_{max}.

The maximum water velocity and acceleration near the sea floor could be predicted for the wave described above through use of any of at least a dozen wave theories (11). Let the theoretical predictions of the peak velocity and acceleration of any theory be represented by u_{max} and $\dot{u}_{max}$, respectively; the symbols for the real maximum velocity and acceleration will be U_{max} and $\dot{U}_{max}$. Kinematics used in this paper will only be of the latter type, making the assumption that measured kinematics are in fact the actual ones. *Every* wave theory errs to at least some degree in predicting U_{max} and $\dot{U}_{max}$ (1), and correction factors are necessary for u_{max} and $\dot{u}_{max}$.

Table 1 contains relevant information obtained at the end of this project (12). The data were obtained for the following wave conditions: $3.0 \leq H \leq 8.2$ ft (0.9–2.5 m); $\bar{H} = 5.0$ ft (1.5 m); $11.5 \leq T \leq 17.4$ sec; $\bar{T} = 16.0$ sec. (Overbars refer to sample mean values.) The kinematical data can be described by: $1.19 \leq U_{max} \leq 3.57$ fps (0.36–1.09 m/sec); $\bar{U}_{max} = 2.33$ fps (0.71 m/sec); $0.27 \leq \dot{U}_{max} \leq 1.97$ ft/sec^2 (0.08–0.60 m/sec^2); $\bar{\dot{U}}_{max} = 0.95$ ft/sec^2 (0.29 m/sec^2). The symbol s_e in Table represents the standard error of estimate.

TABLE 1.—Comparison of Predicted and Measured (Ducted Meter) Peak Kinematics

Kinematical quantity (1)	Prediction of Airy Theory		Prediction of the Stream Function Theory	
	Mean (2)	s_e (3)	Mean (4)	s_e (5)
U_{max}	6.6% low	0.31 fps (0.095 m/sec)	10.7% high	0.31 fps (0.095 m/sec)
$\dot{U}_{max}$	11.2% low	0.26 ft/sec^2 (0.079 m/sec^2)	4.3% high	0.25 ft/sec^2 (0.076 m/sec^2)

Peak Forces.—The equations that will be used to connect the peak kinematics, pipe characteristics, and the maximum forces are the following (4):

$$F'_{max} = C'_{max} \frac{\rho}{2} (Dl)\, U^2_{max} \quad \ldots\ldots\ldots\ldots\ldots\ldots\ldots\ldots\ldots\ldots\ldots\ldots\ldots\ldots (1)$$

and

$$P'_{max} = K'_{max} \frac{\rho}{2} (Dl)\, U^2_{max} \quad \ldots\ldots\ldots\ldots\ldots\ldots\ldots\ldots\ldots\ldots\ldots\ldots\ldots\ldots (2)$$

in which ρ = the water density. Formulations other than Eqs. 1 and 2 are possible (2), but the writers have found these to be the most useful for the data herein. It is apparent that these two equations contain no explicit mention of the peak acceleration $\dot{U}_{max}$, but there is an implicit inclusion of this variable through the realization that the maximum force coefficients C'_{max} and K'_{max} must be functions of the relative effect of acceleration. The parameter that will be used to indicate such a tendency will be an adapted period parameter given by the equation

$$\psi = U^2_{max} / \dot{U}_{max} D \quad \ldots\ldots\ldots\ldots\ldots\ldots\ldots\ldots\ldots\ldots\ldots\ldots\ldots\ldots (3)$$

Parameters and Instantaneous Inertia Force Coefficients.—Other parameters of interest are as follows:

the Reynolds number $N_R = \frac{U_{max} D}{\nu}$ . . . . . (4)

in which ν = the kinematic viscosity of the water;

the relative pipe clearance $= \frac{\Delta}{D}$; . . . . . (5)

the relative roughness of the pipe surface $= \frac{\epsilon}{D}$, ... (6)

in which ϵ = the average height of surface protuberances;

the relative distance of water particle motion $= \frac{s}{D}$, ... (7)

in which s is ideally the horizontal distance of water particle movement. An estimate of s was obtained in this investigation by graphically integrating under

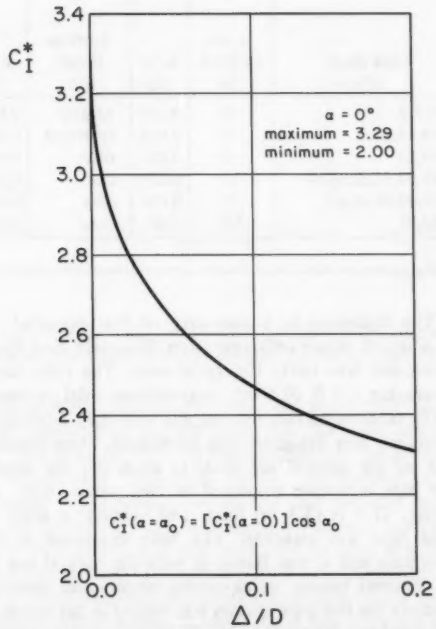

FIG. 1.—Ideal Flow Inertia Coefficient for a Pipe as a Function of Pipe Clearance from the Boundary and Angle of Attack

a U-time t curve from the instant when $U = 0$ to the time of interest, e.g., when $F' = F'_{max}$ or $P' = P'_{max}$.

The instantaneous inertia coefficient is

$$C''_I = \frac{\text{value of } F' \quad \text{when} \quad U = 0}{\rho\left[\left(\frac{\pi D^2}{4}\right) l\right] \dot{U}_*} \quad \ldots\ldots\ldots\ldots\ldots\ldots\ldots\ldots\ldots\ldots (8)$$

in which $\dot{U}_*$ = the flow acceleration when $U = 0$. The ideal-flow counterpart of C''_I will be written C^*_I, and this coefficient is a function of both Δ/D and α as shown in Fig. 1 (14).

Experiment

Experimental Arrangement.—An in-depth account of the design, fabrication, installation, operation, maintenance, and diving aspects of this project is presented

TABLE 2.—Summary of Test Conditions

Phase (1)	Part (2)	Data days (3)	α, in degrees (4)	Δ/D (5)	Surface finish (6)	ϵ/D (7)	No. of waves processed (8)
1	A	3,5,9	0	0.188	natural	0.0001[a]	155
1	B	16,19,20	0	0.031	corroded	0.0025[a]	92
1	C	22,23	0	0.031	ribs	0.016	55
2	A	29,30,31,32,33,34	15	0.031	ribs	0.016	219
2	B	39,40,42,43,44	35	0.031	nuts	0.016	298
2	C	45,46	52	0.031	nuts	0.016	200

[a]Estimated.

by Grace (5,6). The following is a summary of that material. The test site was in 37 ft (11.3 m) of water offshore from Honolulu and the sea floor in the area of the test site was fairly flat coral rock. The tidal range in Hawaii is very small, averaging 1.2 ft (0.4 m); near-bottom tidal currents at the site were negligible. The trade wind fetch to the site was only 2,000 ft (650 m).

A test pipe structure was designed and fabricated, then installed on a thin gravel bed placed on the natural sea floor to even out the subtle peaks and hollows. The test pipe structure consisted of two parts—first, a 16-in. diam (406-mm) steel pipe, 17.5 ft (5.3 m) long, and second, a steel and concrete base to which the pipe was attached. The base measured 16 ft 4 in. by 8 ft (5.0 × 2.4 m) in plan and it was faired in with the natural sea floor through use of dozens of concrete beams, quick-setting underwater cement and epoxy, and steel chain. Before the test pipe system was placed in the ocean, the direction of propagation of Southern Hemisphere swell at the site was established (±5°) through extensive sea floor observation of water motion.

Only a 40-in.-long (1.04-m) near-central portion of the pipe was used as a

force sensor. This segment was attached to the two side portions of the pipe, welded to the base, through two internal strain gage beams. One of these reacted to vertical forces and the other to horizontal ones. On a test day the vertical channel was calibrated by placing known weights on the test section and the horizontal channel was calibrated by using a shunt resistor coupled with the vertical force calibration. The latter technique had been checked earlier in the field, by exerting a known horizontal force on the test section, and found to be accurate within 2%.

Several different pipe arrangements were used during the 4 years of experimentation. In the first year, the pipe was oriented perpendicular to the wave-induced water motion; the pipe clearance from its base was 3 in. (76 mm). The pipe base was 4.5 in. (114 mm) deep. Throught the remainder of the project,

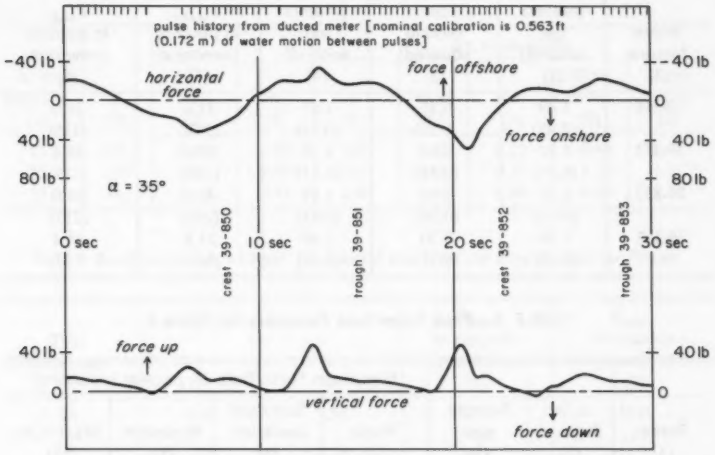

FIG. 2.—Example of Strip Chart Record of Concurrent Variation in Ducted Meter Flow Speed Output and Horizontal and Vertical Forces on Pipe Test Section

the pipe clearance was changed to 0.5 in. (13 mm). This was done by laying keyed, concrete slabs over the old base and the base depth thus became 7 in. (178 mm). The original 3-in. (76-mm) clearance, found to be unnecessary, was used to ensure that coral rock rubble, conceivably swept over the sea floor during heavy wave action, would not jam the test section. The 0.5-in. (13-mm) gap was used as the best compromise between having the pipe directly on the base, to truly simulate a real pipe, and to have it sufficiently far from the base for the test section to function without any possibility of "bottoming." Observations of sand near the test section provided strong evidence that there was no perceptible water motion through the 0.5-in. (13-mm) opening.

Initially, the pipe was used in an "as is" condition. Midway through the second year of work, artificial roughness elements (Table 2) were added to the pipe test section and to adjacent parts of the flanking pipes, and these

were maintained through the rest of the project. The angle between the nominal wave fronts and the pipe during the second year remained at 0°, but for the third year an angle of 15° was employed. Two separate angles were used during the final year of work, first 35° and then 52°. The pipe reorientations were

TABLE 3.—Peak Kinematical and Force Values for Wave Train in Fig. 2

Wave feature (1)	U'_{max}, in feet per second (meters per second) (2)	$\dot{U}_{max}$, in feet per second squared (meters per second squared) (3)	U_{max}, in feet per second (meters per second) (4)	F'_{max}, in pounds (newtons) (5)	P'_{max}, in pounds (newtons) (6)
39-850	1.49	0.85	1.91	31.6	26.0
	(0.45)	(0.26)	(0.58)	(142)	(116)
39-851	1.91	0.91	1.75	35.6	48.8
	(0.58)	(0.28)	(0.53)	(159)	(219)
39-852	1.75	1.10	1.99	48.8	48.0
	(0.53)	(0.34)	(0.61)	(219)	(215)
39-853	1.99	0.70	1.40	22.4	18.4
	(0.61)	(0.21)	(0.43)	(100)	(82)

TABLE 4.—Peak Force Data Summary for Phase 2

Force (1)	α, in degrees (2)	Sample size (3)	Maximum Force Data, in pounds (newtons)			
			Mean (4)	Standard deviation (5)	Minimum (6)	Maximum (7)
F'_{max}	15	212	60.9	25.5	19.5	148.8
			(271)	(113)	(87)	(662)
P'_{max}	15	210	57.4	21.4	18.5	128.1
			(255)	(95)	(82)	(570)
F'_{max}	35	243	38.3	16.1	13.2	116.6
			(170)	(72)	(59)	(519)
P'_{max}	35	229	32.4	9.6	12.2	59.0
			(144)	(43)	(54)	(263)
F'_{max}	52	195	24.0	8.1	10.3	57.7
			(107)	(36)	(46)	(257)
P'_{max}	52	186	18.4	6.5	6.9	40.0
			(82)	(29)	(31)	(178)

carried out, after removal of the fairing beams, through use of a large, air-filled lift bag and a "comealong" pulling from one of the four 1-t anchor blocks on the sea floor used to keep the project boat anchored over the test site. A special vane was used to measure the angle between the pipe and the direction

of wave-induced water motion on any Data Day.

During data-taking days (see Table 2), data were recorded on the project vessel in its forward cabin. Electrical cables connected strip chart recorders, powered by a portable alternator, with the sensors on the sea floor. Two channels of data involved the horizontal and vertical forces on the pipe test section, coming from the strain gage half-bridges, whereas a third channel involved the output from the ducted current meter. This record involved a series of pulses, as magnets in the tips of the three blades of the ducted meter impeller spun past an enclosed reed switch on the side of the meter. All three time histories were recorded on the same chart, as shown in Fig. 2, a retraced raw data history for Data Day 39. Table 3 provides some details on the waves

TABLE 5.—Further Information for Phase 2 Data

α, in degrees (1)	n (2)	r (3)	b (4)	$\Delta\tau$, in seconds				
				n (5)	Mean (6)	s.d. (7)	Minimum (8)	Maximum (9)
15	203	0.90	0.89	210	0.45	0.27	−0.40	3.05
35	174	0.61	0.90	164	0.49	0.37	−1.28	1.71
52	181	0.65	0.74	176	0.48	0.49	−1.20	3.17

TABLE 6.—Correlation of Peak Horizontal and Vertical Pipe Forces for Phase

Test sequence (1)	n (2)	r (3)	$\bar{F}_{max}$, in pounds (newtons) (4)	$\bar{P}_{max}$, in pounds (newtons) (5)
1A	106	0.50	35.8	21.0
			(159)	(93)
1B	80	0.80	58.2	55.2
			(259)	(246)
1C	55	0.94	68.5	66.0
			(305)	(294)

shown in Fig. 2. U^{p}_{max} in this table represents the peak flow speed under the preceding wave feature (i.e., crest or trough).

Force Data.—The ranges of maximum horizontal and vertical forces measured during Phase 2 (Table 2) are presented in Table 4. Additional information of a general nature is shown in Table 5. In that table, the following symbols are used: n = sample size; r = correlation coefficient between same-wave pairs of F'_{max} and P'_{max}; b is a regression slope in the equation $P'_{max} = bF'_{max}$; $\Delta\tau$ is the time delay of F'_{max} relative to the same-wave P'_{max}; and s.d. represents standard deviation. Note that negative $\Delta\tau$ values in Table 5 indicate F'_{max} leading P'_{max}.

The time delay of F_{max} with respect to P_{max} was also investigated for the Data Day 23 data from Phase 1 ($\alpha = 0°$). A sample of size 54 produced a

mean of 0.45 sec, a standard deviation of 0.45 sec, and a range of from −0.60 to 2.90 sec. There were only three negative lags and the high lag of 2.90 sec was one of only two time intervals, both for troughs, larger than 0.90 sec. Fortyone (75%) of the Data Day 23 time delays fell in the interval $0.20 \leq \Delta\tau \leq 0.50$ sec.

The correlation between the peak horizontal and vertical force data from Phase 1 is presented in Table 6. The results suggest that increasing pipe roughness and decreasing pipe clearance promote coupling between maximum horizontal and vertical wave-induced forces for a pipe near a boundary.

Random Effects

A major aim of this research was to chart the manner in which the force coefficients C'_{max} (Eq. 1) and K'_{max} (Eq. 2) vary with Δ/D, ϵ/D, and α (factors under control) as well as Reynolds number and adapted period parameter ψ (parameters determined by the wave environment). It is to be stressed, however, that even for the same test day (same Δ/D, ϵ/D, and, within limits, α) and for two waves having the same U_{max} and $\dot{U}_{max}$ (thus, same Reynolds number and period parameter to say nothing of the same squared velocity appearing in Eqs. 1 and 2), forces are different.

TABLE 7.—Pipe Force Differences Due to Factors Other Than Gross Kinematics Under Particular Wave

Data day (1)	Wave no. (2)	U^p_{max}, in feet per second (meters per second) (3)	$\dot{U}_{max}$, in feet per second squared (meters per second squared) (4)	U_{max}, in feet per second (meters per second) (5)	$(t_{max} - t_0)$, in seconds (6)	F_{max}, in pounds (newtons) (7)	P_{max}, in pounds (newtons) (8)
23	520	2.55	1.36	2.98	2.21	76.1	79.7
		(0.78)	(0.41)	(0.91)		(341)	(357)
23	770	1.47	1.31	2.93	2.14	60.7	58.0
		(0.45)	(0.40)	(0.89)		(272)	(260)
23	044	2.67	1.41	2.24	1.65	74.5	74.5
		(0.81)	(0.43)	(0.68)		(334)	(334)
23	050	2.10	1.39	2.24	2.47	62.0	62.3
		(0.64)	(0.42)	(0.68)		(278)	(279)

The fact that flow history appears to play a strong role in such variability is shown in Table 7. In this presentation, the quantity $(t_{max} - t_0)$ is the time from zero to peak flow speed. Although some of the scatter in the force coefficient data, to be shown presently, may be due to experimental error, the writers attribute the bulk of such variability to effects beyond the factors included mathematically in the analysis. In particular, flow history and flow turbulence,

probably intimately related, play strong dispersive roles. Because of such random effects, force coefficients will be considered later in two senses—mean trends and extreme values.

Instantaneous Inertia Coefficients

Table 8 summarizes the information obtained by the project for the instantaneous inertia coefficient given in Eq. 8. The distributions of C_I'' values for the data sequences shown in Table 8 appeared adequately fitted by the normal

TABLE 8.—Ideal-Flow and Instantaneous Inertia Coefficients

Test sequence (1)	C_I^* (2)	n (3)	Instantaneous Inertia Coefficients			Correlation Coefficients	
			Mean (4)	s.d. (5)	95% confidence interval (6)	With N_R (7)	With ψ (8)
1A	2.32	48	2.12	0.48	1.98–2.26	−0.23	−0.10
1B	2.74	89	2.41	0.65	2.27–2.55	0.28	0.28
1C	2.74	55	2.70	0.74	2.50–2.90	0.08	0.06
2A	2.65	218	2.74	0.81	2.63–2.85	−0.09	0.06
2B	2.24	243	2.38	0.53	2.31–2.45	−0.04	0.00
2C	1.69	195	1.95	0.71	1.85–2.05	0.13	0.18

distribution. The mean coefficient values come satisfactorily close to the theoretical values, C_I^* (Fig. 1).

Peak Forces

Introduction.—Values of C'_{max} or K'_{max} plotted versus adapted period parameter, as in for example Figs. 3–6, yield clouds of points. Two approaches will be used later with these data: on the one hand, a mean line will be derived; on the other, an envelope trend will be considered. Although some work was done with the distribution of residuals about the mean-line curves, this approach will not be used herein as the dispersion of the distribution was correlated with the independent variable (in a predictor sense) ψ.

The correlation coefficient between C'_{max} and ψ Test Sequence 2A, for example, (211 points) is −0.75. But the correlation coefficient between C'_{max} and N_R for these same data is −0.68. It is then logical to inquire whether C'_{max} is really varying in a negative way with both of these parameters or if it is perhaps varying in such a way with only one and the two parameters are in themselves positively correlated. For these data the correlation coefficient between ψ and N_R is 0.85.

To answer this question, C'_{max} (also K'_{max}) was plotted both against N_R for specific ψ ranges and again against ψ for specific N_R ranges. Adapted period parameter classes were taken of 0.2-unit width with $N_R \times 10^{-5}$ ranges of 1.0–2.5, 2.5–4.0, and >4.0. The data showed clearly that there were no visible trends purely on the basis of N_R; thus the data have been presented as in Figs. 3–6,

i.e., versus ψ—with no identification on the individual points as to the applicable range of N_R. A similar approach, but statistical, appears in Tables 9 and 10. The $\alpha = 0°$ case, missing in these tables, is discussed in Appendix I. Table 11 presents general correlation information for Phase 2 data.

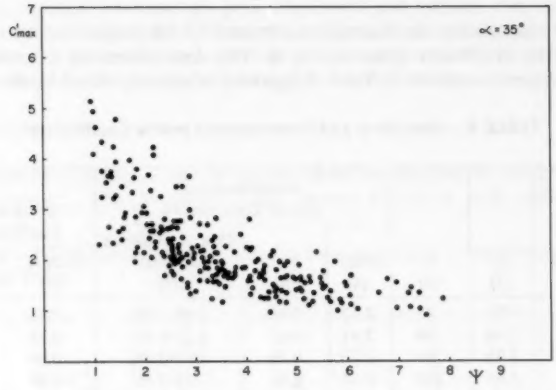

FIG. 3.—Variation of Maximum Horizontal Pipe Force Coefficient with Adapted Period Parameter ($\alpha = 35°$)

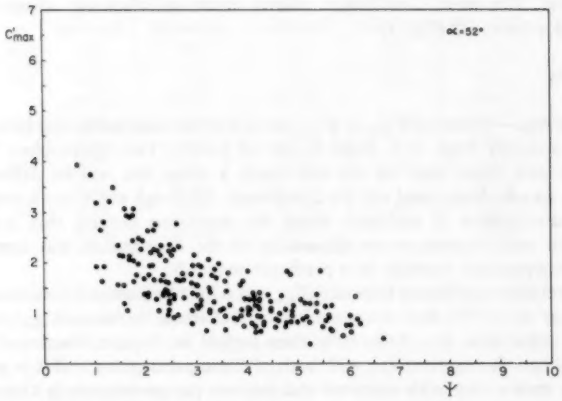

FIG. 4.—Variation of Maximum Horizontal Pipe Force Coefficient with Adapted Period Parameter ($\alpha = 52°$)

Maximum Force Coefficients: Mean Trends.—The following forms of expressions have been found useful in fitting the classified mean trends for C'_{max} and K'_{max} versus adapted period parameter:

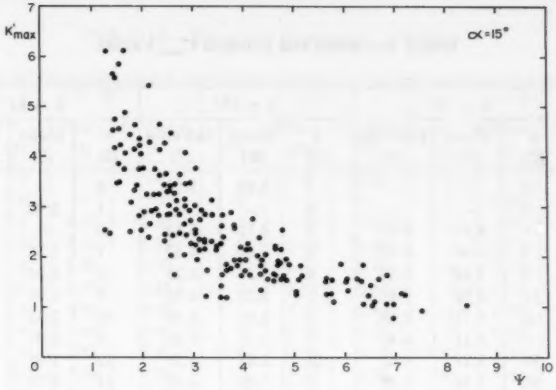

FIG. 5.—Variation of Maximum Vertical Pipe Force Coefficient with Adapted Period Parameter ($\alpha = 15°$)

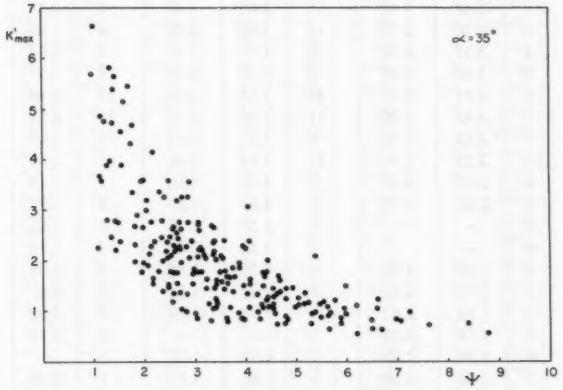

FIG. 6.—Variation of Maximum Vertical Pipe Force Coefficient with Adapted Period Parameter ($\alpha = 35°$)

$$\overline{C'_{\max}} = C'_H + B_1 e^{-A_1\psi} + \frac{G_1}{\psi^2}, \quad 1 \leqslant \psi \quad \ldots\ldots\ldots\ldots\ldots\ldots\ldots (9)$$

and $$\overline{K'_{\max}} = C'_H + B_2 e^{-A_2\psi} + \frac{G_2}{\psi^2}, \quad 1 \leqslant \psi \quad \ldots\ldots\ldots\ldots\ldots\ldots\ldots (10)$$

The velocity-dependent horizontal force coefficient C'_H in Eqs. 9 and 10 came from an analysis wherein peak forces were predicted by a Morison form of

TABLE 9.—Mean and Extreme C'_{max} Values

	$\alpha = 15°$			$\alpha = 35°$			$\alpha = 52°$		
ψ (1)	n (2)	Mean (3)	Extreme (4)	n (5)	Mean (6)	Extreme (7)	n (8)	Mean (9)	Extreme (10)
0.4	0	—	—	1	8.98	8.98	0	—	—
0.6	0	—	—	0	—	—	1	3.92	3.92
0.8	1	6.97	6.97	3	4.72	5.14	0	—	—
1.0	3	5.91	6.57	5	3.65	4.62	7	2.39	3.18
1.2	3	3.82	5.06	8	3.37	4.25	2	3.35	3.49
1.4	12	4.02	5.68	9	3.20	4.78	7	1.99	3.09
1.6	6	3.71	5.29	5	3.05	3.99	10	2.32	3.08
1.8	9	3.31	4.40	7	2.75	3.80	9	2.07	2.48
2.0	10	3.27	4.42	13	2.85	4.36	10	1.97	2.65
2.2	10	3.38	4.09	8	2.49	3.29	11	1.75	2.78
2.4	13	2.95	3.65	18	2.26	2.74	14	1.60	2.41
2.6	10	2.84	3.40	16	2.33	3.45	8	1.76	2.79
2.8	13	2.90	3.47	10	2.19	3.62	7	1.52	2.13
3.0	14	2.73	3.85	11	2.10	2.71	11	1.29	1.93
3.2	9	2.48	3.39	18	2.05	2.81	8	1.43	2.06
3.4	9	2.20	2.73	12	1.83	2.26	9	1.29	2.00
3.6	8	2.37	2.90	8	1.77	2.16	3	1.27	1.78
3.8	8	2.46	3.09	4	2.10	2.50	8	1.17	1.62
4.0	8	2.41	2.87	13	1.85	2.80	13	1.14	1.39
4.2	8	2.42	3.00	11	1.60	2.19	10	1.01	1.39
4.4	7	2.12	2.72	9	1.57	2.08	6	1.07	1.35
4.6	10	2.23	3.10	11	1.63	2.00	7	1.08	1.81
4.8	6	2.12	2.85	3	1.56	1.66	5	1.13	1.76
5.0	5	2.06	2.29	6	1.69	1.89	4	1.03	1.25
5.2	0	—	—	6	1.50	2.13	7	1.01	1.32
5.4	0	—	—	6	1.52	1.79	4	1.13	1.82
5.6	6	1.60	1.88	4	1.39	1.96	5	0.86	1.14
5.8	1	2.01	2.01	4	1.34	1.54	2	0.65	0.75
6.0	3	1.84	2.01	4	1.28	1.70	5	0.90	1.32
6.2	4	1.78	2.25	0	—	—	1	0.78	0.78
6.4	4	1.74	1.93	1	1.32	1.32	0	—	—
6.6	2	1.63	1.88	1	1.61	1.61	1	0.50	0.50
6.8	4	1.64	2.06	2	1.28	1.53	0	—	—
7.0	1	1.31	1.31	2	1.18	1.33	0	—	—
7.2	1	1.70	1.70	2	1.25	1.44	0	—	—
7.4	2	1.38	1.59	1	0.90	0.90	0	—	—
7.6	0	—	—	0	—	—	0	—	—
7.8	0	—	—	1	1.22	1.22	0	—	—
8.0	0	—	—	0	—	—	0	—	—
8.2	1	1.05	1.05	0	—	—	0	—	—
8.4	0	—	—	0	—	—	0	—	—
8.6	0	—	—	0	—	—	0	—	—
8.8	211			243			200		

TABLE 10.—Mean and Extreme K'_{max} Values

	$\alpha = 15°$			$\alpha = 35°$			$\alpha = 52°$		
ψ (1)	n (2)	Mean (3)	Extreme (4)	n (5)	Mean (6)	Extreme (7)	n (8)	Mean (9)	Extreme (10)
0.4	0	—	—	1	12.41	12.41	0	—	—
0.6	0	—	—	0	—	—	1	1.97	1.97
0.8	1	9.32	9.32	3	7.53	8.93	1	3.18	3.18
1.0	3	7.13	7.79	5	4.18	6.62	7	2.71	3.64
1.2	3	3.69	6.09	8	4.22	5.80	4	2.33	4.02
1.4	12	4.50	5.86	9	3.47	5.62	7	1.58	3.23
1.6	6	3.80	4.89	5	4.06	5.44	11	1.88	4.39
1.8	9	3.69	4.63	9	2.87	5.14	9	1.60	2.28
2.0	8	3.58	5.41	10	2.54	4.15	10	1.32	3.15
2.2	10	3.50	4.65	7	2.43	3.33	10	1.71	2.52
2.4	14	3.18	4.46	16	2.10	3.63	14	1.39	2.60
2.6	9	2.81	3.63	15	2.13	3.22	8	1.52	3.07
2.8	12	2.95	4.09	11	2.02	3.23	6	1.21	1.98
3.0	14	2.77	3.78	11	1.96	2.68	10	0.95	1.26
3.2	9	2.33	3.11	14	1.77	2.68	7	1.17	2.28
3.4	9	2.00	2.62	10	1.71	2.39	8	0.94	1.58
3.6	7	2.11	2.93	8	1.35	1.86	3	1.22	1.60
3.8	8	2.16	2.67	8	1.56	2.30	5	0.80	1.16
4.0	8	1.98	2.27	5	1.86	3.04	10	1.03	1.72
4.2	9	2.12	2.83	11	1.35	2.20	9	1.03	1.25
4.4	7	1.79	2.41	7	1.19	1.77	5	0.98	1.12
4.6	10	1.97	2.57	8	1.28	1.60	7	0.73	1.13
4.8	5	1.94	2.64	4	1.26	1.66	6	0.75	1.01
5.0	6	1.58	1.89	4	1.21	1.35	3	0.81	1.11
5.2	0	—	—	5	1.18	2.06	7	0.66	0.99
5.4	0	—	—	4	1.06	1.19	4	0.87	1.49
5.6	7	1.38	1.58	4	0.92	1.21	5	0.65	0.85
5.8	1	1.87	1.87	4	1.06	1.39	2	0.57	0.66
6.0	3	1.48	1.59	1	1.10	1.10	5	0.76	1.31
6.2	4	1.51	1.87	0	—	—	1	0.40	0.40
6.4	4	1.25	1.46	3	0.84	1.04	0	—	—
6.6	2	1.35	1.57	2	0.98	1.27	1	0.50	0.50
6.8	4	1.14	1.63	1	0.84	0.84	0	—	—
7.0	1	1.29	1.29	1	0.81	0.81	0	—	—
7.2	1	1.29	1.29	1	0.99	0.99	0	—	—
7.4	2	1.07	1.20	0	—	—	0	—	—
7.6	0	—	—	1	0.71	0.71	0	—	—
7.8	0	—	—	0	—	—	0	—	—
8.0	0	—	—	0	—	—	0	—	—
8.2	0	—	—	1	0.75	0.75	0	—	—
8.4	1	1.04	1.04	0	—	—	0	—	—
8.6	0	—	—	1	0.58	0.58	0	—	—
8.8	209			218			200		

the equation where C_I^* was the acceleration-related coefficient and C'_H was the velocity-dependent one. The use of this coefficient as the asymptote for the maximum horizontal force coefficient is certainly reasonable. It was used as an asymptote for the maximum vertical force coefficient since it appeared, after various trials using other values, to be the best choice.

The coefficients, B, A, and G appearing in Eqs. 9 and 10 were chosen from the three horizontal and vertical data sets in Phase 2; they are also listed in Table 12. The fit of the resulting six lines to the mean trends of the C'_{max} and K'_{max} data was excellent, and Figs. 7 and 8 present the resulting curves. Two comments are perhaps in order to assist in understanding these two figures. On the one hand, the same data classes were used as for Tables 9 and 10,

TABLE 11.—Correlation Information for Phase 2 Data

α, in degrees (1)	Coefficient or parameter (2)	Correlation Coefficient with Parameter		
		n (3)	ψ (4)	N_R (5)
15	C'_{max}	212	−0.75	−0.68
	K'_{max}	210	−0.76	−0.69
	N_R	219	0.85	1.00
35	C'_{max}	243	−0.70	−0.69
	K'_{max}	229	−0.65	−0.69
	N_R	298	0.84	1.00
52	C'_{max}	195	−0.70	−0.75
	K'_{max}	186	−0.60	−0.68
	N_R	200	0.84	1.00

TABLE 12.—Coefficients for Eqs. 9 and 10

Test sequence (1)	C'_H (2)	B_1 (3)	A_1 (4)	G_1 (5)	B_2 (6)	A_2 (7)	G_2 (8)
2A	1.11	2.87	0.239	1.99	6.50	0.478	0.38
2B	0.77	2.20	0.222	1.81	4.95	0.525	1.39
2C	0.41	2.26	0.285	1.16	2.03	0.337	0.82

i.e., $0.4 < \psi \leq 0.6$, $0.6 < \psi \leq 0.8$, etc. Secondly, the open symbols in the figures indicate that only one value was involved in these classes; thus, the particular values do not have the same weight as those obtained in other classes from samples of size two or greater.

It is of interest to compare the $\overline{C'_{max}}$ and $\overline{K'_{max}}$ values for $\alpha = 35°$ and 52° to those obtained for $\alpha = 15°$ or, equivalently as it turns out, to those values applicable for $\alpha = 0°$. In all four cases, there is no apparent trend in the ratios with increasing adapted period parameter. Summary results for the four cases are presented in Table 13. Note that situations involving only one value in a class were ignored.

Maximum Force Coefficients: Extreme Values.—It is also of interest to consider

the extreme values of the maximum force coefficients in Tables 9 and 10. For each class in each table, excepting those situations where there is only one point, the ratios obtained by dividing the extreme coefficient value by the mean have been computed. Down playing the tendency towards lower ratios for high ψ values, because of the small class sample sizes, there appear to

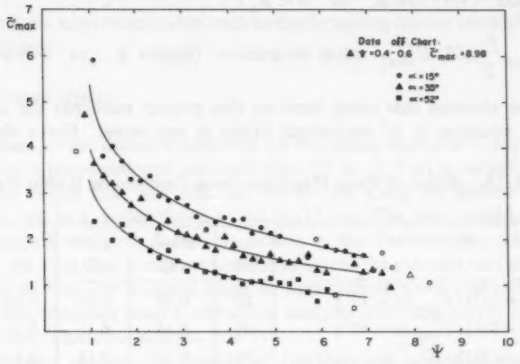

FIG. 7.—Variation of Class-Average Maximum Horizontal Pipe Force Coefficient with Adapted Period Parameter for Three Test Pipe Orientations

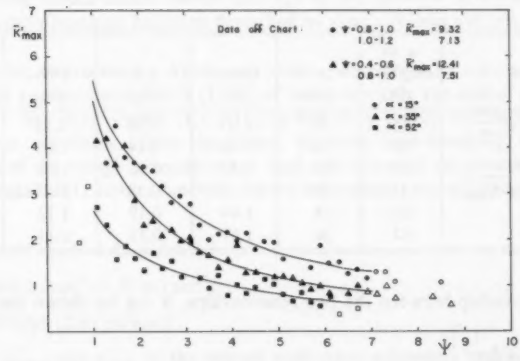

FIG. 8.—Variation of Class-Average Maximum Vertical Pipe Force Coefficient with Adapted Period Parameter for Three Test Pipe Orientations

be no tendencies among the six separate groups towards systematic down or up trends with increasing ψ values. For that reason, it is convenient to view overall information and the results are given in Table 14. It is clear that for both horizontal and vertical maximum force coefficients, the averages increase as the angle α increases.

The Question of Very Low ψ Values.—The complete equations for use in computing peak horizontal forces are the following:

$$F'_{max} = C_f^* \rho \left[\left(\frac{\pi D^2}{4} \right) l \right] \dot{U}_{max}$$

no separation (very low ψ, or $\psi < \psi_*$) . . . . . (11*a*)

$$F'_{max} = C'_{max} \frac{\rho}{2} (Dl) U^2_{max}, \quad \text{after separation (higher } \psi, \text{ or } \psi > \psi_*) \quad (11b)$$

It should be stressed that work done on this project concerns the latter case; the former situation is of theoretical origin in any event. For a short region

TABLE 13.—Ratios of Mean Maximum Force Coefficients Within Classes

Ratio (1)	*n* (2)	Mean (3)	s.d. (4)	Low (5)	High (6)
$\overline{C'_{max}}\ (\alpha = 35°)/\overline{C'_{max}}\ (\alpha = 15')$	23	0.78	0.07	0.62	0.88
$\overline{C'_{max}}\ (\alpha = 52°)/\overline{C'_{max}}\ (\alpha = 15°)$	23	0.54	0.10	0.40	0.88
$\overline{K'_{max}}\ (\alpha = 35')/\overline{K'_{max}}\ (\alpha = 15')$	24	0.75	0.13	0.59	1.14
$\overline{K'_{max}}\ (\alpha = 52°)/\overline{K'_{max}}\ (\alpha = 15°)$	23	0.46	0.08	0.34	0.63

TABLE 14.—Ratios of Extreme Mean Maximum Force Coefficients

Ratio (1)	α, in degrees (2)	*n* (3)	Mean (4)	s.d. (5)	Low (6)	High (7)
$\overline{C'_{max\ extreme}}/\overline{C'_{max}}$	15	28	1.25	0.10	1.11	1.42
	35	30	1.30	0.14	1.06	1.65
	52	26	1.40	0.16	1.04	1.68
$\overline{K'_{max\ extreme}}/\overline{K'_{max}}$	15	28	1.29	0.13	1.07	1.65
	35	28	1.44	0.19	1.12	1.79
	52	26	1.61	0.33	1.14	2.39

or point of overlap between the two relationships, it can be shown that

$$C'_{max} = \left[\frac{\pi}{2} C_f^* \frac{1}{\psi} \right] \quad \ldots \ldots \ldots \ldots \ldots \ldots \ldots \ldots \ldots \ldots \quad (12)$$

The point of intersection between the hyperbolic relationship given in Eq. 12 with the mean lines shown in Fig. 7 theoretically gives an estimate of the cutoff value, ψ_*, between the two forms of Eq. 11. Unfortunately, for each of Test Sequences 2A, 2B, and 2C, the two lines do not actually cross for low ψ values but virtually parallel each other. In terms of both the closeness of the lines and the paucity of points in this investigation for $\psi < 1$, it is proposed that $\psi_* = 1.0$. Thus, Eq. 11 can be rewritten

$$F'_{max} = C_I^* \rho \left[\left(\frac{\pi D^2}{4} \right) l \right] \dot{U}_{max}, \quad \psi \leq 1 \quad \ldots \quad (13a)$$

$$F'_{max} = C'_{max} \frac{\rho}{2} (Dl) U^2_{max}, \quad \psi > 1 \quad \ldots \quad (13b)$$

Note that there is no relationship such as the foregoing for the vertical maximum force coefficient.

Submarine Pipeline Design

Introduction.—One option considered for the sewer outfall at Wanganui, New Zealand, was a post-tensioned concrete pipe, 67 in. (1.7 m) in outside diameter. A possibility in this case was that the line be laid along the seabed some 6200 ft (1900 m) out to a water depth of 40 ft (12 m). The pipe would be stapled to the seabed as required. Storm conditions in the Tasman Sea, which offlies Wanganui, are such that is was reasonable to assess tha planned outfall's stability to breaking waves. The steepest angle of approaching wave orthogonals to the pipe, 35°, was obtained from a refraction analysis involving waves approaching from due west. Thus, for design, $\alpha = 55°$.

In the present section, the results of this research investigation in Hawaii will be used to evaluate the peak horizontal and vertical forces on the (assumed rigid) Wanganui outfall in 40 ft (12 m) of water. Some consideration will also be given to the distribution of force along the outfall in this depth. The problem of computing forces under waves that are in the process of breaking rather than incipiently breaking has been described by Grace (4) and will not be covered here.

Kinematics, Parameters.—Assume a 10-sec period for the waves incipiently breaking in approximately 40 ft (12 m) of water towards the end of the outfall. Although it has been shown (1,3,9,11,13) that Airy theory accurately predicts near-bottom velocities under the crests of even near-breaking waves, the prediction of the trough velocity is too high and the peak acceleration too low. Use of tabulated (1) stream function theory information and extensive interpolation gives

$$u^P_{max} = -4.84 \text{ fps } (-1.48 \text{ m/sec}) \quad \ldots \quad (14a)$$

$$\dot{u}_{max} = 5.48 \text{ ft/sec}^2 \text{ } (1.67 \text{ m/sec}^2) \quad \ldots \quad (14b)$$

$$u_{max} = 8.67 \text{ fps } (2.64 \text{ m/sec}) \quad \ldots \quad (14c)$$

in which u^P_{max} and u_{max} = the trough and crest velocities, respectively, and $\dot{u}_{max}$ = the peak water particle acceleration occurring between trough and crest or between crest and trough. Assume, for simplicity, that these three theoretical kinematical values are equal to the real quantities U^P_{max}, U_{max}, and $\dot{U}_{max}$, respectively.

The values of adapted period parameter for the trough and crest are, respectively,

$$\psi' = \frac{(U^P_{max})^2}{\dot{U}_{max} D} = 0.77 \quad \ldots \quad (15a)$$

and $$\psi = \frac{U_{max}^2}{\dot{U}_{max} D} = 2.46 \quad \ldots \quad (15b)$$

Both values in Eq. 15 are necessary since the distribution of force on the pipe should be computed. The value of ψ' indicates use of Eq. 13*a*, whereas the value of ψ points to Eq. 13*b*. For the trough case, Fig. 1 ($\Delta/D = 0.00$ and $\alpha = 55°$) yields $C_I^* = 1.9$, and Eq. 13*a* gives

$$_tF'_{max} \equiv C_I^* \rho \left[\left(\frac{\pi D^2}{4} \right) l \right] \dot{U}_{max} \quad \ldots \quad (16a)$$

or $$\frac{_tF'_{max}}{l} = 530 \text{ lb/ft } (7.7 \text{ kN/m}) \quad \ldots \quad (16b)$$

in which the presubscript t indicates trough. In the crest case, interpolation and extrapolation in Figs. 7 and 8 yield $C'_{max} = 1.7$ and $K'_{max} = 1.3$, respectively (for $\psi = 2.46$). Thus,

$$_cF'_{max} \equiv C'_{max} \left(\frac{\rho}{2} \right) (Dl)\, U_{max}^2 \quad \ldots \quad (17a)$$

or $$\frac{_cF'_{max}}{l} = 710 \text{ lb/ft } (10.3 \text{ kN/m}) \quad \ldots \quad (17b)$$

$$_cP'_{max} \equiv K'_{max} \left(\frac{\rho}{2} \right) (Dl)\, U_{max}^2 \quad \ldots \quad (18a)$$

or $$\frac{_cP'_{max}}{l} = 540 \text{ lb/ft } (7.9 \text{ kN/m}) \quad \ldots \quad (18b)$$

Since no formulation such as Eq. 13*a* is available for vertical forces, the assumption will be made that

$$_tP'_{max} = {}_tF'_{max} \quad \ldots \quad (19a)$$

or $$\frac{_tP'_{max}}{l} = 530 \text{ lb/ft } (7.7 \text{ kN/m}) \quad \ldots \quad (19b)$$

For pipes in very close proximity to the bottom, the approximate validity of Eq. 19*a* was assured by information gathered during this project.

The wave length (L) of the 30.4-ft (9.3-m) high design wave is, according to the stream function theory, 344 ft (105 m). If the depth were reasonably constant, the wave feature would theoretically repeat itself at intervals of

$$\mathscr{L} \equiv L(\csc \alpha) \quad \ldots \quad (20a)$$

$$\mathscr{L} = 420 \text{ ft } (128 \text{ m}) \quad \ldots \quad (20b)$$

along the pipe. The depth change over this distance is approximately

$$\Delta d = \frac{420}{6200} (40) \quad \ldots \quad (21a)$$

$$\Delta d = 2.7 \text{ ft } (0.8 \text{ m}) \quad \ldots \quad (21b)$$

so that the original assumption of constant depth is adequately substantiated.

Assume a wave crest at the offshore end of the pipe. Horizontal forces of 710 lb/ft (10.3 kN/m) and vertical forces of 540 lb/ft (7.9 kN/m) exist at the end of the pipe and 420 ft (128 m) inshore of that location; horizontal and vertical forces of 530 lb/ft (7.7 kN/m) and 530 lb/ft (7.7 kN/m), respectively, occur 210 ft (64 m) shoreward of the end of the outfall. The horizontal crest and trough forces act in opposite directions and the horizontal force distribution along the pipe can be approximated by fairing in a smooth curve that joins these points. The vertical crest and trough forces both act upward. The distribution of vertical force along the pipe passes through these values and dips in between. This minimum vertical force can be assumed equal to zero as shown in Fig. 2.

Conclusions

Ocean experiments with a test pipe have resulted in extensive wave force data for angles between wave fronts and the pipe of 0°, 15°, 35°, and 52°. The horizontal and vertical pipe force data have been converted into maximum force coefficients through use of measured kinematics and these coefficients have been related to values of an adapted period parameter. This information is useful to engineers appraising peak wave forces on exposed and rigid submarine pipes.

Acknowledgments

This project was financially supported by two United States Federal agencies, the Sea Grant Program office and the Department of Energy, as well as by the State of Hawaii and the American Gas Association. Those involved in the project, besides the writers, were as follows: Donald Evans, Russell Luke, Susan Petty, Mark Kaya, Henry Ho, Kent Reinhard, Frederick Casciano, Joseph Castiel, Sylvia Khong, Arthur Shak, Elizabeth Leis, Charles Schuster, James Sands, Steven Nicinski, Herbert Thatcher, Shepard Williams, Edgar Bilderback, Michael Rayfuse, Edward Noda, Wilfred Ii, George Mason, George Weber, Daryl Koreyasu, Barbara Downs, Andrew Oshita, and Terence Dibble.

Appendix I.—Accuracy of Phase I Force Coefficients

This appendix is included in order to explain the absence of the Phase 1 ($\alpha = 0°$) force coefficient data from Tables 9 and 10 and Figs. 6 and 7. It has been shown in Table 2 that the three parts of Phase 1 had different clearance/roughness combinations. However, the force coefficient data from Test Sequences 1B and 1C (different roughness only) were indistinguishable and the two sets of data have been pooled in what follows. The combined 1B and 1C information [pipe clearance of 0.5 in. (13 mm)] is reproduced in the format of Tables 9 and 10 in Table 15. Comparison of these data with those for $\alpha = 15°$ in Tables 9 and 10 shows clearly that the trends in Table 15 lie somewhat lower than those in Test Sequence 2A. On the average (excepting ψ classes with $n \leq 1$) the coefficient ratios are 0.83 and 0.85 in the horizontal and vertical directions, respectively.

The finding that the ratio of these coefficients is not very close to, and

TABLE 15.—Classified Mean and Extreme Behavior of Maximum Force Coefficient for Test Sequences 1B and 1C

	C_{max}			K_{max}		
ψ (1)	n (2)	Mean (3)	Extreme (4)	n (5)	Mean (6)	Extreme (7)
0.4	0	—	—	0	—	—
0.6	0	—	—	0	—	—
0.8	2	3.25	3.36	2	3.34	3.37
1.0	0	—	—	0	—	—
1.2	1	2.39	2.39	1	3.67	3.67
1.4	6	2.69	3.13	6	3.03	3.86
1.6	4	2.67	3.72	4	3.02	3.68
1.8	6	2.90	4.02	6	3.21	4.14
2.0	9	2.70	3.58	9	2.70	4.00
2.2	9	2.73	3.74	9	3.00	4.33
2.4	5	2.37	2.68	4	3.04	3.26
2.6	9	2.35	3.45	8	2.43	4.00
2.8	9	2.16	2.73	8	2.25	3.33
3.0	8	2.63	3.14	7	2.37	2.97
3.2	11	2.11	2.86	11	1.86	3.02
3.4	9	2.24	2.99	9	2.38	3.21
3.6	4	1.78	2.33	4	1.54	2.43
3.8	5	1.95	2.39	4	1.55	1.99
4.0	4	1.89	2.53	3	1.29	1.65
4.2	3	2.04	2.52	2	1.78	1.87
4.4	5	1.81	2.21	5	1.63	2.22
4.6	3	2.10	2.89	2	1.69	2.14
4.8	3	1.73	1.97	3	1.42	2.04
5.0	0	—	—	0	—	—
5.2	7	1.59	2.21	7	1.30	1.91
5.4	3	1.34	1.50	2	1.07	1.13
5.6	5	1.72	2.00	5	1.87	2.32
5.8	2	1.69	1.70	2	1.57	1.70
6.0	3	1.19	1.35	2	1.04	1.21
6.2	0	—	—	0	—	—
6.4	2	1.40	1.65	2	1.10	1.22
6.6	1	1.42	1.42	1	0.79	0.79
6.8	1	1.64	1.64	1	1.46	1.46
7.0	2	1.29	1.36	2	0.99	1.07
7.2	0	—	—	0	—	—
7.4	1	1.56	1.56	0	—	—
7.6	0	—	—	0	—	—
7.8	0	—	—	0	—	—
8.0	0	—	—	0	—	—
8.2	1	1.16	1.16	1	0.80	0.80
8.4	0	—	—	0	—	—
8.6	0	—	—	0	—	—
8.8						
	133			122		

perhaps somewhat greater than, unity is surprising. However, it is the impression of the writers that the $\alpha = 0°$ and 15° cases *are* essentially the same and that the 0.83 and 0.85 ratios resulted from an irregularity in the data gathering and reduction. The ducted current meter used in this project has different calibration (10%) depending upon whether flow enters one end or the other of the duct. That this difference was as large as 10% did not surface until detailed unsteady-flow calibration of the meter (which, incidentally, demonstrated the excellent dynamic response of the sensor) was carried out between Phases 1 and 2. Whereas very careful attention to the fore and aft orientation of the meter was maintained throughout Phase 2, this was unfortunately not always the case during Phase 1. The writers believe that during one and perhaps two of the Data Days in Test Sequences 1B and 1C in Table 2, the meter orientation was inadvertently switched. This would have resulted in flow speeds too high for the crest case, the primary one for which data were processed, leading to coefficients that were too low.

Before leaving the Phase 1 data, it is worthwhile considering differences among the 1A, 1B, and 1C data sets. Table 2 presents the different conditions for the three parts of Phase 1.

There were no discernable mean-trend or extreme-value differences for the horizontal maximum force coefficients across Test Sequences 1A, 1B, and 1C. There were no detectable extreme-value differences across the three data sets for vertical peak force coefficients, and the same applied to the 1B and 1C mean-value trends. However, the 1A mean-value line clearly lay below those for Test sequences 1B and 1C.

These overall results indicate, first, the very small role that reasonable-scale roughness plays in determining wave forces on real ocean submarine pipes. The writers believe that the heavy wake and nonwake turbulence swept back and forth over an uneven sea floor is responsible for this result. In other words, turbulence effects overwhelm roughness effects. The second observation concerns pipe clearance. Although the lack of change in horizontal peak force coefficients might have been anticipated from steady flow results (10), the absence of change in the extreme values for the vertical maximum force coefficients is an unexpected and important result.

Appendix II.—References

1. Dean, R. G., "Evaluation and Development of Wave Theories for Engineering Application," *Special Report No. 1*, U.S. Army, Corps of Engineers, Coastal Engineering Research Center, Fort Belvoir, Virginia, Nov., 1974.
2. Grace, R. A., "Available Data for the Design of Unburied, Submarine Pipelines to Withstand Wave Action," Institution of Engineers, Australia, *National Conference Publication No. 73/1*, 1973, pp. 59–66.
3. Grace, R. A., "Near-Bottom Water Motion Under Ocean Waves," *Proceedings of the Fifteenth Conference on Coastal Engineering, Honolulu, Hawaii*, July, 1976, pp. 2371–2386.
4. Grace, R. A., *Marine Outfall Systems: Planning, Design and Construction*, Prentice-Hall, Inc., Englewood Cliffs, N.J., 1978.
5. Grace, R. A., "A Slanted Look at Ocean Wave Forces on Pipes," report prepared for the American Gas Association, Alexandria, Virginia, at the University of Hawaii, Honolulu, Aug., 1979.
6. Grace, R. A., "Hawaii Ocean Test Pipe Project: Experimental Setup," *Civil Engineering in the Oceans IV*, ASCE, Sept., 1979, pp. 77–98.

7. Grace, R. A., and Nicinski, S. A., "Wave Force Coefficients from Pipeline Research in the Ocean," *Proceedings of the Eighth Annual Offshore Technology Conference, Houston, Texas,* May, 1976, pp. 681–694.
8. Grace, R. A., Castrel, J., Shak, A. T., and Zee, G. T. Y., "Hawaii Ocean Test Pipe Project: Force Coefficients," *Civil Engineering in the Oceans IV,* ASCE, Sept., 1979, pp. 99–110.
9. Iwagaki, Y., and Sakai, T., "Horizontal Water Particle Velocity of Finite Amplitude Waves," *Proceedings of the Twelfth Coastal Engineering Conference, Washington D.C.,* Sept., 1970, pp. 309–326.
10. Jones, W. T., "On-Bottom Pipeline Stability in Steady Water Currents," *Proceedings of the Eighth Annual Offshore Technology Conference, Houston, Texas,* Vol. 2, May, 1978, pp. 763–778.
11. LeMéhauté, B., Divoky, D., and Lin, A., "Shallow Water Waves: A Comparison of Theories and Experiments," *Proceedings of the Eleventh Conference on Coastal Engineering, London, England,* Sept., 1968, pp. 86–107.
12. Luke, R. K. H., "Wave-Induced Water Motion near the Sea Floor," presented to the University of Hawaii, at Honolulu, Hawaii, in 1979, in partial fulfillment of the requirements for the degree of Master of Science.
13. Tsuchiya, Y., and Yamaguchi, M., "Horizontal and Vertical Water Particle Velocities Induced by Waves," *Proceedings of the Thirteenth International Conference on Coastal Engineering, Vancouver, Canada,* Vol. 1, 1972, pp. 555–568.
14. Yamamoto, T., "Hydrodynamic Forces on Multiple Circular Cylinders," *Journal of the Hydraulics Division,* ASCE, Vol. 102, No. HY9, Sept., 1976, pp. 1193–1210.

LONG-TERM DISTRIBUTIONS OF OCEAN WAVES: A REVIEW

By Michael de St. Q. Isaacson,[1] M. ASCE and Neil G. MacKenzie[2]

INTRODUCTION

Important advances have now been made into various aspects of the design of offshore structures with respect to wave action. These include: (1) The development of highly accurate wave theories; (2) the prediction of wave forces on slender structural elements in terms of the incident fluid flow, and on large bodies on the basis of diffraction theory; (3) realistic wave hindcasting from known wind field data; and (4) spectral descriptions of wave and wave loading variations during a given sea state. One important step often encountered in design is the estimation of an extreme design wave (or sea state) on the basis of recorded or hindcast wave data. This generally involves selecting and fitting a suitable probability distribution to wave height data, and extrapolating this to locate a suitable design value. However, even though the procedure is of considerable practical importance, there appears no systematic account in the literature of the various steps involved as applied to all the different distributions that have generally been adopted.

The selection of a design wave from a series of wave records is usually carried out in the following stages:

1. Data consisting of wave heights and periods are collected over a long time (e.g., a few years) at the site of interest. Alternatively, a hindcasting technique may be used to provide wave height data over a much longer time span (say 50 yr or more).
2. A plotting formula is used to reduce the data to a set of points describing the long-term probability distribution of wave heights.
3. These points are plotted on an extreme value probability paper corresponding to a chosen probability distribution function.
4. A straight line is fitted, often by eye, through the points to represent a trend.

[1]Assoc. Prof., Dept. of Civ. Engrg., Univ. of British Columbia, Vancouver, British Columbia, V6T 1W5 Canada.

[2]Civ. Engr., Swan Wooster Engrg. Co., Vancouver, British Columbia, Canada.

Note.—Discussion open until October 1, 1981. To extend the closing date one month, a written request must be filed with the Manager of Technical and Professional Publications, ASCE. Manuscript was submitted for review for possible publication on March 24, 1980. This paper is part of the Journal of the Waterway, Port, Coastal and Ocean Division, Proceedings of the American Society of Civil Engineers, ©ASCE, Vol. 107, No. WW2, May, 1981. ISSN 0148-9895/81/0002-0093/$01.00.

5. The line is then extrapolated to locate a design value corresponding to a chosen return period, T_R, or a chosen encounter probability, E.

An indication of some of the preceding steps is provided by the wave height exceedence diagram sketched in Fig. 1. (Relationships between alternative ordinate scales based on the reduced variety, the exceedence, $Q(H)$, the return period, T_R, and the encounter probability, E, are shown. The scale for E is derived for a design lifetime, L, of 30 yr.) Much of the information needed to carry out the aforementioned procedure is widely scattered in the literature, often being described in any one case for one specific probability distribution and fitting technique only. Furthermore, as emphasized by Nolte (23), quite different models have been used as a basis for defining the individual data points to which a distribution is fitted. The present paper serves to assemble the results needed in applying any of the more common alternative distributions

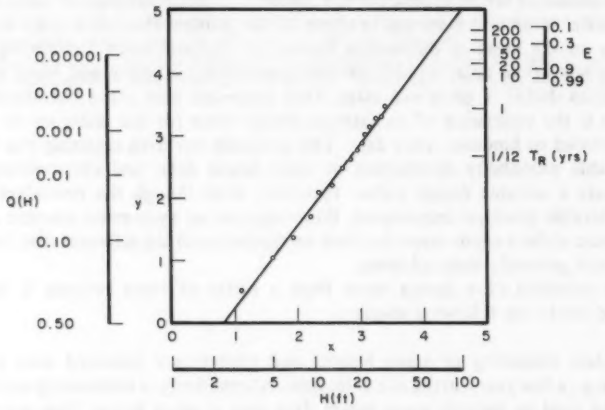

FIG. 1.—Wave-Height Exceedence Diagram Based on Log-Normal Distribution

used, and to review the estimation procedure with its principal variations and areas of difficulty. The emphasis of the paper is given to the selection and fitting of a probability distribution to the data. The complimentary step of wave hindcasting from a known wind field is not itself treated here, although the extrapolation of such hindcast data to extreme conditions is covered as part of the general procedure described.

Extreme Value Probability Distributions

Several probability distributions have been used or proposed to describe extreme wave statistics. These include the log-normal distribution, and the Extremal Types I, II, and III (both lower-bound and upper-bound) probability distributions. Although these all have a theoretical base, they are used here essentially as an empirical fit to the data.

In the following, the cumulative probability, $P(H) = \text{Prob}(H(t) \leq H)$, is the probability that the argument H is not exceeded by any randomly chosen value, $H(t)$, and the probability density, $p(H) = dP(H)/dH$. In describing the distributions, it is convenient to adopt the following notation for the parameters used to define any specific distribution: α = the shape parameter which determines the basic shape of a particular distribution; θ = the scale parameter which controls the degree of spread along the abscissa (variate axis); and ϵ = the location parameter which locates the position of the density function along the abscissa. In the special case of the Type III distributions to be described, ϵ locates one end of the density function.

Table 1 gives the expressions for $P(H)$ defining the different distributions considered here, and also includes expressions for their means and variances. Sketches of each of the corresponding probability densities, plotted with linear scales along both axes, are shown in Fig. 2 for various parameter values.

It is common practice to plot any set of measured data such that the selected distribution lies on a straight line, since this aids visualization of the extrapolation procedure and permits eye fitting where appropriate. Thus, a particular probability paper is first selected, or equivalently corresponding scales are constructed, in order to meet this requirement. The linear ordinate scale, y, is related to the cumulative probability, $P(\ )$, and the linear abscissa scale, x, is related to the variate, H, according to the relationships given in Table 2. There now exists a linear relationship between x and y, $y = ax + b$, with slope a and intercept b which are given in terms of the parameters α, θ, and ϵ, as indicated in the table. In the light of the preceding comments, each distribution is now briefly mentioned in turn.

TABLE 1.—Probability Distributions Used to Describe Long-Term Wave Heights

Distribution (1)	Range (2)	Cumulative probability, $P(H)$ (3)	Mean (4)	Variance (5)
Lognormal	$0 < H < \infty$ $-\infty < \theta < \infty$ $0 < \alpha < \infty$	$(1/\sqrt{2\pi}) \int_0^H \frac{1}{\alpha h} \exp\left[-\frac{1}{2}\left(\frac{\ln(h)-\theta}{\alpha}\right)^2\right] dh$	$\exp\left(\theta + \frac{\alpha^2}{2}\right)$	$\exp(2\theta + \alpha^2)[\exp(\alpha^2) - 1]$
Type I	$-\infty < H < \infty$ $-\infty < \epsilon < \infty$ $0 < \theta < \infty$	$\exp\left\{-\exp\left[-\left(\frac{H-\epsilon}{\theta}\right)\right]\right\}$	$\epsilon + \gamma\theta$ $(\simeq \epsilon + 0.58\theta)$	$\frac{\pi^2}{6}\theta^2$ $(\simeq 1.64\theta^2)$
Type II	$0 < H < \infty$ $0 < \theta < \infty$ $0 < \alpha < \infty$	$\exp\left[-\left(\frac{H}{\theta}\right)^{-\alpha}\right]$	$\theta\Gamma\left(1 - \frac{1}{\alpha}\right)$	$\theta^2\left[\Gamma\left(1 - \frac{2}{\alpha}\right) - \Gamma^2\left(1 - \frac{1}{\alpha}\right)\right]$
Type III$_L$ (Lower Bound)	$\epsilon < H < \infty$ $0 < \theta < \infty$ $0 < \alpha < \infty$	$1 - \exp\left[-\left(\frac{H-\epsilon}{\theta}\right)^{\alpha}\right]$	$\epsilon + \theta\Gamma\left(1 - \frac{1}{\alpha}\right)$	$\theta^2\left[\Gamma\left(1 + \frac{2}{\alpha}\right) - \Gamma^2\left(1 + \frac{1}{\alpha}\right)\right]$
Type III$_U$ (Upper Bound)	$-\infty < H < \epsilon$ $0 < \theta < \infty$ $0 < \alpha < \infty$	$\exp\left[-\left(\frac{\epsilon-H}{\theta}\right)^{\alpha}\right]$	$\epsilon - \theta\Gamma\left(1 + \frac{1}{\alpha}\right)$	$\theta^2\left[\Gamma\left(1 + \frac{2}{\alpha}\right) - \Gamma^2\left(1 + \frac{1}{\alpha}\right)\right]$

Log-Normal Distribution.—The log-normal distribution corresponds to $\ln(H)$ possessing a normal distribution. It was the first distribution to be fitted to long-term wave height data (see Ref. 19) and has commonly been used in extreme wave prediction following the work of Draper (8). Some examples illustrating this approach include those given by Draper (9), Powers, Draper, and Briggs (28), Singh and Draper (32), Draper and Driver (10), and Dattari (7). These examples and others have been compared by Ouellet (25).

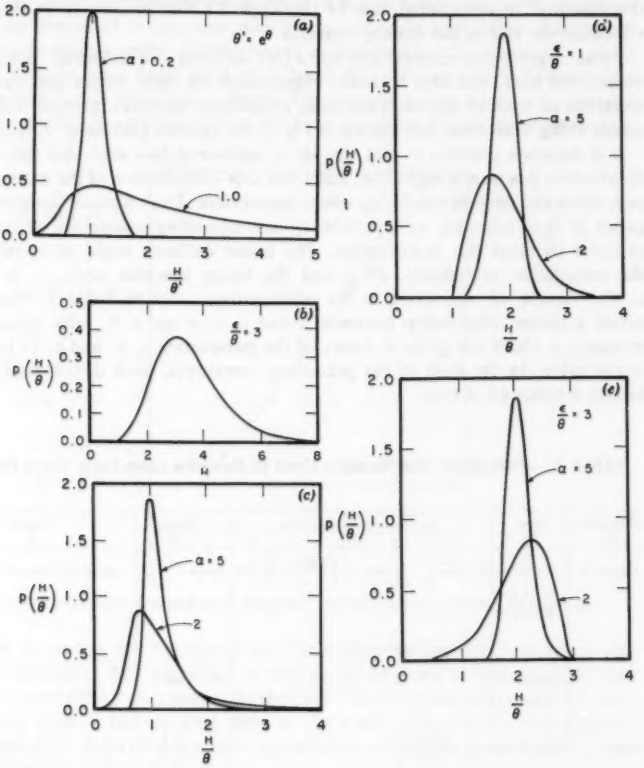

FIG. 2.—Probability Densities of Selected Distributions Plotted with Linear Scales: (*a*) Log-Normal; (*b*) Type I; (*c*) Type II; (*d*) Type III$_L$; (*e*) Type III$_U$

Typical densities with linear scaling and with different values of α are shown in Fig. 2(*a*). The corresponding log-normal probability paper is readily available, and is easy to construct since the ordinate scale, relating y to P as given in Table 2, is listed in probability tables (e.g., see Ref. 1).

Extremal Type I Distribution (Also Termed Gumbel or Fisher-Tippett I Distribu-

tion).—Gumbel (15) developed this distribution to a considerable degree in the context of flood prediction and it is also frequently used in extreme wind prediction (e.g., see Ref. 31). The Type I distribution has been examined in the context of extreme wave prediction by St. Denis (29,30), and an example of its use has been given by Khanna and Andru (20).

A sketch of the density function with linear scaling is shown in Fig. 2(*b*). The corresponding extremal ("Gumbel") probability paper is easily constructed, with the ordinate given as $y = -\ln[-\ln(P)]$ and the abscissa scale given directly as H.

Extremal Type II Distribution (Also Termed Fretchet or Fisher-Tippett II Distribution).—The Type II distribution is often used in the prediction of extreme wind speeds following the work of Thom (33). Its application to extreme wave prediction deriving from the use of wave hindcast formulas to wind speed distributions has subsequently been proposed [Thom (34,35), and reviewed by Yang, Tayfun, and Fallah (38)].

TABLE 2.—Scale Relationships for Probability Papers

Distribution (1)	Abscissa scale x (2)	Ordinate scale y (3)	Slope a (4)	Intercept b (5)
Lognormal	$\ln(H)$	$P(H) = \frac{1}{\sqrt{2\pi}} \int_0^y e^{-1/2t^2}\, dt$	$1/\alpha$	$-\theta/\alpha$
Type I	H	$-\ln\{-\ln[P(H)]\}$	$1/\theta$	$-\epsilon/\theta$
Type II	$\ln(H)$	$-\ln\{-\ln[P(H)]\}$	α	$-\alpha \ln\theta$
Type III_L (Lower Bound)	$\ln(H - \epsilon)$	$\ln\{-\ln[Q(H)]\}$	α	$-\alpha \ln\theta$
Type III_L (Lower Bound)	H	$\{-\ln[Q(H)]\}^{1/\alpha}$	$1/\theta$	$-\epsilon/\theta$
Type III_U (Upper Bound)	$-\ln(\epsilon - H)$	$-\ln\{-\ln[P(H)]\}$	α	$\alpha \ln\theta$
Type III_U (Upper Bound)	H	$-\{-\ln[P(H)]\}^{1/\alpha}$	$1/\theta$	$-\epsilon/\theta$

Fig. 2(*c*) shows Type II density functions for different values of α. The distribution corresponds to $\ln(H)$ possessing a Type I distribution, and thus plots as a straight line on log-extremal paper (sometimes termed "Weibull" paper), in which the ordinate is scaled as with extremal paper, $y = -\ln[-\ln(P)]$, while $\ln(H)$ in place of H is plotted linearly along the abscissa.

Extremal Type III Distribution (Also Termed Weibull Distribution).—There are two alternative forms which have been adopted or proposed for extreme wave prediction. These are lower-bound and upper-bound distributions, denoted here by Types III_L and III_U, which depend on whether the location parameter, ϵ, is used to described a lower-bound (Type III_L) or an upper-bound (Type III_U) to the wave heights. Thus, in either case ϵ represents a limiting value of the variate, H, beyond which no occurrence is possible. The Type III_L distribution was initially developed by Gumbel (14) for estimating worst possible droughts. Since the intention is to provide an empirical fit to the data, the use of either Type III_L or III_U is justified, even though the limits or the distribution's shape may or may not be physically appealing. Figs. 2(*d*) and 2(*e*) show typical plots on linear scales of these two distributions for different

values of α. For particular parameter values, the Weibull distribution reduces to the Rayleigh distribution (when $\alpha = 2$, $\epsilon = 0$) or to the Exponential distribution (when $\alpha = 1$).

It will be seen that the Type III distributions depend on three parameters, rather than two as with the other distributions considered, and so provide added flexibility in attempting to fit data. Against this is the fact that the theoretical variation on log-extremal paper does not fall on a straight line. In order to obtain a straight line plot it becomes necessary to adopt scales which depend on one or other of the parameters to be estimated. Thus, one may plot $\ln(H - \epsilon)$ in the case of Type III_L, or $-\ln(\epsilon - H)$ in the case of Type III, along the abscissa, while the ordinate scale is an appropriate function only of $P(\ )$ as given in Table 2. Alternatively, one may plot $[-\ln(1 - P)]^{1/\alpha}$ for Type III_L, or $-[-\ln(P)]^{1/\alpha}$ for Type III_U along the ordinate, while H is plotted directly along the abscissa. Scales providing a straight line plot thus depend on making an estimate of α or ϵ before plotting the data.

However, in published applications, authors have invariably adopted chosen values of ϵ (e.g., see Ref. 2) or α (e.g., see Ref. 27), rather than best estimates of these parameters. This simplification enables data to be plotted directly, and the Type III_L distribution has been used quite successfully in this way.

In the Type III_L distribution, ϵ may be considered to correspond to a small wave height representing low level background wave activity which is always present, or a lower bound to the wave heights included in the data sample. The Type III_U distribution has not generally been adopted for extreme wave prediction, although its use has been advocated by St. Denis (30), and by Borgman (5). The upper height limit entailed in the Type III_U distribution makes it particularly attractive, e.g., at locations where height may be limited by water depth, fetch, or other such feature, or in any case where a finite maximum wave height corresponding to $P = 1$ is preferred.

Collection of Data Sample

Various methods have been used to assemble a sample of wave statistics to which the extrapolation procedure is to be applied. The individual data points used may be defined in quite different ways as have been reviewed and compared by Nolte (23).

A common method of collecting wave data consists of recording the free surface elevation over a recording period (of say 20 min) with successive recordings commencing at the start of each recording interval (of say several hours). The procedure for converting an individual wave record into characteristic wave statistics is well known and has been described, e.g., by Tucker (36). For data obtained in this way, one may assign one statistic to each successive recording interval, characterizing that particular sea state, and this may be chosen as the significant wave height, expected maximum height, most probable maximum height, zero-crossing period, etc. This approach has been used by Draper (8), Draper and Driver (10), Dattari (7), and others.

A common form of presenting such wave data is with a bivariate histogram or "scatter diagram." Each recording interval has an associated significant wave height and (e.g., zero-crossing or peak) wave period. In the scatter diagram, all such wave heights and periods are divided into equal ranges, and the number

of occurrences of different class combinations of these are tabulated. This data may then be fitted by a long-term distribution of wave heights.

As an alternative procedure, such data may be used to obtain the long-term distribution of *individual* wave heights, $I(H)$. This distribution $I(H)$ may be given in terms of the long-term distribution of significant wave heights, $P(H_s)$, and the Rayleigh distribution, $R(H|H_s)$, which describes the short-term distribution of individual wave heights, H, corresponding to a particular H_s. Pedersen (26) expresses this distribution, $I(H)$, as

$$I(H) = \int_0^\infty R(H|H_s)\, p(H_s)\, dH_s \quad \ldots\ldots\ldots\ldots\ldots\ldots\ldots\ldots\ldots\ldots\ldots\ldots (1)$$

Battjes (2) proposed an improvement to this formula to account for the correlation between H_s and T, the characteristic wave period pertaining to any recording interval. The modified expression is

$$I(H) = \frac{1}{\overline{T^{-1}}} \int_0^\infty \int_0^\infty \frac{R(H|H_s)}{T}\, p(H_s, T)\, dH_s\, dT \quad \ldots\ldots\ldots\ldots\ldots\ldots\ldots (2)$$

in which $\overline{T^{-1}}$ = the long-term average number of waves per unit time; and $p(H_s, T)$ = the long-term bivariate probability density of H_s and T.

Nolte (23) has illustrated how unreliable a design wave estimate can be when based on a single year's wave records. An example he provides shows 100-yr wave estimates differing by a *factor* of about 3 when based on wave records of two successive years. This emphasizes the importance of an adequate data base for reliable predictions to be made.

The alternative procedure involving hindcasting from meteorological data has the considerable advantage that data deriving from a relatively long time span may be reconstructed. Such an alternative is commonly used for hurricane generated waves (e.g., see Ref. 6). A statistic that is generally used in this context is the most probable maximum height occurring in an individual storm greater than a certain intensity [e.g., see Durning (11), Haring and Heideman (16), Petrauskas and Aagaard (27)]. Jahns and Wheeler (18) describe the estimation of this statistic, and also other relevant storm parameters based on hindcast data.

In the case of hurricane generated waves, Ward, Borgman, and Cardone (27) have described an alternative approach to estimating the probability distribution of large individual wave heights. This is obtained in terms of empirical probability distributions of hurricane tracks, affecting the closest distance of approach to the site in question, of hurricane intensities and of the frequency of hurricane occurrence.

Plotting Formulas

In order to plot the data one must first assign a value of $P(H)$ to each value in the sample. To do this, the data are first ordered according to wave height. The suffix m is then used to denote its rank, with $m = 1$ corresponding to the largest value, and $m = N$ to the smallest value in a sample containing N wave heights.

A simple estimate of the exceedence, $Q(H) = 1 - P(H)$, for each of the

N heights is then given as:

$$Q(H_m) = 1 - P(H_m) = \frac{m}{N+1} \quad \ldots\ldots\ldots\ldots\ldots\ldots\ldots\ldots\ldots\ldots (3)$$

In those cases in which N is large (such as when a scatter diagram or an individual wave height distribution is used), $Q(H)$ may be calculated for fewer heights selected at convenient intervals obtained directly from a scatter diagram, or selected to be the largest heights in the sample. In this case, the formula of Eq. 3 still applies, but now takes the following form:

$$Q(H) = 1 - P(H) = \frac{\text{Number of height values} \geq H}{N+1} \quad \ldots\ldots\ldots\ldots\ldots\ldots (4)$$

Gumbel (15) has shown that the expected probability for the mth ordered observation is given by $m/(N + 1)$ as noted in the foregoing, and that this is independent of the distribution adopted. However, Eq. 3 is not unique, and in fact has been demonstrated [e.g., see Kimball (21), and Gringorten (12)] to introduce a slight bias peculiar to the distribution being estimated. An unbiased formula depends on the particular distribution being used, and also on the specific parameters involved. A more general plotting formula may be written in the form:

$$Q(H_m) = 1 - P(H_m) = \frac{m - A}{N + B} \quad \ldots\ldots\ldots\ldots\ldots\ldots\ldots\ldots\ldots\ldots (5)$$

in which A and B = constants to be determined. For the Type I distribution, Gringorten (12) gives $A = 0.44$, $B = 0.12$; and for the Type III$_L$ distribution with prescribed α, Petrauskas and Aagaard (27) give $A = 0.30 + 0.18/\alpha$, and $B = 0.21 + 0.32/\alpha$. Even so, most authors have adopted Eq. 3 as a plotting formula for reducing the data, because of its simplicity, but in spite of it resulting in a possible departure from any "true" underlying distribution (Ref. 12).

Methods of Parameter Estimation

Each of the five distributions considered here is actually a family of distributions, whose properties depend upon the parameter values assigned to them. Having selected one distribution as a likely model, it remains to estimate the parameter values which will provide the best empirical fit between the distribution and the data.

The most straightforward approach is to plot the individual data points on the selected probability paper and then draw a straight line through these by eye. (In the case of the Type III distributions, this would apply only if α or ϵ were chosen in advance.) Alternatively, the best-fit line may be derived by three possible methods: (1) The method of moments; (2) the method of least squares; and (3) the method of maximum likelihood. Each of these three methods may give a different estimate of the parameters based on the same sample. In the following, the estimated values of the parameters are distinguished by a caret over the symbol.

Method of Moments.—The method of moments operates by equating the first

two or three moments of the distribution to those of the data. Since the lowest moments tend to exert the strongest influence on the shape of a distribution, this procedure often leads to an acceptable model.

The estimated values of the parameters, $\hat{\alpha}$, $\hat{\theta}$, and $\hat{\epsilon}$ are expressed in terms of $\bar{H}$, $\bar{H}^2$, and $\bar{H}^3$, as indicated in Table 3. Here $\bar{H}$, $\bar{H}^2$, and $\bar{H}^3$ are obtained

TABLE 3.—Parameters of Distributions as Estimated by Method of Moments

Distribution (1)	Estimated Parameters $\hat{\alpha}$ (2)	$\hat{\theta}$ (3)	$\hat{\epsilon}$ (4)
Log-normal	$[\ln(\bar{H}^2) - 2\ln(\bar{H})]^{1/2}$	$2\ln(\bar{H}) - \frac{1}{2}\ln(\bar{H}^2)$	—
Type I	—	$\frac{\sqrt{6}}{\pi}[\bar{H} - (\bar{H})^2]^{1/2}$	$\bar{H} - \gamma\hat{\theta}$
Type II	$\frac{\bar{H}^2}{(\bar{H})^2} = \frac{\Gamma(1-2/\hat{\alpha})}{\Gamma^2(1-1/\hat{\alpha})}$	$\frac{\bar{H}}{\Gamma(1-1/\hat{\alpha})}$	—
Type III	$\sqrt{\beta} = f(\hat{\alpha})$, see Eqs. 7 and 8	$\left[\frac{\bar{H}^2 - (\bar{H})^2}{\Gamma(1+2/\hat{\alpha}) - \Gamma^2(1+1/\hat{\alpha})}\right]^{1/2}$	$\bar{H} + K\hat{\theta}\Gamma(1+1/\hat{\alpha})$

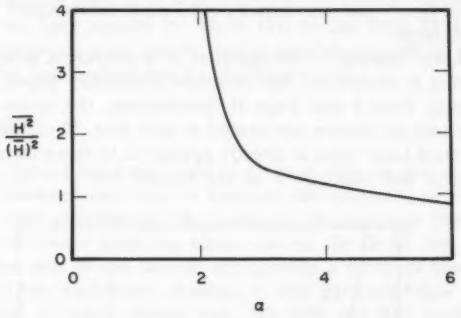

FIG. 3.—Variation of $\bar{H}^2/(\bar{H})^2$ with Shape Parameter, α, for Type II Distribution

directly from the data and are defined as follows:

$$\bar{H} = \frac{1}{N}\sum_{m=1}^{N} H_m; \quad \bar{H}^2 = \frac{1}{N}\sum_{m=1}^{N} H_m^2; \quad \bar{H}^3 = \frac{1}{N}\sum_{m=1}^{N} H_m^3 \quad \ldots\ldots\ldots\ldots (6)$$

The log-normal, Type I and Type II distributions each involve only two parameters, and these can be obtained by equating the first and second moments of the sample to those of the model. In the case of the Type II distribution, the

relationship between $\bar{H}^2/(\bar{H})^2$ and $\hat{\alpha}$ used in the Type II distribution is sketched in Fig. 3. The curve is discontinuous for $\hat{\alpha} < 2$ because of discontinuties in the Gamma function, and $\bar{H}^2/(\bar{H})^2$ is seen to be increasingly insensitive to $\hat{\alpha}$ as $\hat{\alpha}$ becomes large. The Type III distributions involve three parameters, and of these, $\hat{\alpha}$ may first be estimated by equating the skewness, $\sqrt{\beta}$, of the sample to that of the model. The remaining parameters can then be estimated by equating the first and second moments of the sample and the fitted distribution.

The skewness, $\sqrt{\beta}$, is defined as $\sqrt{\beta} = \mu_3/\mu_2^{3/2}$, in which μ_2 and μ_3 are the second and third central moments of the distribution. The sample skewness is given as

$$\sqrt{\beta} = \frac{\bar{H}^3 - 3(\bar{H})(\bar{H}^2) + 2(\bar{H})^3}{[\bar{H}^2 - (\bar{H})^2]^{3/2}} \quad \ldots\ldots\ldots\ldots\ldots\ldots\ldots\ldots\ldots\ldots (7)$$

The dependence of $\hat{\alpha}$ on the skewness, referred to in Table 3, is given by

$$\sqrt{\beta} = K \left\{ \frac{\Gamma\left(1+\frac{3}{\hat{\alpha}}\right) - 3\Gamma\left(1+\frac{2}{\hat{\alpha}}\right)\Gamma\left(1+\frac{2}{\hat{\alpha}}\right) + 2\Gamma^2\left(1+\frac{1}{\hat{\alpha}}\right)}{\left[\Gamma\left(1+\frac{2}{\hat{\alpha}}\right) - \Gamma^2\left(1+\frac{1}{\hat{\alpha}}\right)\right]^{3/2}} \right\} \quad (8)$$

in which $K = 1$ for the Type III_L distribution; $K = -1$ for the Type III_U distribution; and Γ = the Gamma function. Thus, $\hat{\alpha}$ is estimated by Eq. 8 in which the sample skewness, Eq. 7, is applied. This result for the Type III_L distribution was given by Gumbel (14). The relationship given by Eq. 8 is plotted in Fig. 4. It is noted that the skewness becomes increasingly insensitive to $\hat{\alpha}$ as $\hat{\alpha}$ becomes large.

Method of Least Squares.—The intention is to provide a straight line fit to the data when it is plotted on the pertinent probability paper. In the cases of the lognormal, Type I and Type II distributions, the scales are known *a priori* and only two parameters are needed in each case. Thus, the least-squares method in its most basic form is directly applicable to these distributions. This gives the slope a and intercept b of the best-fit line $y = ax + b$ in terms

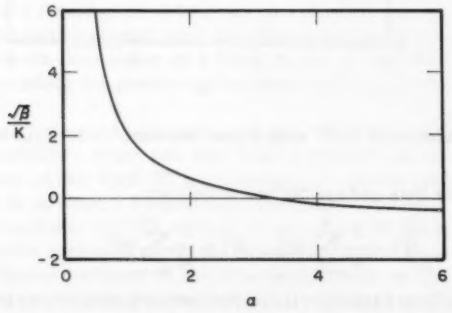

FIG. 4.—Variation of $\sqrt{\beta}/K$ with Shape Parameter, α, for Type III Distributions

of the coordinates (x_i, y_i) of all the data points. The corresponding estimated values of the parameters of the distribution, if required, may then be obtained from the slope and intercept by the expressions given in Table 2.

In the case of the Type III distributions, either the ordinate or abscissa is dependent upon one of the parameters to be estimated, and thus without prior knowledge of this parameter the data cannot even be plotted [unless ϵ or α is chosen to take some trial value, as carried out by Battjes (2) and Petrauskas and Aagaard (27)]. In any case, the least-squares procedure can readily be extended to provide estimates of a, b, and ϵ, or a, b, and α, or both, and involves an iterative procedure which entails no serious difficulty.

Method of Maximum Likelihood.—The method of maximum likelihood attempts to provide estimated parameters which would give the data sample the highest probability of being observed in its particular form. The available sample is considered to consist of a series of independent observations from the same distribution and the probability of the intersection of these events is the product of their individual probabilities. The likelihood function is defined as:

$$L = \Pi_{m-1}^{N} p(H_m) \quad (9)$$

in which $p(\ )$ = the probability density of the chosen distribution; and H_m = the measured wave heights. The method of maximum likelihood then selects values of each parameter which maximizes L. [Since most of the common density functions have an exponential form, this procedure is simplified by maximizing instead $\ln(L)$.]

The method results in estimated parameters which are unbiased and have a relatively small variance. However, the solution usually requires lengthy iterative manipulation, and the method is consequently rarely used in the present context. The method has been applied by Thom (33) to the Type II distribution for the analysis of extreme wind speeds, and its possible application to the distributions considered here is described by Mackenzie (22).

Confidence Intervals

Once a distribution has been fitted to a set of data by one or other method described, it becomes desirable to appraise the closeness of fit of the data points to the fitted distribution. The scatter of the data may best be described in terms of confidence limits on either side of the fitted line. Thus, curves drawn on either side of the best-fit line provide a series of confidence bands which indicate the confidence attached to any particular data point. This is sketched in Fig. 5, which shows, e.g., the 50% and 90% confidence bands, within which data are expected to lie with probabilities of 50% and 90%, respectively. (In this figure, the symbols x shows an example of a pair of calculated height limits used to derive the confidence bands.)

A procedure for constructing confidence bands was developed by Gumbel (15), and has been described by St. Denis (29) in the context of wave prediction. The method is simple to use, but is based on an approximation which is really only suitable for data near the center of the ordered sample, and becomes invalid for the highest points in the sample (which is of greater concern in the present case). Furthermore, the method described applies only to the Type I distribution.

The more complete derivation of confidence bands, as applied to any chosen distribution, is described by Borgman (3) and Gringorten (13). For a given sample size N, rank m, and chosen confidence probability level, this method provides a pair of height limits for the mth statistic. These values may then be plotted on either side of the mth data point, and a faired line drawn through equivalent limits for the remaining points. This procedure is indicated in Fig. 5. It is emphasized that this method cannot be used for prediction (cf. Ref. 29), but strictly applies only to the available data points.

An alternative approach has been used by Petrauskas and Aagaard (27) and involves Monte Carlo simulation to generate random sets of data deriving from the best-fit distribution that has been obtained. The spread of this simulated data can then be used to describe the confidence or uncertainty attached to any chosen value. The major advantage of this approach is that it can be used

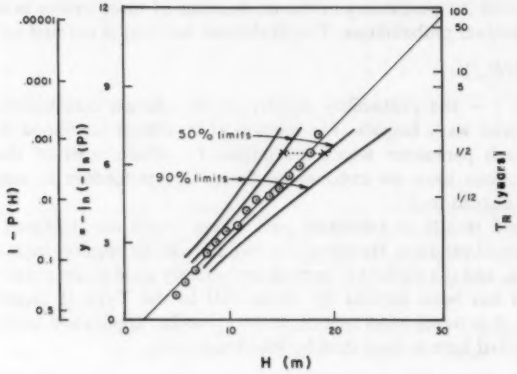

FIG. 5.—Wave-Height Exceedence Diagram Showing Use of Confidence Bands

for any values of height, including predicted values, and thus, enables confidence limits to be attached to any chosen design wave height.

Design Wave Selection

The processes of selecting a particular distribution, together with estimating the most suitable parameters, have so far been described, and we now consider methods of using the best-fit line to predict a design wave height selected to correspond to a prescribed return period. The *return period* (or recurrence interval), T_R, is the average time interval between successive events of the design wave being equalled or exceeded. The wave height selected for this purpose, would initially be defined in the same way as the recorded wave heights (e.g., the significant wave height over a recording interval, or the most probable maximum height in an individual storm). The return period, T_R, may be expressed in dimensionless form as the expected waiting time, $R = T_R/r$, in which r = the recording interval associated with each data point. (Thus, in the case

where each data point corresponds to an individual storm, r would be the average time interval between such storms.) The expected waiting time is directly related to the probability, $P(H)$, as

$$R = \frac{T_R}{r} = \frac{1}{1 - P(H)} \quad \ldots\ldots\ldots\ldots\ldots\ldots\ldots\ldots\ldots\ldots\ldots\ldots\ldots\ldots \quad (10)$$

From this formula, return periods may be scaled along the ordinate, as indicated in Fig. 1. Thus, a prescribed return period has an associated value of $P(H)$, and the corresponding wave height may then be determined from the (extrapolated) best-fit line that has been plotted. This design value will be defined in the same way as were the individual data points (e.g., the significant height over a recording interval), and should be equalled or exceeded on the average once over the duration of any return period. The probability distribution of *individual* wave heights during the corresponding extreme sea state, or other characteristic heights of that sea state, such as the most probable maximum height or the height corresponding to a chosen probability value, may then be obtained in terms of the design height obtained by the use of statistical formulas applicable to short-term (stationary) variations.

It is easily shown that the return period for the common ordinate scale, $y = -\ln[-\ln(P)]$, used in the Types I, II, and III_U distributions may be approximated as

$$\frac{T_R}{r} \simeq \frac{1}{2} + \exp(y) \quad \text{for} \quad \frac{T_R}{r} > 7 \quad \ldots\ldots\ldots\ldots\ldots\ldots\ldots\ldots\ldots\ldots \quad (11)$$

Nolte (23) has indicated that in many cases a correction to the return period is necessary, because its intended meaning is distorted due to the occurrence of more than one data point in a single storm; i.e., the occurrence of large valued data points will tend to group together, and the average duration between successive storms containing a design wave, which is really the intended requirement, will thus be larger than the true return period. The corresponding "grouping correction factor" is relatively important when an individual wave model is used (since more data points will tend to occur in groups), and is unnecessary when a storm model is used

Encounter Probability

In many cases, design is carried out with wave heights corresponding to some prescribed return period, e.g., 50 yr or 100 yr. However, it is appropriate in the context of offshore design to consider also the *encounter probability*, E. This is the probability that the design wave is equalled or exceeded during a prescribed period, L, say the design life-time of a structure; and indeed it may be preferable instead to select T_R to correspond to prescribed values of E and L. The relationship between these quantities (e.g., see Ref. 4) is:

$$E = 1 - \left(1 - \frac{r}{T_R}\right)^{L/r} \quad \ldots\ldots\ldots\ldots\ldots\ldots\ldots\ldots\ldots\ldots\ldots\ldots \quad (12)$$

In which $T_R^2/Lr >> 1$ (i.e., generally when $T/r >> 1$), a suitable approximation to E, which is independent of the recording interval is:

$$E \simeq 1 - \exp\left(-\frac{L}{T_R}\right) \quad \ldots\ldots\ldots\ldots\ldots\ldots\ldots\ldots\ldots\ldots\ldots\ldots \quad (13)$$

Thus, e.g., the return period giving rise to an encounter probability of 0.1 for a design life-time $L = 50$ yr, is 475 yr; and again, the probabilities of a 50-yr design wave being exceeded within 10 yr, 50 yr, and 100 yr are 0.181, 0.632, and 0.865, respectively.

If the design life-time of the structure is prescribed, the encounter probability, E, may be scaled along the ordinate alongside, or in place of, T_R, as sketched in Fig. 1.

Extreme Wave Period

There are various approaches to estimating the extreme wave period associated with the design wave height which has been obtained. The first is to repeat the entire procedure using wave periods instead of wave heights as statistics. Thus, when using a scatter diagram, marginal frequencies are obtained by summing the number of wave occurrences in each period range. By using the same return period as the heights, one may obtain a predicted value of the 50-yr zero-crossing period, T_z, for a hypothetical wave record with the same recording interval. Draper (8) has suggested that this value of T_z may be used with the predicted height, but this suggestion is based on the fact that there is a noticeable correlation between the two variables in the scatter diagram.

An alternative approach involves using the predicted wave height to set a lower limit to the wave period (due to wave breaking), and then using a series of values of the wave period above this lower limit to find the worst effect on the structure. By assuming a Pierson-Moskowitz spectrum, Battjes (2) has shown that for deep water and intermediate depths, a characteristic wave steepness defined as $2\pi H_s/gT^2$ is limited by

$$\frac{2\pi H_s}{gT^2} \leq \frac{1}{16} \quad \ldots\ldots\ldots\ldots\ldots\ldots\ldots\ldots\ldots\ldots\ldots\ldots\ldots\ldots \quad (14)$$

in which g = the gravitational constant [9.801 m/s^2 (32.2 ft/sec^2)]. Thus, a lower limit of period T_L for a given significant height, may be set as:

$$T_L = \left\{\frac{32\pi H_s}{g}\right\}^{1/2} \quad \ldots\ldots\ldots\ldots\ldots\ldots\ldots\ldots\ldots\ldots\ldots\ldots \quad (15)$$

Research has recently been directed [e.g., Houmb and Overvik (17), and Ochi (24)] towards fitting a bivariate probability distribution to long-term data of both wave heights and periods. This predicts different combinations of height and period corresponding to known probabilities of occurrence and should account for limits on height-period combinations due to wave breaking. Such a distribution can conveniently be presented as contours of known probabilities on a scatter diagram. Ochi (24) has employed a bivariate log-normal distribution in this way.

Application

A variety of examples of the foregoing procedures have been provided in

the various references cited herein and will not be repeated here. These have invariably adopted one distribution or another as a fit to the wave data. It is clear, though, that an estimated design wave height from a given set of data depends to some extent on the particular distribution selected and the method of curve fitting applied. Moreover, in many cases (e.g., see Ref. 7), the tail of the data, corresponding to the most extreme measurements made, shows the most noticeable departure from a curve fitted to all the data, even though this extreme range is precisely that over which the best possible fit is required. Thus, it may be preferable to apply, e.g., a least-squares fit to the tail of the data rather than to all of it.

This approach has been explored by MacKenzie (22). A computer program has been prepared by the writers in which wave height data is analyzed to predict design values. In their approach, any one probability distribution is not chosen *a priori*, but rather the five distributions described herein are all fitted to the data using a least-squares fit—a three-parameter fit is used in the case of the Type III distributions. Confidence bands are then constructed about the fitted curves and on the basis of these the most appropriate distribution is selected. This is then used to derive design wave heights in the usual way. This procedure has been illustrated by MacKenzie (22) using data gathered at Tinier Point, New Brunswick.

Summary

The various steps involved in the estimation of extreme design waves have been reviewed. These include methods of data collection, the use of a plotting formula, the selection of a suitable distribution and its parameters, the plotting of confidence bands about the best-fit line, and the selection of a design wave corresponding to a prescribed return period or encounter probability.

The probability distributions that have been used or proposed include the log-normal and Extremal Types I, II, and III distributions (Gumbel, Fretchet, and Weibull distributions, respectively). These distributions are described and their properties and other results required for fitting to data are assembled in tabular form for ready reference.

Additional research is required to enable bivariate probability distributions to be fitted to long-term wave height and period data, taking into account the limits imposed by wave breaking.

Appendix I.—References

1. Abramowitz, M., and Stegun, I. A., *Handbook of Mathematical Functions*, Dover Publications, Inc., New York, N.Y., 1965.
2. Battjes, J. A., "Long-Term Wave Height Distribution at Seven Stations Around the British Isles," *Internal Report No. A44*, National Institute of Oceanography, England, 1970.
3. Borgman, L. E., "The Frequency Distribution of Near Extremes," *Journal of Geophysical Research*, Vol. 66, No. 10, Oct., 1961, pp. 3295–3307.
4. Borgman, L. E., "Risk Criteria," *Journal of the Waterways and Harbors Division*, ASCE, Vol. 89, No. WW3, Proc. Paper 3607, Aug., 1963, pp. 1–35.
5. Borgman, L. E., "Extremal Statistics in Ocean Engineering," *Civil Engineering in the Oceans, III*, ASCE, 1975, pp. 117–133.
6. Cardone, V. J., Pierson, W. J., and Ward, E. G., "Hindcasting the Directional Spectra

of Hurricane Generated Waves," *Journal of Petroleum Technology*, Vol. 28, Apr., 1976, pp. 385–394.
7. Dattari, J., "Waves Off Mangalore Harbor—West Coast of India," *Journal of the Waterways, Harbors and Coastal Engineering Division*, ASCE, Vol. 99, No. WW1, Proc. Paper 9532, Feb., 1973, pp. 39–58.
8. Draper, L., "Derivation of a Design Wave from Instrumental Records of Sea States," *Proceedings of the Institution of Civil Engineers*, Vol. 26, 1963, pp. 291–304.
9. Draper, L., "The Analysis and Presentation of Wave Data—A Plea for Uniformity," *Proceedings of the 10th Coastal Engineering Conference*, Vol. I, 1966, pp. 1–11.
10. Draper, L., and Driver, J. S., "Winter Waves in the Northern North Sea at 57° 30′ N 3° 00′ E, Recorded by M. V. Famita," *Proceedings of the 1st International Conference on Port and Ocean Engineering Under Arctic Conditions*, Vol. II, 1971, pp. 966–978.
11. Durning, P. J., "Prediction of Maximum Wave Height From Historical Data," *Paper No. OTC 1343, Proceedings*, Offshore Technology Conference, Apr., 1971.
12. Gringorten, I. I., "A Plotting Rule for Extreme Probability Paper," *Journal of Geophysical Research*, Vol. 68, No. 3, Feb., 1963, pp. 813–814.
13. Gringorten, I. I., "Envelopes for Ordered Observations Applied to Meteorological Extremes," *Journal of Geophysical Research*, Vol. 68, No. 3, Feb., 1963, pp. 815–826.
14. Gumbel, E. J., "Statistical Theory of Droughts," *Proceedings*, ASCE, Vol. 80, Separate No. 439, May, 1954, pp. 1–19.
15. Gumbel, E. J., *Statistics of Extremes*, Columbia University Press, New York, N.Y., 1958.
16. Haring, R. E., and Heideman, J. C., "Gulf of Mexico Rare Wave Return Periods," *Paper No. OTC 3230, Proceedings*, Offshore Technology Conference, May, 1978.
17. Houmb, O. G., and Overvik, T., "Parameterization of Wave Spectra and Long Term Joint Distribution of Wave Height and Period," *Proceedings of the 1st International Conference, Behaviour of Off-Shore Structures*, Vol. I, Aug., 1976, pp. 144–169.
18. Jahns, H. O., and Wheeler, J. D., "Long-Term Wave Probabilities Based on Hindcasting of Severe Storms," *Journal of Petroleum Technology*, Vol. 25, Apr., 1973, pp. 473–486.
19. Jasper, N. H., "Statistical Distribution Patterns of Ocean Waves and of Wave-Induced Ship Stresses and Motions with Engineering Applications," *Proceedings of the Society of Naval Architects and Marine Engineers*, Vol. 6, 1956, p. 41.
20. Khanna, J., and Andru, P., "Lifetime Wave Height Curve for Saint John Deep, Canada," *International Symposium on Ocean Wave Measurement and Analysis*, ASCE, Vol. I, 1974, pp. 301–319.
21. Kimball, B. F., "On the Choice of Plotting Positions on Probability Paper," *Journal of the American Statistical Association*, Vol. 55, 1960, pp. 546–560.
22. MacKenzie, N. G., "The Statistical Estimation of Extreme Waves," thesis presented to the University of British Columbia, at Vancouver, British Columbia, Canada, in partial fulfillment of the requirements for the degree of Master of Applied Science.
23. Nolte, K. G., "Statistical Methods for Determining Extreme Sea States," *Proceedings of the 2nd International Conference on Port and Ocean Engineering Under Arctic Conditions*, 1973, pp. 705–742.
24. Ochi, M. K., "On Long-Term Statistics for Ocean and Coastal Waves," *Proceedings*, 16th Coastal Engineering Conference, Vol. I, Sept., 1978, pp. 59–75.
25. Ouellet, Y., "On the Need of Wave Data for the Design of Rubble Mound Breakwaters," *International Symposium on Ocean Wave Measurement and Analysis*, ASCE, Vol. I, 1974, pp. 500–522.
26. Pedersen, B., "Prediction of Long-Term Wave Conditions with Special Emphasis on the North Sea," *Proceedings of the 1st International Conference on Port and Ocean Engineering Under Arctic Conditions*, Vol. II, 1971, pp. 979–992.
27. Petrauskas, C., and Aagaard, P., "Extrapolation of Historical Storm Data for Estimating Design-Wave Heights," *Journal of the Society of Petroleum Engineers*, Vol. 11, Mar., 1971, pp. 23–37.
28. Powers, W. H., Draper, L., and Briggs, P. M., "Waves at Camp Pendleton, California," *Proceedings of the 11th Conference on Coastal Engineering*, Sept., 1968, pp. 1–8.
29. St. Denis, M., "Determination of Extreme Waves," *Topics in Ocean Engineering*, C. L. Bretshneider, ed., Vol. 1, Gulf Publishing Co., Texas, 1969, pp. 37–41.
30. St. Denis, M., "Some Cautions on the Employment of the Spectral Technique to

Describe the Waves of the Sea and the Response Thereto of Oceanic Systems," *Paper No. OTC 1819, Proceedings,* Offshore Technology Conference, May, 1973.
31. Simiu, E., and Filliken, J. J., "Probability Distributions of Extreme Wind Speeds," *Journal of the Structural Division,* ASCE, Vol. 102, No. ST9, Proc. Paper 12507, Sept., 1976, pp. 1861–1877.
32. Singh, K. Y., and Draper, L., "Waves off Benghazi Harbor—Lybia," *Proceedings of the 11th Conference on Coastal Engineering,* Sept., 1968, pp. 9–18.
33. Thom, H. C. S., "Frequency of Maximum Wind-Speeds," *Proceedings,* ASCE, Vol. 80, Separate No. 539, Nov., 1954, pp. 1–11.
34. Thom, H. C. S., "Asymptotic Extreme-Value Distributions of Wave Heights in the Open Ocean," *Journal of Marine Research,* Vol. 29, 1971, pp. 19–27.
35. Thom, H. C. S., "Extreme Wave Height Distributions Over Oceans," *Journal of the Waterways, Harbors and Coastal Engineering Division,* ASCE, Vol. 99, No. WW3, Proc. Paper 9939, Aug., 1973, pp. 355–374.
36. Tucker, J., "Analysis of Records of Sea Waves," *Proceedings,* Institution of Civil Engineers, Vol. 26, 1963, pp. 305–316.
37. Ward, E. G., Borgman, L. E., and Cardone, V. J., "Statistics of Hurricane Waves in the Gulf of Mexico," *Paper No. OTC 3229, Proceedings,* Offshore Technology Conference, May, 1978.
38. Yang, C. Y., Tayfun, M. A., and Fallah, M. H., "Extreme Wind, Wave and Tide," *Civil Engineering in the Oceans, III,* ASCE, 1975, pp. 134–141.

Appendix II.—Notation

The following symbols are used in this paper:

a = slope;
b = intercept;
E = encounter probability;
g = gravitational constant;
H = wave height;
H_m = wave height of mth data point;
H_s = significant wave height;
I = long-term cumulative probability of individual wave heights;
L = design life-time;
m = rank;
N = sample size;
P = cumulative probability;
p = probability density;
Q = $1 - P$ = exceedence probability;
R = cumulative probability of Rayleigh distribution;
r = recording interval;
T = wave period;
$\bar{T}^{-1}$ = long-term average number of waves per unit time;
T_R = return period;
T_z = zero-crossing period;
x = abscissa scale;
y = ordinate scale;
α = shape parameter;
$\sqrt{\beta}$ = skewness;
Γ = gamma function;
ϵ = location parameter; and
θ = scale parameter.

TECHNICAL NOTES

Note.—Discussion open until October 1, 1981. To extend the closing date one month, a written request must be filed with the Manager of Technical and Professional Publications, ASCE. This paper is part of the Journal of the Waterway, Port, Coastal and Ocean Division, Proceedings of the American Society of Civil Engineers, ©ASCE, Vol. 107, No. WW2, May, 1981.

Technical Notes

To provide a place within ASCE for publication of technical ideas that have not advanced, as yet, to the point where they warrant publication as a Proceedings paper in a *Journal*, the publication of Technical Notes was authorized by the Board of Direction on October 16–18, 1967, under the following guidelines:

1. An original manuscript and two copies are to be submitted to the Manager of Technical and Professional Publications, ASCE, 345 East 47th Street, New York, N.Y., 10017, along with a request by the author that it be considered as a Technical Note.
2. The two copies will be sent to an appropriate Technical Division or Council for review.
3. If the Division or Council approves the contribution for publication, it shall be returned to Society Headquarters with appropriate comments.
4. The technical publications staff will prepare the material for use in the earliest possible issue of the *Journal*, after proper coordination with the author.
5. Each Technical Note is not to exceed 4 pages in the *Journal*. As an approximation, each full manuscript page of text, tables, or figures is the equivalent of one-half a *Journal* page.
6. The Technical Notes will be grouped in a special section of each *Journal*.
7. Information retrieval abstracts and key words will be unnecessary for Technical Notes.
8. The final date on which a Discussion should reach the Society is given as a footnote with each Technical Note.
9. Technical Notes will not be included in *Transactions*.
10. Technical Notes will be included in ASCE's annual and cumulative subject and author indexes.

The manuscripts for Technical Notes must meet the following requirements:

1. Titles must have a length not exceeding 50 characters and spaces.
2. The author's full name, Society membership grade, and a footnote reference stating present employment must appear on the first page of the manuscript. Authors need not be Society members.
3. The manuscript is to be submitted as an original copy (with two duplicates) that is typed double-spaced on one side of 8-1/2-in. (220-mm) by 11-in. (280-mm) white bond paper.
4. All mathematics must be typewritten and special symbols must be properly identified. The letter symbols used must be defined where they first appear, in figures or text, and arranged alphabetically in an Appendix.—Notation.
5. Standard definitions and symbols must be used. Reference must be made to the lists published by the American National Standards Institute and to the *Authors' Guide to the Publications of ASCE*.
6. Tables must be typed double-spaced (an original ribbon copy and two duplicate copies) on one side of 8-1/2-in. (220-mm) by 11-in. (280-mm) paper. An explanation of each table must appear in the text.
7. Figures must be drawn in black ink on one side of 8-1/2-in. (220-mm) by 11-in. (280-mm) paper. Because figures will be reproduced with a width of between 3 in. (76 mm) to 4-1/2 in. (110 mm), the lettering must be large enough to be legible at this width. Photographs must be submitted as glossy prints. Explanations and descriptions must be made within the text for each figure.
8. References cited in text must be typed at the end of the Technical Note in alphabetical order in an Appendix.—References.
9. Dual units, i.e., U.S. Customary followed by SI (International System) units in parentheses, should be used throughout the paper.

Cable Analysis Using Orthogonal Collocation

By Herman Migliore[1] and Ernest McReynolds[2]

The capability to analyze and design cable systems during the deployment and retrieval phase must encompass the dynamic effects of paying out and reeling in the cable system. Past cable payout/reel in work has been preponderantly treated in a quasidynamic manner (4). With this quasidynamic approach, a dynamic analysis was performed at a fixed length, for several lengths of cable. More recently, spatially-discrete methods, such as the lumped parameter and finite element methods, have been employed in a manner where the length of the cable system is changed at each time integration step (11). These adjustments present a rather adrupt change in configuration and as a result, numerical oscillations can be introduced. Alternatively, cable systems undergoing changing length can be treated in a continuous fashion where full dynamic effects due to payout or reel in are considered (5).

Consider a spherical load of mass, M, and radius, R, supported by an extensible permeable cable; $S(t)$ = the unstretched length of cable between the load and the top support at time, t. Under the assumption that only vertical motion is present, the equations of motion for this one-dimensional system are:

$$0 \le s \le S(t), \quad \frac{\partial T(s,t)}{\partial t} = Ea \frac{\partial v(s,t)}{\partial s} \quad \ldots\ldots\ldots\ldots\ldots\ldots\ldots (1)$$

$$0 < s < S(t), \quad m \frac{\partial v(s,t)}{\partial t} = \frac{\partial T(s,t)}{\partial s} - (m - m_d)g - \frac{\pi}{2} \rho_f C_t D v|v| \quad \ldots\ldots (2)$$

$$s = 0, \quad (M + M_a) \frac{\partial v(0,t)}{\partial t} = -(M - M_d)g + T(0,t) - \frac{1}{2} C_{DS} \rho_f \pi R^2 v|v| \quad (3)$$

$$s = S(t), \quad v[S(t),t] = -\frac{dS(t)}{dt} + u(t) \quad \ldots\ldots\ldots\ldots\ldots\ldots\ldots (4)$$

in which E = elastic modulus (assumed to be linear); a = cable cross section

[1]Assoc. Prof. of Mech. Engrg., Portland State Univ., P.O. Box 751, Portland, Oreg. 97207.

[2]Research Assoc., Portland State Univ., P.O. Box 751, Portland, Oreg. 97207.

Note.—Discussion open until October 1, 1981. To extend the closing date one month, a written request must be filed with the Manager of Technical and Professional Publications, ASCE. Manuscript was submitted for review for possible publication on June 3, 1980. This paper is part of the Journal of the Waterway, Port, Coastal and Ocean Division, Proceedings of the American Society of Civil Engineers, ©ASCE, Vol. 107, No. WW2, May, 1981. ISSN 0148-9895/81/0002-0113/$01.00.

area; m = cable mass per unit unstretched length of cable; m_d = mass of displaced fluid per unit length of cable; M_a = added mass of load in the fluid (the sphere); M_d = mass of displaced fluid of the load (the sphere); C_{DS} = drag coefficient of load; C_t = drag coefficient tangential to cable; ρ_f = fluid density (per unit of volume); D = diameter of cable; and u = deterministic ship motion.

The independent variables are the time, t, and the material coordinate, s, which is the distance along the unstretched length from the load to the cable mass element. The dependent variables, T and v = the tension and vertical velocity (positive up), respectively. Eqs. 1 and 2 are the usual equations for longitudinal oscillations of an elastic cable. Boundary conditions are given by Eqs. 3 and 4.

The boundary condition of Eq. 4 is very awkward to handle since it is applied at a variable material coordinate, i.e., at $s = S(t)$ in which $S(t)$ = the unstretched length of cable in the system. To resolve this difficulty, a material coordinate transformation will be made so that the new "material coordinate" is not time dependent. This is accomplished by the following change of variables: $\sigma = s/S(t)$; $\bar{T}(\sigma, t) = T[s, S(t), t]$; and $\bar{v}(\sigma, t) = v[s, S(t), t]$.

The transformed equations are:

$$0 \le \sigma \le 1, \quad \frac{\partial \bar{T}}{\partial t} = \frac{Ea}{S(t)} \frac{\partial \bar{v}}{\partial \sigma} + \frac{\dot{S}(t)}{S(t)} \sigma \frac{\partial \bar{T}}{\partial \sigma} \quad \ldots\ldots\ldots\ldots\ldots\ldots (5)$$

$$0 < \sigma < 1, \quad \frac{\partial \bar{v}}{\partial t} = \frac{1}{mS(t)} \frac{\partial \bar{T}}{\partial \sigma} - \frac{(m - m_d)g}{m} + \sigma \frac{\dot{S}(t)}{S(t)} \frac{\partial \bar{v}}{\partial \sigma} -$$

$$- \frac{\pi \rho_f C_t D}{2m} \bar{v}|\bar{v}| \quad \ldots\ldots\ldots\ldots\ldots\ldots\ldots\ldots\ldots\ldots\ldots\ldots (6)$$

$$\text{at} \quad \sigma = 0, \quad \frac{\partial \bar{v}}{\partial t} = -\frac{(M - M_D)g}{M + M_a} + \frac{\bar{T}(0, t)}{M + M_a} - \frac{1}{2} \rho_f \frac{C_{DS} \pi R^2 \bar{v}|\bar{v}|}{M + M_a} \quad \ldots\ldots (7)$$

$$\sigma = 1, \quad \bar{v} = -\dot{S}(t) + u(t) \quad \ldots\ldots\ldots\ldots\ldots\ldots\ldots\ldots\ldots\ldots (8)$$

The method of weighted residuals, in particular that of orthogonal collocation, provides an approach to approximate the solution of the preceding nonlinear system of partial differential equations.

A positive integrable weight function, $W(\sigma)$, is chosen as an integrating weight to obtain a Gaussian quadrature for any integrable function, $f(\sigma)$, for $0 < \sigma < 1$. The quadrature formula is of the form

$$\int_0^1 W(\sigma) f(\sigma)\, d\sigma \simeq \sum_{k=1}^{n} w_k f(\sigma_k) \quad \ldots\ldots\ldots\ldots\ldots\ldots\ldots\ldots\ldots\ldots (9)$$

in which the w_k = nonzero coefficients; and the σ_k = values lying in the interval $0 < \sigma < 1$.

If i denotes the number of terms in the preceding summation, and is then varied over the positive integers, a set of polynomials is obtained:

$$P_i(\sigma) = (\sigma - \sigma_1)(\sigma - \sigma_2) \ldots (\sigma - \sigma_i), \quad \text{defining} \quad P_o(\sigma) = 1. \quad \ldots\ldots\ldots (10)$$

For the selected weight function, these polynomials will be orthogonal over the interval of integration (3).

Trial solutions of Eqs. 5–8 are taken as linear combination of polynomials from this set having degree less than or equal to $n - 1$, for some integer n. Following the method of Galerkin, i.e., taking the interior equations of that system with these expansions substituted as interior residuals (1):

$$R_1(\sigma,t) = \frac{\partial \bar{T}}{\partial t} - \frac{Ea}{S(t)}\frac{\partial \bar{v}}{\partial \sigma} - \frac{\dot{S}(t)}{S(t)}\sigma\frac{\partial \bar{T}}{\partial \sigma} \quad \ldots\ldots\ldots\ldots\ldots\ldots \quad (11)$$

$$R_2(\sigma,t) = \frac{\partial \bar{v}}{\partial t} - \frac{1}{mS(t)}\frac{\partial \bar{T}}{\partial \sigma} + \frac{(m-m_d)g}{m} - \sigma\frac{\dot{S}(t)}{S(t)}\frac{\partial \bar{v}}{\partial \sigma}$$

$$+ \frac{\pi \rho_f C_t D}{2m}\bar{v}|\bar{v}| \quad \ldots\ldots\ldots\ldots\ldots\ldots\ldots\ldots\ldots\ldots \quad (12)$$

The inner product of these residuals are taken with the first n polynomials of P over (0, 1) and set to zero. Thus

$$\int_0^1 W(\sigma)\, R_j(\sigma,t)\, P_i(\sigma)\, d\sigma = 0 \quad \ldots\ldots\ldots\ldots\ldots\ldots\ldots\ldots \quad (13)$$

in which $j = 1, 2$; and $i = 0, n - 1$. Taking an nth order Gaussian quadrature of the preceding integrals yields:

$$\sum_{k=1}^{n} w_k R_j(\sigma_k,t)\, P_i(\sigma_k) = 0 \quad \ldots\ldots\ldots\ldots\ldots\ldots\ldots\ldots \quad (14)$$

in which again, $j = 1, 2$; $i = 0, n - 1$; and σ_k = the roots of $P_n(\sigma)$.

For each j, the aforementioned equations determine a homogeneous system of n linear equations in the variables $w_k R_j(\sigma_k,t)$, $k = 1, n$, with the coefficient matrix given by:

$$\mathbf{A} = (a_{ik}), \quad a_{ik} = P_i(\sigma_k) \quad \ldots\ldots\ldots\ldots\ldots\ldots\ldots\ldots \quad (15)$$

This matrix is composed of n linearly independent functions evaluated at n distinct points which will make it nonsingular. Therefore, the preceding system must have the solution

$$R_j(\sigma_k,t) = 0 \quad j = 1, 2 \quad k = 1, n \quad \ldots\ldots\ldots\ldots\ldots\ldots \quad (16)$$

To the aforementioned set of equations are added the boundary conditions yielding a system of $2n + 4$ ordinary differential equations in $4n + 6$ variables. The set of points (0, 1, σ_k; $k = 1, n$) are the so-called orthogonal collocation points (9).

Derivatives with respect to the normalized coordinate appearing in the residuals are eliminated as variables by the consideration of the polynomial trial solutions (2). For example:

$$\bar{v}(\sigma,t) = \sum_{i=0}^{n+1} a_i(t) P_i(\sigma) = \sum_{i=0}^{n+1} \bar{a}_i(t) \sigma^i \quad \ldots \ldots \ldots \ldots \ldots \ldots \quad (17)$$

Differentiating and evaluating this quantity at the collocation points yields

$$\bar{v}(\sigma_k,t) = \sum_{i=0}^{n+1} \bar{a}_i(t) \sigma_k^i; \quad \frac{\partial \bar{v}}{\partial \sigma}(\sigma_k,t) = \sum_{i=0}^{n+1} \bar{a}_i(t) i \sigma_k^{i-1}; \quad k = 0,\ n+1 \ \ldots \quad (18)$$

The matrix $\mathbf{B} = (b_{kl})$, $b_{kl} = \sigma_k^l$, is composed of $n + 2$ linearly independent functions evaluated at $n + 2$ distinct points which will allow the aforementioned $\bar{a}_i(t)$ to be expressed in terms of the $\bar{v}(\sigma_k,t)$. In this manner, a system of $2n + 4$ time-varying ordinary differential equations in $2n + 4$ unknowns is obtained. These equations were solved using the Hamming predictor-corrector method with a fourth order Runge-Kutta method startup procedure (8).

Available experimental data were then compared to analytic results in order to gain confidence in applying the developed computer program (10). The model anchor was a sphere. Two different types of cable were used; they were solid rubber and braided nylon. The cable and anchor were reeled in or paid out at the top of a tank by means of a winching mechanism. The winching mechanism also provided a measure of the payout/reel in velocity and acceleration. The simulation of ship motion was accomplished by an oscillator which caused the winching mechanism and winching platform to oscillate in the vertical direction. Cable tension was measured at the top.

Preliminary comparison between experimental and analytic results revealed the importance of modeling the payout/reel in acceleration. Spline functions were employed to continuously approximate the experimentally-derived data, and these conditions were input into the collocation program. For both experimental and analytic results, the response of the modeled system, in terms of tension at this winch end, exhibited transient oscillation due to the initiation of payout/reel in for both experimental and analytic results. The tension then settled to a steady-state configuration encompassing effects due to change of system length and hydrodynamic drag forces on the cable. The salient features of the analytic results agreed reasonably well with the experimental data; however amplitude comparisons revealed significant differences, in that the computer output tended to be overactive.

Two remedies were incorporated into the computer program. Dynamic uniaxial tension tests revealed measurable material damping for the case of the rubber cable. Material damping was incorporated in the analytic model for rubber (6). The other problem was specification of system drag in the case of braided nylon. The system was subjected to velocity conditions which were successively transient, periodic, and constant in nature. Based on sophistication involved with conducting previous drag studies (7), no attempt could be made to conclusively investigate drag for this particular system. As a result, load drag was somewhat arbitrarily increased from 0.50–1.0 for the nylon case. Steady-state response from the experimental case revealed a constant component for increased drag, irrespective of parametric variation of **EA**, masses, or cable drag.

Since the same payout/reel in program was utilized for parametric analysis, numerical difficulties cannot be ruled out as a contribution. Lower order numerical

integration was employed due to word-size limitations and the procedure for approximating derivatives.

Conclusions

The method of weighted residual, orthogonal collocation technique was used to solve the continuous equations of motion for cable payout and reel in. The method was compared to experimental data for two types of cable under payout and reel in with and without ship motion excitation. Results were within about 35% for the case of rubber cable using a constant coefficient of drag. For the case of nylon cable, the collocation method showed similar results relative to experiments, but some differences in phase and frequency were encountered. Changes in coefficient of drag lessened these differences. As demonstrated by both analytic and experimental results significant dynamic tension were encountered due to solely initiating payout/reel in and bringing the cable system to an abrupt stop.

As suggested in previous sections, the thrust of this investigation was development and exercise of a numerical solution technique for an accepted cable model (6). Future work will include alternative numerical integration procedures and investigation of NWR solution to cable-fluid models which may not incorporate velocity-squared drag. In addition, a two-dimensional solution of the current form of equations of motion are under development and will be compared to experimental results.

Acknowledgment

This investigation was sponsored by the Office of Naval Research, Ocean Technology Branch, under contract number N00014-78-C-0631. The Civil Engineering Lab, Naval Construction Battalion is acknowledged for providing experimental data.

Appendix.—References

1. Ames, W. F., *Numerical Methods for Partial Differential Equations*, Academic Press, New York, N.Y., 1977.
2. Findlayson, B. A., *The Method of Weighted Residuals and Variational Principles*, Academic Press, New York, N.Y., 1972.
3. Hamming, R. W., *Numerical Methods For Scientists and Engineers*, McGraw-Hill Book Co., Inc., New York, N.Y., 1973.
4. Migliore, H. J., and Zwibel, H. J., "Rigorous Treatment of Cable Systems Which Change Length With Time," *Technical Memo. No. M-44-76-8*, Civil Engineering Lab, Naval Construction Battalion, Ft. Hueneme, Calif., Jan., 1976.
5. Migliore, H. J., and Zwibel, H. J., "Dynamic Treatment of Cables Which Change Length With Time," presented at the May, 1977, Sixth Canadian Congress on Applied Mechanics, held at Vancouver, British Columbia, Canada.
6. Reid, R. O., "Dynamic of Deep-Sea Mooring Lines," *Texas A&M Project 204, Reference 68-11F*, Texas A&M Univ., College Station, Tex., July, 1968.
7. Sarpkaya, T., "Periodic Flow Above Bluff Bodies: Part I: Forces on Cylinders and Spheres in a Sinusoidally Oscillating Fluid," *NPS-595L74091*, Naval Postgraduate School, Monterey, Calif., Sept., 1974.
8. Thresher, R. W., and Nath, J. H., "Anchor-Last Deployment Simulation by Lumped Masses," *Journal of the Waterways, Harbors, and Coastal Engineering Division*, ASCE,

Vol. 101, No. WW4, Proc. Paper 11709, Nov., 1975, pp. 419–433.
9. Villadsen, J., and Michelsen, M. L., *Solution of Differential Equation Models By Polynomial Approximation*, Prentice-Hall, Englewood Cliffs, N.J., 1978.
10. Ward, T. M., "Experimental Study of the Dynamics of Variable-Length Cable Systems," *GALCIT Report No. HSWT-1129*, Graduate Aeronautical Laboratories, California Institute of Technology, Pasadena, Calif., 1979.
11. Webster, R. L., "Nonlinear Static and Dynamic Response of Underwater Cable Structures Using the Finite Element Method," presented at the May, 1975, Offshore Technology Conference, held at Houston, Texas, *Paper Number OTC 2322*.

DISCUSSION

Note.—This paper is part of the Journal of the Waterway, Port, Coastal and Ocean Division, Proceedings of the American Society of Civil Engineers, ©ASCE, Vol. 107, No. WW2, May, 1981. ISSN 0148-9895/81/0002-0121/$01.00.

Discussions

Discussions may be submitted on any Proceedings paper or technical note published in any *Journal* or on any paper presented at any Specialty Conference or other meeting, the *Proceedings* of which have been published by ASCE. Discussion of a paper/technical note is open to anyone who has significant comments or questions regarding the content of the paper/technical note. Discussions are accepted for a period of 4 months following the date of publication of a paper/technical note and they should be sent to the Manager of Technical and Professional Publications, ASCE, 345 East 47th Street, New York, N.Y. 10017. The discussion period may be extended by a written request from a discusser.

The original and three copies of the Discussion should be submitted on 8-1/2-in. (220-mm) by 11-in. (280-mm) white bond paper, typed double-spaced with wide margins. The length of a Discussion is restricted to two *Journal* pages (about four typewritten double-spaced pages of manuscript including figures and tables); the editors will delete matter extraneous to the subject under discussion. If a Discussion is over two pages long it will be returned for shortening. All Discussions will be reviewed by the editors and the Division's or Council's Publications Committees. In some cases, Discussions will be returned to discussers for rewriting, or they may be encouraged to submit a paper or technical note rather than a Discussion.

Standards for Discussions are the same as those for Proceedings Papers. A Discussion is subject to rejection if it contains matter readily found elsewhere, advocates special interests, is carelessly prepared, controverts established fact, is purely speculative, introduces personalities, or is foreign to the purposes of the Society. All Discussions should be written in the third person, and the discusser should use the term "the writer" when referring to himself. The author of the original paper/technical note is referred to as "the author."

Discussions have a specific format. The title of the original paper/technical note appears at the top of the first page with a superscript that corresponds to a footnote indicating the month, year, author(s), and number of the original paper/technical note. The discusser's full name should be indicated below the title (see Discussions herein as an example) together with his ASCE membership grade (if applicable).

The discusser's title, company affiliation, and business address should appear on the first page of the manuscript, along with the *Proceedings* paper number of the original paper/technical note, the date and name of the *Journal* in which it appeared, and the original author's name.

Note that the discusser's identification footnote should follow consecutively from the original paper/technical note. If the paper/technical note under discussion contained footnote numbers 1 and 2, the first Discussion would begin with footnote 3, and subsequent Discussions would continue in sequence.

Figures supplied by the discusser should be designated by letters, starting with A. This also applies separately to tables and references. In referring to a figure, table, or reference that appeared in the original paper/technical note use the same number used in the original.

It is suggested that potential discussers request a copy of the *ASCE Authors' Guide to the Publications of ASCE* for more detailed information on preparation and submission of manuscripts.

Sand Bed Friction Factors for Oscillatory Flows[a]

Closure by Philip Vitale[5]

The writer thanks the three discussors for the significant and interesting comments they have made. Eq. 31, derived by Jonsson, is a concise relation which will prove most useful. Lofquist's use of Eq. 28 to relate Eqs. 24 and 26 provides a valuable link between different sections of the report. Both of these analyses suggest that the $R_A^{-1/2}$ factors in the rippled bed trends of Eqs. 26 may be due simply to the constant period of the data. Nielsen's Eq. 32 extends the original results and allows for a more direct comparison with Jonsson's values of f_w. The relationship between f and f_w are discussed in Refs. 8 and 15.

A point brought up by all three discussors concerns the small contribution of the ripples to the total resistance, as predicted by Eq. 25. Lofquist notes that the sand grain component of the roughness (see Eq. 21) includes some effect of the ripples due to the alteration of the flow patterns and skin friction distribution; therefore, Eq. 25 does not take the "ripple effect" into account completely. Nielsen mentions two references (21,22) which demonstrate the importance of sand grain roughness. Jonsson suggest that the 30% contribution of the ripples is too small. To this point, the writer refers to his interpretation of the data which seemed best explained by using Eq. 21 for the bed roughness. This can be seen in the series of graphs in Figs. 10–13. Fig. 10 divides the data into three groups: the turbulent data, defined in Fig. 3, and represented by the symbol *A*; the Area II data, defined in Fig. 2, and represented by the symbol *C*; and the balance of the data which is represented by the symbol *B*. In Fig. 11, which uses Eq. 21 for the abscissa, the rippled and flatbed data group together to allow a single straight line to be drawn through the *A* data. As the ripple effect is increased in the abscissas of Figs. 12 and 13, the rippled data move away from the flat-bed data making it necessary to draw one line for each group.

The writer recognizes the problem with comparing Eqs. 23 and 24 to past determinations of $k_s \approx 2.5\ D_s$ for flat beds and $k_s \approx 2.5\eta$ for rippled beds. In fact, it was this existence of two different k_s relations which led the writer to the analysis of the data of Carstens, Neilsen, and Altinbilek (4) in an attempt to find a roughness factor which would allow for a smooth variation of the roughness as the bed changes, with increasing flow, from rippled to flat-bed sheet flow. (Lofquist points out that the flat-bed condition to which Eq. 24 applies is sheet flow.) Eqs. 23 and 24 allow for this smooth transition.

---

[a]August, 1979, by Philip Vitale (Proc. Paper 14754).

[5]Hydr. Engr., Dept. of the Army, U.S. Army Coastal Engrg. Research Center, Corps of Engrs., Kingman Building, Fort Belvoir, Va. 22060.

The issues of the preceding two paragraphs inspire additional tests which would specifically look into the relative roles of ripple and sand grain roughnesses. These would include tests of similar fixed-bed smooth, fixed-bed rough, and

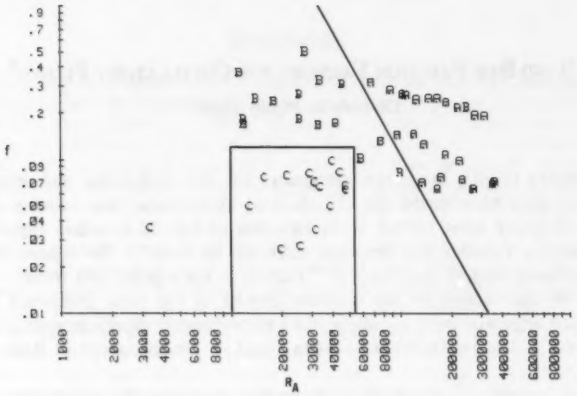

FIG. 10.—Data Separated into Three Groups as Defined in Text

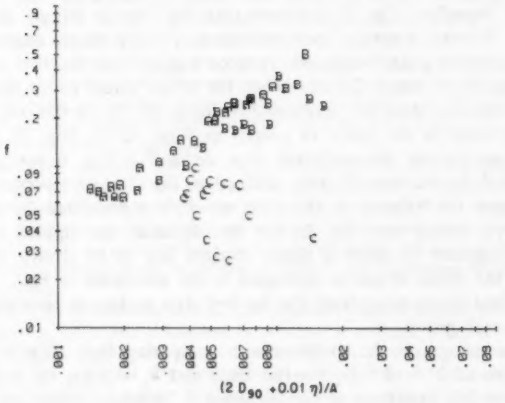

FIG. 11.—Eq. 21 Is Abscissa; Rippled and Flat-Bed Data Group Allow Single Straight Line

movable-bed ripples under identical flow conditions. Also, flow over movable-bed ripples can be gradually increased until sheet flow is produced while the roughness factor is continually determined to track its evolution.

As regards the turbulent zone in Fig. 3, the writer was purposefully conservative

in placing it to insure that the points used in Fig. 4 were indeed turbulent. This is demonstrated by the tight grouping of the *A* data points in Fig. 11. It is possible to make a good case, as Jonsson does, for shifting the line to

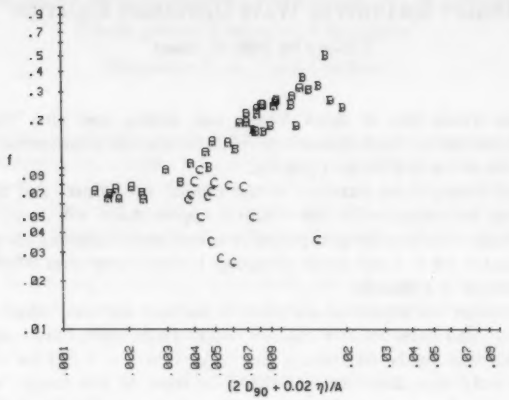

FIG. 12.—Ripple Effect Is Increased

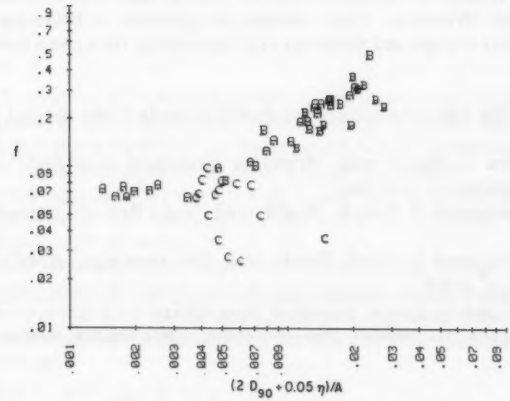

FIG. 13.—Greater Increase in Ripple Effect

the left. This would then include in the turbulent zone a number of the *B* data points in Fig. 11, some of which fall close to the *A* group.

Direct Solution of Wave Dispersion Equation[a]

Closure by John N. Hunt[5]

The writer would like to thank Young and Sobey, and also Venezian for their helpful comments. Both discussions relate to practical alternatives to iterative solution of the wave dispersion equation.

Young and Sobey draw attention to the tabular procedure, and compare its computational efficiency with the writer's approximate solutions, with very favorable results. Some of the gain probably arises from exploiting the deep-water simplification for $mh > 5$, but some advantage is clearly apparent when sufficient computer storage is available.

Venezian raises the important question of balance between range of validity and accuracy, and presents two shallow water Padé approximations, Eqs. 12 and 13, which are highly efficient in the range $0 \leq y < 1$. These expressions are not the only approximants that could be used in this range, nor indeed was the writer's Eq. 6 the only approximant that could be used in $0 \leq y < \infty$.

Both discussions emphasize the desirability of subdividing the range $0 \leq y < \infty$, and it may be that more than two subintervals would further improve computational efficiency. There remains the problem of balancing computer time, computer storage, and simplicity of programming, for a given computational accuracy.

Errata.—The following corrections should be made to the original paper:

Page 457, line 7: Should read "from the relation $c^2 = \sigma^2/m^2$." instead of "from the relation $\sigma^2 = \sigma^2/m^2$."

Page 458, paragraph 3, line 3: Should read "e.g., Ref. 1" instead of "e.g., Ref. 15"

Page 458, paragraph 5, line 6: Should read "the term $d_9 y^9$ gives" instead of "the term $d_g y^9$ gives"

---

[a]November, 1979, by John N. Hunt (Proc. Paper 14944).

[5]Prof. of Applied Mathematics, Univ. of Reading, White Knights, Reading RG6 2AX, England.

Irregularities in Solutions of Nonlinear Wave Diffraction Problem by Vertical Cylinder[a]

Discussion by A. Yücel Odabasi[3]

In the original paper the author pointed out Isaacson's incorrect conclusion (24) that a perturbation solution for the diffraction problem may not be formally extended beyond the linearized approximation due to the irregularity of higher-order solutions along the contour of intersection of the vertical pile and the free surface, and suggested a procedure to compute the solution on the contour of intersection.

Although the present contributor agrees with Miloh's view on the incorrectness of Isaacson's conclusions, some further consideration needs to be paid before the adoption of the solution proposed in the original paper. The aim of this contribution is therefore to complement the views of Miloh by shedding more light into the origin and the nature of these irregularities which may then lead to a solution procedure.

Since the apparent ease in using a polar cylindrical coordinate seems to hinder the source of this irregularity, we shall use a different notation. Then the boundary conditions creating the irregular behavior may be written as:

$$\phi_{tt}^{(k)} + g\,\phi_n^{(k)} = f^{(k)}(\phi^{(k-1)}, \ldots) \quad \text{on} \quad S_F \qquad (30)$$

$$\phi_n^{(k)} = 0 \quad \text{on} \quad S_B \qquad (31)$$

in which $\phi^{(k)} = \phi_I^{(k)} + \phi_s^{(k)}$ = the kth order potential as a sum of the incident ($\phi_I^{(k)}$) and scattered ($\phi_s^{(k)}$) potentials; subscripts t and n denote the derivation with respect to time and normal, respectively; and S_F and S_B = the sets consisting of the points on the free surface and body surface, respectively.

If the points of intersection form a new set S_I the first question to be answered is the choice between the following options: (1) $S_I \subset S_B$, $S_I \not\subset S_F$; (2) $S_I \subset S_F$, $S_I \not\subset S_B$; or (3) $S_I = S_B \cap S_F$.

For the first or second option there is no problem and thus no irregularity in the solution, since the usual perturbation solution without any correction satisfies the needs of these problems. If, however, the third option is the real situation, then the problem is not simply the satisfaction of Eqs. 3 and 5. Rewriting Eqs. 30 and 31 as:

$$a\,\phi_{tt}^{(k)} + b\,\phi_n^{(k)} = cf^{(k)} \quad \text{on} \quad S_B \cup S_F \qquad (32)$$

we can detect that:

1. For points belonging to $S_B - S_I$, $a = 0$, $b = 1$, $c = 0$; for points belonging to $S_F - S_I$, $a = 1$, $b = g$, $c = 1$. However, for points belonging to S_I there

[a] May, 1980, by Touvia Miloh (Proc. Paper 15385).

[3] Named Appointment, The British Ship Research Association, Wallsend Research Station, Wallsend, Tyne and Wear, NE28 6UY, England.

is jump on the values of a, b, and c. Such a jump in itself is sufficient to create an irregularity, solution of which will normally require the extension of two-dimensional complex variable techniques to three-dimensional.

2. For points belonging to S_I, the direction of normal is undefined. In the problem treated by the author this manifests itself as radial or vertical derivatives depending on the direction of approach. In a study on the boundary discontinuity effect for Neumann problem, Craggs, Mangler and Zamir (20) indicated that the behavior of the singularity strongly depends on the vertex angle.

Since a Rankine source distribution on both the body surface and the free surface also leads to a solution, as done by Gadd (23) and Dawson (21) in the ship-wave resistance theory, the simultaneous satisfaction of Eqs. 30 and 31 first raises the question of the existence of a solution on S_I since these conditions may overdetermine the system of equations.

The remedy of the second singularity arising from the nonuniqueness of the boundary normal may be easier to treat. Recently Eggers (22) gave a rigorous treatment of the singularities arising from the boundary discontinuities which may be extended to the present case.

From the foregoing discussions it is clear that neither the problem nor the origin of the irregularity is well-defined unless one of the options on the orientation of the set S_I is chosen. Furthermore, if there is an irregularity this would also exist in the first-order solution since both the jump in the coefficients and the nonuniqueness of normal on S_I also exist in the first-order problem.

Appendix.—References

20. Craggs, J. W., Mangler, K. W., and Zamir, M., "Some Remarks on the Behaviour of Surface Source Distribution Near the Edge of a Body," *Aeronautical Quarterly*, Vol. 24, Part 1, 1973, pp. 25–33.
21. Dawson, C. W., "A Practical Computer Method for Solving Ship-Wave Problems," *Proceedings*, Second International Conference on Numerical Ship Hydrodynamics, 1977, pp. 30–38.
22. Eggers, K., "On Irregularities of the Wave-Flow Due to Source Panels and How to Compensate them by Adding Kelvin-Source Line Elements," Contribution to the Oct. 10–12, 1980, Continued Workshop on Wave Resistance Calculations, held at Izu, Japan.
23. Gadd, G. E., "A Method of Computing the Flow and Surface Wave Pattern Around Full Forms," *Transactions of the Royal Institute of Naval Archives*, Vol. 118, 1976, pp. 207–219.
24. Isaacson, M. de St. Q., "Nonlinear Wave Forces on Large Offshore Structures," *Journal of the Waterways, Harbors, and Coastal Engineering Division*, ASCE, Vol. 103, No. WW1, 1977, pp. 166–170.

SHALLOW WATER SURFACE WAVE ELEVATION[a]

Errata

The following reference should be added to the original paper:

8. Thompson, E. F., "Energy Spectra in Shallow U.S. Coastal Waters," *Technical Paper No. 80-2,* U.S. Army Coastal Engineering Research Center, Fort Belvoir, Va., Feb., 1980.

INLINE FORCES ON FIXED VERTICAL CYLINDER IN WAVES[b]

Discussion by George C. Christodoulou,[3] A. M. ASCE

The author has presented a noteworthy experimental study concerning the inline forces acting on fixed smooth vertical cylinders in a wave tank. Detailed force measurements and application of fifth-order stream function wave theory resulted in defining a relationship between the (local) Morison equation coefficients C_M, C_D and the Keulegan-Carpenter number, KC (Fig. 3). The potential value of the study in improving offshore structure design is obvious.

However, there is a severe limitation of the present results, associated with the Reynolds number parameter. Besides its small values, no distinction of R could practically be made, because of the small range of variation, i.e., 2×10^4–3×10^4. The author suggests that the scatter of the experimental data about the mean curves in Fig. 3 is partly due to the change of R. Previous studies (3,5,15) indicate a strong dependence of the coefficients, especially C_D, on R. Therefore it may be further suggested that the Reynolds number change is responsible, to some extent, for the trend of the mean curves as well, i.e., the gradual decrease of C_D and increase of C_M for KC > 10. This would be a consequence of positive correlation between R and KC. Such a remark is supported by Fig. 7, where it is observed that the curves of C_M, C_D obtained by the author are generally closer to the broken lines for $R = 2 \times 10^4$ at low KC values and closer to those for $R = 3 \times 10^4$ at high KC values.

---

[a]May, 1980, by Edward F. Thompson (Proc. Paper 15385).
[b]May, 1980, by Subrata K. Chakrabarti (Proc. Paper 15403).
[3]Lect., Applied Hydr. Lab., National Technical Univ. of Athens, Athens 624, Greece.

It can be further seen in Fig. 7 that there is no appreciable difference between the values of the coefficients C_M, C_D obtained for wave-flow and those for two-dimensional harmonic flow. The major discrepancies occur at the high end of the KC range, where the sparsity of data makes the wave-flow results less reliable, as the author has mentioned. The agreement is remarkable in view of the empirical nature of these coefficients, their dependence on the wave theory describing the flow field, and some unrealistic assumptions commonly involved in their evaluation, e.g., constancy over the wave cycle. Certainly, wave flow experiments are more representative of field conditions than harmonic flow ones, however the limited present results lead to the tentative conclusion that no significant differences in the coefficients should be expected for the two cases. This could be clarified only by further similar experiments, which would cover a wider range of R and, most importantly, extend to higher ranges encountered in the field. It would be very useful if this procedure could establish more reliable estimates of the Morison coefficients, the lack of which necessarily leads to oversimplifications in design practice (15).

Nevertheless, the more accurate evaluation of the Morison coefficients may not be the only way to proceed in future research. Given the drawbacks associated with their empirical nature and the immense growth of computing capabilities since the Morison formula was proposed, a more generalized correlation of wave characteristics with resulting forces seems now both feasible and more sound. For example, the approach proposed by Jen (14) could lead to such generalized relationships.

Concerning the comparison between measured and calculated total forces on the cylinder, shown in Figs. 4, 5, 6, it should be kept in mind that there is a considerable "feedback" between the forces measured and those calculated. Indeed, the coefficients used in the theoretical force calculation had been obtained by local force measurements on the same cylinders, in the same experimental arrangement and by using, backwards, the same wave theory, Therefore, one would expect a good agreement between essentially the local forces and the integrated forces on the same members. It may be noticed that, although still satisfactory considering the complexity of the problem, the agreement is relatively poorer for the shallow cylinder (Fig. 6), which is the one with the smallest input in the evaluation of the mean C_M, C_D curves. To better establish the validity of the proposed functions of C_M, C_D versus KC it would seem essential to compare them to additional data derived from independent experiments.

Appendix.—References

14. Jen, Y., "Wave Force Analysis: An Alternate Procedure," *Journal of the Waterway, Port, Coastal and Ocean Division*, ASCE, Vol. 106, No. WW1, Proc. Paper 15166, Feb., 1980, pp. 117–121.
15. U.S. Army Corps of Engineers, *Shore Protection Manual*, Coastal Engineering Research Center, Vol. II, 1975.

Impact of Gravel Mining on River System Stability[a]

Discussion by Glendon T. Stevens, Jr.[4] and Claude N. Strauser,[5] Members, ASCE

After reviewing the original paper the writers would like to state that the authors have done a commendable job of constructing a broad array of data, alluding to the impact of gravel mining on river stability. However, certain facets of the data and the conclusions drawn therefrom inspire comment.

At the outset, the title of this article appears to be misleading if one carefully examines the content. It becomes readily apparent in perusing the body of the article that the authors are discussing "armoring"; as a descriptor, armoring is, at the very best, a vaporous term. Simply put, it refers to the natural phenomenon of prevention of erosion or scour of the banks or bed of an alluvial river. The term is derived from a supposition that the fines, sand and silt of the bed, are placed in suspension by scour, leaving materials which are too large to be carried by the flow. That supposition fails to take into account some factors which are difficult to ignore. First of all, the armoring concept presented might be plausible if: (1) There was no increase in flow sufficient to increase the carrying capacity; and (2) there was no inflow of fines from upstream. Such conditions might exist below a large reservoir. However, to postulate that gravel of the size normally mined for commercial purposes can prevent scour on a river subjected to as wide a range of flow as the Mississippi, is to dance on the fringes of fantasy. After all, concrete mattresses are being destroyed constantly.

The authors have unrestrainedly discussed the detrimental effects of commercial gravel mining, ignoring completely the possibility that the dredged areas could serve as storage areas within which the sediment naturally carried by the river could be trapped. Sediments trapped in this manner are unlikely to be a hazard to navigation since most commercial gravel mining takes place well aside from the navigation channel. If the process spoken of operates as proclaimed, then it should alleviate to a small degree the need for channel dredging, in regard to maintenance of open-channels for navigation.

In addition to substantive questions in reference to this article, this reviewer is constrained to question the location of the photographs shown in Figs. 1, 2, and 3. These pictures seem to reveal that the lower Mississippi River was dry at the time they were taken. The history of the Mississippi River records no such condition. The writer believes the gravel found in the lower Mississippi

[a]August, 1980, by Peter F. Lagasse, Brien R. Winkley, and Daryl B. Simmons (Proc. Paper 15643).

[4]Assoc. Prof. of Civ. Engrg., Univ. of Missouri-Rolla, Inst. of River Studies, 302 Engrg. Research Labs., Rolla, Mo. 65401.

[5]Potamologist, St. Louis Dist. Corps of Engrs., 210 N. 12th Street, St. Louis, Mo. 63101.

River, because of years of transport and deposition, would be smoother and more rounded than that depicted. (Reproduction might have caused a distortion.)

It should be noted in critique of this article that the amount of material commercially dredged (sand and gravel) from the Mississippi River during any given year is less than 5% of the material naturally transported by the river. Therefore, the authors are correct when they state that some or all of the changes examined in the paper might have occurred without the removal of gravel from the river bed.

In addition, the writer is compelled to point out that when data are collected and manipulated in the manner they were in plotting Figs. 4, 5, and 6, they lose their identity. Data collected at a specific point if analyzed in this fashion may be acceptable. However, data collected over a 200-mile reach under varying flow conditions and analyzed as they were is questionable.

Further, Fig. 6 indicates that in a relatively few years the bed material of the river will achieve uniform gradation. This is a proposition to which the writer has yet to find agreement and one which is exceedingly difficult to accept.

Technical Papers

Original papers should be submitted in triplicate to the Manager of Technical and Professional Publications, ASCE, 345 East 47th Street, New York, N.Y. 10017. Authors must indicate the Technical Division or Council, Technical Committee, Subcommittee, and Task Committee (if any) to which the paper should be referred. Those who are planning to submit material will expedite the review and publication procedures by complying with the following basic requirements:

1. Titles must have a length not exceeding 50 characters and spaces.

2. The manuscript (an original ribbon copy and two duplicate copies) should be double-spaced on one side of 8-1/2-in. (220-mm) by 11-in. (280-mm) paper. Three copies of all figures and tables must be included.

3. Generally, the maximum length of a paper is 10,000 word-equivalents. As an *approximation*, each full manuscript page of text, tables or figures is the equivalent of 300 words. If a particular subject cannot be adequately presented within the 10,000-word limit, the paper should be accompanied by a rationale for the overlength. This will permit rapid review and approval by the Division or Council Publications and Executive Committees and the Society's Committee on Publications. Valuable contributions to the Society's publications are not intended to be discouraged by this procedure.

4. The author's full name, Society membership grade, and a footnote stating present employment must appear on the first page of the paper. Authors need not be Society members.

5. All mathematics must be typewritten and special symbols must be identified properly. The letter symbols used should be defined where they first appear, in figures, tables, or text, and arranged alphabetically in an appendix at the end of the paper titled Appendix.—Notation.

6. Standard definitions and symbols should be used. Reference should be made to the lists published by the American National Standards Institute and to the *Authors' Guide to the Publications of ASCE*.

7. Figures should be drawn in black ink, at a size that, with a 50% reduction, would have a published width in the *Journals* of from 3 in. (76 mm) to 4-1/2 in. (110 mm). The lettering must be legible at the reduced size. Photographs should be submitted as glossy prints. Explanations and descriptions must be placed in text rather than within the figure.

8. Tables should be typed (an original ribbon copy and two duplicates) on one side of 8-1/2-in. (220-mm) by 11-in. (280-mm) paper. An explanation of each table must appear in the text.

9. References cited in text should be arranged in alphabetical order in an appendix at the end of the paper, or preceding the Appendix.—Notation, as an Appendix.—References.

10. A list of key words and an information retrieval abstract of 175 words should be provided with each paper.

11. A summary of approximately 40 words must accompany the paper.

12. A set of conclusions must end the paper.

13. Dual units, i.e., U.S. Customary followed by SI (International System) units in parentheses, should be used throughout the paper.

14. A practical applications section should be included also, if appropriate.